Title
Droplet Microfluidic Tools and Methods for Enzyme Screening

Author
Tran, Tuan M.

Publication Date
2017

Peer reviewed|Thesis/dissertation

Droplet Microfluidic Tools and Methods for Enzyme Screening

by

Tuan Minh Tran

DISSERTATION

Submitted in partial satisfaction of the requirements for the degree of

DOCTOR OF PHILOSOPHY

in

Bioengineering

in the

GRADUATE DIVISION

of the

UNIVERSITY OF CALIFORNIA, SAN FRANCISCO

AND

UNIVERSITY OF CALIFORNIA, BERKELEY

[redacted]

Acknowledgements

Elements of this dissertation have been published elsewhere. Chapters 2-5 have been published in Journal of Physics D: Applied Physics, Biomicrofluidics, PNAS, and Biomicrofluidics respectively.

I would like to thank all members of the Abate lab for providing a supportive and enjoyable environment for science. First and foremost, I would like to thank Prof. Adam Abate for his hard work and dedication to the lab and his pragmatic mentorship. Without his efforts, I would not have had the productive experience that I had as a graduate student. I would like to thank Prof. Philip Romero, who is now at the University of Wisconsin-Madison. I worked with Prof. Romero when he was a post-doc in the Abate lab. Prof. Romero was and still is one of the best mentors I could have asked for. I would also like to thank Dr. Shaun Lim, Dr. Shea Lance, Dr. Freeman Lan, and Dr. John Haliburton. We all joined the Abate lab the same year and helped each other out tremendously throughout our journeys.

I would also like to thank all of the professors who have helped me throughout my graduate career. Professor Dorian Liepmann, Professors Lydia Sohn, Patricia Babbitt, James Wells, Tanja Kortemme dedicated much time to helping me during my early years in graduate school. In particular, I would like to thank Professor James Wells. I always looked forward to my meetings with Prof. Wells, as his enthusiasm for science always renewed mine.

I would like to thank my collaborators at Northwestern, Professor Michael Jewett and Dr. Yongchan Kwon who devoted a large amount of resources to our projects.

Finally, none of my work would have been possible without the love and support of my mom, dad, three brothers, and numerous friends I made during my graduate career. I cannot thank them enough for their unwavering support through good and challenging times.

Droplet Microfluidic Tools and Methods for Enzyme Screening

Abstract

The ability to engineer enzymes has wide ranging applications in industry and biotechnology. Recently, methods and tools have been developed to engineer enzymes to catalyze a broad range of reactions and conditions. Despite these achievements, the task of enzyme engineering remains quite challenging due to the vast amount of possible sequences and interactions within a protein. This dissertation describes droplet microfluidic tools and methods for ultra-high-throughput screening of enzymes. By screening through variants faster and with less reagent, we increase our chances of finding improved variants. We first describe a fabrication method to make 3-D double emulsion devices in PDMS. We then describe a droplet microfluidic method for high throughput sequence-function mapping. Finally, we detail a detergent-free method to lyse cells in droplets using electroporation. By enabling us to screen enzymes at high throughput, these droplet microfluidic technologies can be a powerful tool for enzyme discovery.

Contents

List of Figures

Chapter 1: Introduction

Our ability to understand and engineer enzymes has significant implications for industry and human health. However, the vast number of possible amino acid combinations and interactions for a single protein presents a major hurdle for enzyme engineering. To tackle the complexity of protein sequence space, two common approaches are used: rational enzyme engineering and directed evolution. These approaches try to overcome the sequence space problem in two complimentary ways. Rational enzyme engineering uses computational models and existing data to predict what sequences will be functional. Directed evolution uses no prior knowledge of the sequence-function relationship. Instead, enzyme libraries with randomized mutations are generated and screened to find the most functional variants. While both approaches have yielded successes, there remains a need to screen variants at a faster and economical rate. By having a method that can screen variants at high throughput, we can build better models for rational enzyme engineering and provide a faster method to screen through variants for directed evolution.

Droplet microfluidics is an emerging field that enables biologists to perform reactions in picolitre sized droplets. These aqueous droplets in oil can be generated at kilohertz rates. Biocompatible surfactant is used to stabilize the emulsion and prevent coalescence. Most biological reagents can be used without compromising the stability of the emulsion. In addition, many devices have been developed to further manipulate the droplets in a precise high throughput manner. Droplets can be split, merged with other droplets, injected with reagents, and sorted. These modules can be combined to perform complex biological workflows. For instance, enzymes libraries can be screened at high throughput using droplet microfluidics. Bacteria expressing an enzyme variant can be encapsulated with a fluorescent assay and lysis reagents in

a droplet. When the bacteria lyse and release the enzyme, the enzyme will catalyze a reaction and produce a fluorescent substrate. The droplet localizes the reaction product, therefore providing a phenotype to genotype linkage. The droplets can be sorted at kilohertz rates based on fluorescence. The variants are then recovered for further analysis and screening. The interchangeability of the modules and flexibility of reagents can accommodate a wide range of enzymatic assays. Droplet microfluidics therefore provides a general platform for enzyme engineering. Millions of enzyme variants can be screened per hour and we can explore the sequence-function landscape of an enzyme in great detail to discover new enzymes.

This dissertation details recent progress on droplet microfluidic devices and how droplet microfluidics can be used to explore the sequence-function landscape of an enzyme.

Chapter 2 provides an extensive review of the droplet microfluidics field. We describe the various types of microfluidic modules. We then discuss the potential biological applications of droplets for high throughput biology.

Chapter 3 describes a new microfluidic device with a 3-D flow focusing geometry in PDMS. We fully characterized this device and demonstrate the ability to generate monodisperse double and single emulsions.

Chapter 4 describes a new method of sequence-function mapping using droplet microfluidics. We demonstrate that we can interrogate millions of variants within several hours. This detailed mapping enabled us to distinguish new functional residues for beta-glucosidase function never before reported.

Chapter 5 describes a new device for detergent free lysis of bacteria in droplets by using electroporation. For enzymes which may be affected by the presence of detergents, this device

offers an alternative lysis method. This is important for directed evolution where the enzyme that is evolved tends to work best in the conditions it was screened in and not its native condition.

Chapter 2: From tubes to drops: Droplet-based microfluidics for ultrahigh-throughput biology

The following section is reprinted from "From tubes to drops: Droplet-based microfluidics for ultrahigh-throughput biology" by Tuan M. Tran*, Freeman Lan*, C. Shea Thompson*, and Adam R. Abate. The article was published in the Journal of Physics D: Applied Physics Volume 46, Number 11 on 22 February 2013. Tuan M. Tran, Freeman Lan, C. Shea Thompson gathered the relevant information and co-wrote the publication. Adam Abate co-wrote the publication and supervised the project.

2.1 Abstract

Droplet-based microfluidics holds enormous potential for transforming the way that many biological screens are performed by affording unprecedented increases in screening throughput and reductions in reagent usage. In this Review, we describe this maturing field and the pioneering work that has laid the foundation for its application to ultrahigh-throughput biological analysis. We begin by introducing the basic elements of the approach and describe the numerous microfluidic components that have been developed for droplet manipulation, with special emphasis on the ones most useful for ultrahigh-throughput analysis. We conclude with a discussion of the first demonstrations of this approach to perform novel, ultrahigh-throughput biological screens.

2.2 Introduction

There are many examples in biological research in which the major barrier to progress is the need to screen massive numbers of separate biological reactions. For example, in drug discovery applications it is often necessary to screen hundreds-of-thousands of compounds, each of which must be separately tested for activities of interest [1–3]. When engineering proteins

through directed evolution, it is often necessary to screen millions of variants of the target protein to find the rare variants with the best activity [4–7]. To detect rare cells or pathogens in a mixed sample, it is often necessary to screen and classify hundreds-of-millions of candidate cells [8]. In all of these examples, and many others like them, the ability to perform ultrahigh-throughput screening on a system-wide scale is essential.

There is now a growing arsenal of tools available to researchers in the biological sciences that are amenable to ultrahigh-throughput, system-scale analysis. To analyze systems at the genomic and transcriptional level, Next Generation Sequencing (NGS) has been transformative because it is able to sequence hundreds-of-millions of DNA molecules, allowing every variant in the system to be characterized. For proteomic analysis, mass spectrometry is becoming an ever more powerful tool, allowing the detection and classification of hundreds of proteins in a complex mixture, and even the determination of protein-protein interactions [9]. This has opened up entirely new frontiers in systems biology, in which complex protein interaction networks are systematically constructed from the rapidly elucidated interactions among pairs of proteins. To analyze systems at the cellular level, fluorescence-activated cell sorting (FACS) is a universal tool, allowing millions of single cells to be individually screened and sorted according to their fluorescence and light-scattering properties.

There is, nevertheless, an important and unmet need in ultrahigh-throughput biological studies, which is the ability to rapidly execute and screen liquid-phase reactions. For example, when enhancing the activity of an enzyme through directed evolution, a critical step is characterizing the catalytic activity of each enzyme variant in the pool. However, because the product of an enzymatic reaction is a molecule that is released into the surrounding solution, there is no physical linkage between the enzyme, its gene, and the quantity of product it produces,

precluding the direct use of technologies like FACS for the ultrahigh-throughput screening. Instead, the reactions must be modified to link gene, protein, and product [6,10–13], an extremely challenging task; alternatively, each variant can be tested in a separate well using plate-based screening [5,7,14–20]. Well-plate formats, however, due to their limited throughput, can only screen ~10^5 variants in total; this is far too small to cover the sequence space of even the active site of most enzymes, making it ineffective for many directed evolution studies. As an alternative to well-plate formats, electrowetting-on-dielectric (EWOD) is a growing field in microfluidics that compartmentalizes reactions in droplets positioned on a checkerboard-like array. Using electrowetting forces, the droplets can be moved around the board and split, merged, and passed over sensors to probe their contents. The precision, automation, and flexibility of this approach hold immense potential for liquid reaction screening, but current technologies are still limited in throughput to just a few reactions per second [21]. Increasing the throughput of liquid-reaction processing would benefit a number of important biological screens, including drug discovery, genomics, and the development of therapeutic antibodies, to name just a few examples.

In this Review, we describe the burgeoning field of microchannel droplet-based microfluidics, a frontier in microfluidics that holds potential for transforming the way that many biological screens are conducted. In this approach, microdroplets, tiny spheres of aqueous liquid dispersed in an inert carrier oil, are used as “test tubes” for reactions with single cells and biomolecules. In many ways, these devices are similar to automated well-plate screening platforms, except that the wells are thousands of times smaller and processed at rates thousands of times faster. The combination of small volumes and massive screening throughput allows screening on a scale that is infeasible with conventional approaches – in which millions of reactions are screened in hours using microlitres of total reagent. Here, we will describe the basic

elements of the approach and the multitude of microfluidic components that have been developed for droplet manipulation, screening, and sorting, with special emphasis on the ones most amenable to ultrahigh-throughput applications: in which droplets the volume of picolitres are screened at rates of kilohertz. We conclude with a discussion of the recent efforts of researchers to build integrated platforms and their application to biological screens that are the first of their kind.

2.3 Fabricating droplet-based microfluidic devices

2.3.1 Photolithography of SU-8 masters

A key explanation for the explosion of microfluidics in the last decade is the development of soft lithography in poly(dimethylsiloxane) (PDMS), a fabrication process that allows creation of microfluidic devices with a range of channel geometries and with precision and ease. PDMS has several properties that make it attractive as a material for microfluidic devices: it is naturally hydrophobic, optically transparent, minimally fluorescent at UV and visible wavelengths, and chemically inert [22]. It is, however, also permeable to vapors and gases, which can be problematic for certain applications. Alternative materials that have been used for creating droplet microfluidic devices for biological applications include glass [23] and PMMA [24]. We will focus on devices fabricated in PDMS, because they are by far the most widely used and the best for ultrahigh-throughput droplet-based screening in academic research settings.

PDMS devices are normally fabricated by molding them from masters containing positive (protruding) channels of the epoxy SU-8 glued to a silicon wafer [25]. The masters are fabricated through a lithographic process in which the photocurable epoxy is spin-coated onto the silicon wafer at a controlled thickness. The wafer is then baked to drive excess solvent out of the epoxy and to cause it to harden, but not crosslink, when cooled. The epoxy-coated wafer is then covered with a “mask” consisting of a printout of the desired microfluidic device in inverse – that is, in

which most of the mask is coated with UV-absorbent ink, but the portions that are to become the positive channels are transparent. The wafers are then exposed to collimated UV light, such that the light passes through the transparent regions but is blocked by the absorbent regions; this crosslinks the SU-8 under the transparent regions. The wafer can then be "developed" by bathing it in a solvent that dissolves uncrosslinked SU-8, leaving behind positive features in the shape needed to mold the PDMS device [26]. This approach produces planar microfluidic channels with rectangular cross sections; however, by iterating coatings of different thickness with exposures through different masks, it is possible to fabricate non-planar devices in which the channel heights vary too [27]. In the majority of research labs utilizing this process, clean room facilities are used, although they are not absolutely required: Depending on the sizes of features in the device and the particular use for which it is intended, often a tidy research lab suffices.

2.3.2 Molding PDMS replicates

Once the master has been fabricated, the PDMS mold can be replicated. This is accomplished by preparing a batch of silicone elastomer (Sylgard 184) and pouring it over the master. The mold is evacuated to remove entrained air bubbles and baked. The baking accelerates crosslinking of the PDMS elastomer, causing it to solidify and become a transparent rubber. It is then sliced and peeled from the master, punched with inlet ports, and washed and bonded to a solid support, such as a glass slide.

2.3.3 Bonding and sealing PDMS channels

The bonding of the PDMS device to a solid support is a critical step in the fabrication process because it adds the final wall that encloses the channels. The most common method for bonding PDMS channels for ultrahigh-throughput biological applications is oxygen plasma treatment. In this approach, a fully-cured PDMS replicate is treated with oxygen plasma

immediately before bonding it to another piece of PDMS or glass. The oxygen plasma makes the surfaces of the PDMS reactive so that when they are placed into contact they irreversibly bond. Plasma bonding produces strong bonds in a matter of minutes. However, it also requires an oxygen plasma cleaner, an expensive piece of hardware that is not available in most research labs. A less-expensive alternative is a handheld corona wand [28], which bonds devices through a similar process at a fraction of the cost. However, because the treatment is performed by hand in the atmosphere rather than in a controlled oxygen environment, the results are less consistent. Both methods make the channels temporarily hydrophilic [29]. To enable the formation of the aqueous-in-oil emulsions that are used in ultrahigh-throughput biological applications, the channels must be made hydrophobic, which is normally achieved using chemical treatments.

2.3.4 Channel wettability

To form droplets in lithographically-fabricated microfluidic channels, the wetting properties of the channels are critical. In planar microfluidic devices like the ones normally fabricated in PDMS, all fluids are initially in contact with the channel walls. To form aqueous droplets, the channel walls must therefore be hydrophobic to allow the oil phase to lift the aqueous phase from the walls, surround it, and encapsulate it into drops. Hydrophobic channels can be obtained by plasma bonding the PDMS channels to a PDMS surface and baking the device for several days at 65°C, during which time the channels revert to their native hydrophobic state [29]. Alternatively, to make the channels hydrophobic more quickly, they can be functionalized with hydrophobic silanes or the glass treatment Aquapel.

2.3.5 Oils and surfactants

Just as important as the aqueous droplets that comprise the “test tubes” is the oil phase surrounding the droplets and comprising the “walls” of the test tubes. The carrier phase must allow the droplets to be stable against coalescence, have a viscosity that is close to that of water, and be inert with respect to the biological reagents contained in the drops and the material of which the device is composed. Several oils have been used in droplet-based microfluidics, each with their own pros and cons.

Low viscosity silicone oils swell PDMS [30,31], changing the cross-sectional dimensions of the channels and influencing the flow properties of the devices [32]. This also depletes the carrier phase from the channels, limiting on-chip incubation time and interfering with droplet recovery [33]. Silicone oils, however, can be used in microfluidic devices fabricated in glass [34,23], which are impermeable to these oils; however, glass devices are much harder to fabricate than PDMS devices and, thus, less widely used. High viscosity silicone oils can be used in PDMS devices with minimal swelling at the expense of significantly increasing the pressures required to pump them through the microchannels. Hydrocarbon oils can also be obtained in a range of viscosities and have the benefit that there are a large number of commercially-available surfactants for them that can stabilize aqueous-in-oil emulsions. However, they also swell PDMS [32,33]{Citation} and tend to exhibit poor retention of encapsulated organic reagents, which are often partially soluble in these oils [35].

By far the preferred oils for biological applications of droplet-based microfluidics are fluorocarbon oils, because even low viscosity versions of these oils do not swell PDMS [32]. In addition, they tend to exhibit excellent retention of reagents in the drops [36,37] and have high solubility for gases, allowing oxygen and carbon dioxide to passively diffuse in and out of the

drops, for unperturbed cellular respiration [38–40]. This allows yeast (figure 2.1 (a)) [39], algae [41], mammalian cells [40,42], and even the multicellular organism *C. elegans* [42] to survive in fluorocarbon oil emulsions for hours after encapsulation. A disadvantage of fluorocarbon oils, however, is that, due to their much lower prevalence compared to silicone and hydrocarbon oils, there are few commercially-available surfactants for stabilizing aqueous-in-fluorocarbon emulsions. Surfactants are essential for reducing the surface tension of the oil-water interface [43] and minimizing droplet coalescence [33]. The choice of which surfactant to use is also imperative for limiting the transfer of reagents between drops [44,45]. A comprehensive review of surfactants for droplet-based microfluidics is available [46]. The surfactants utilized in droplet-based microfluidics normally consist of a hydrophilic head group and hydrophobic tail. The amphiphilic character of these molecules allows them to assemble at the oil-water interface of the droplet, thereby lowering its interfacial tension and enhancing stability [43,47] as depicted in figure 2.1

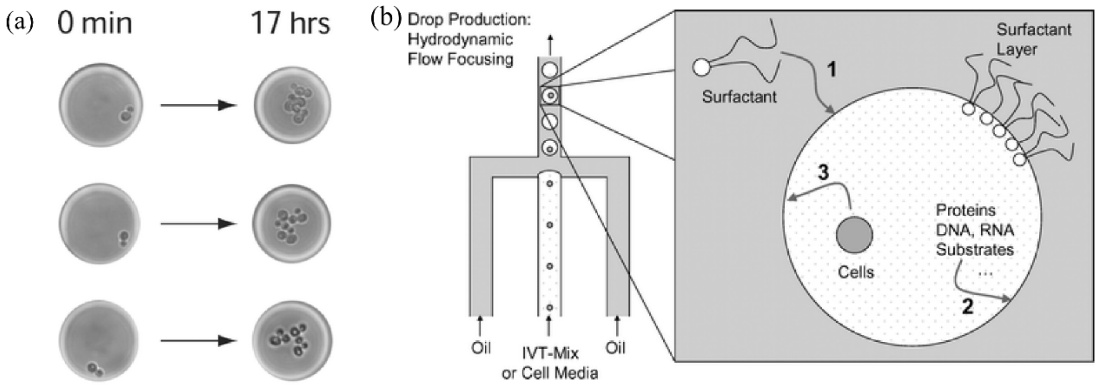

Figure 2.1 Fluorinated oils and non-ionic surfactants are currently thought to afford the best combination of properties for biological applications of droplet-based microfluidics, and are thus the most commonly used combination. They have been demonstrated to be compatible with different kinds of cells, including mammalian cells, bacteria, and yeast cells, which can still divide and proliferate long after encapsulation, (a). Adapted from [47] with permission of The Royal Society of Chemistry. The surfactants stabilize the droplets by adsorbing to the oil-water interface, lowering its interfacial tension and coating the inner surface with a hydrophilic, non-ionic, and biocompatible layer, such as polyethylene glycol, that is resistant to protein adsorption and non-toxic to cells, (b). Reproduced from [47] with permission of The Royal Society of Chemistry.

(b). The chemical properties of the head group of the surfactant impact the biocompatibility of the droplet interface. Surfactants with non-ionic head groups, for instance, have been found to minimize the adsorption of macromolecules like proteins and DNA to the droplet interface, minimally impacting biological assays performed in the drops [47,48]. Several fluorosurfactants that can be readily synthesized in the lab have been described, as has their effectiveness at stabilizing emulsions and yielding biocompatible droplets [42,43,47–49]. Additives to the aqueous phase can also enhance biocompatibility by increasing the retention of small molecules in the droplets and minimizing adsorption at the oil-water interface [40,50,51]. The choice of the surfactant should be made with the oil that is to be used since the properties of the resultant emulsion depend on the combination [24,52]. Different oils can be mixed to optimize the properties of the emulsion for the particular application [53] and methods have been described for easily characterizing the properties of the combination that has been selected [52].

2.4 Generating droplets and encapsulating cells and biomolecules

2.4.1 Droplet generation geometries

The starting point for most droplet-based microfluidic screens is droplet generation [54–56]. There are three common droplet generation geometries in microfluidics: co-flow, T-junction, and flow focus drop formation, each illustrated in figure 2.2. In co-flow drop formation, the dispersed phase is injected through a small capillary centered within a larger capillary, flowing parallel to the flow of the continuous phase, as shown in figure 2.2 (a) [57,58]. Droplets are generated by the viscous shear of the continuous phase over the dispersed phase in a process that resembles a dripping faucet; as the emerging droplet grows, the viscous drag of the continuous phase increases. This continues until the drag is equal to the interfacial tension force adhering the base of the droplet to the capillary tip, at which point a droplet buds off and is carried downstream

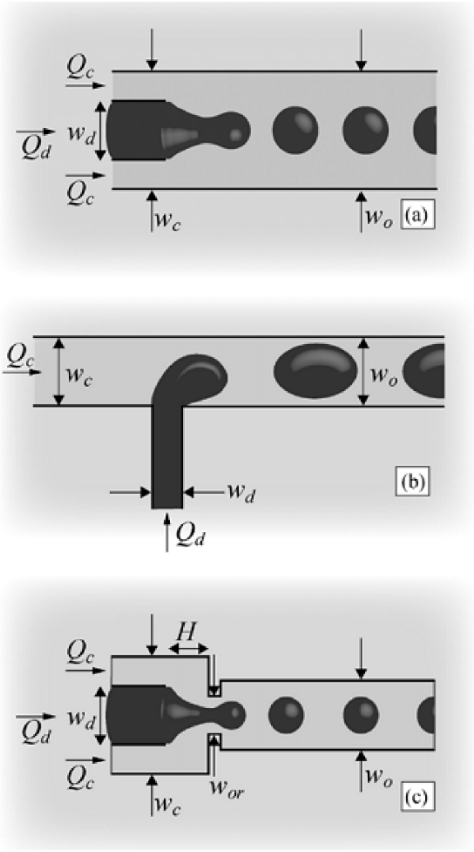

Figure 2.2 The three most commonly used droplet-formation geometries in microfluidics are co-flow (a), T-junction (b), flow-focus (c) drop formation. T-junction and flow focus drop formation are the most widely used because they are easily fabricated in PDMS devices consisting of planar microchannels. Important dimensions for determining droplet size are labeled including w_d, w_c, w_o, which are the widths of the dispersed, continuous and outer phase streams, respectively. w_{or} is the width of the orifice. Q_d and Q_c are the dispersed and continuous phase flow rates. Reproduced with permission from [54].

[59]. In co-flow drop formation, the flows are "unconfined" in the sense that the outer capillary is much larger than the inner capillary and the droplets that are formed; consequently, the drop formation mechanism depends mainly on viscous shear and surface tension, and interactions with the outer capillary wall can be neglected [60]. A disadvantage of this geometry is that it is difficult to fabricate with lithographic processes because it requires the inner capillary to be smaller than, and nested within, the outer capillary. As a result, this geometry is rarely used in ultrahigh-

throughput biological applications, which typically utilize microfluidic devices fabricated with soft lithography and, thus, consisting of planar channel networks.

A more commonly used drop formation geometry, and one that is an example of "confined" drop formation, is the T-junction. In this geometry, the dispersed phase is injected from a channel that is perpendicular to the channel carrying the continuous phase, as illustrated in figure 2.2 (b) [61]. The mechanism by which monodisperse drops are formed depends on the Capillary number (Ca) of the flow. At high Ca, the large viscous drag of the continuous phase shears droplets of the dispersed phase from the inlet channel. A characteristic of drops formed by this mechanism is that they are smaller than the channel. Alternatively, at low Ca drops can also be produced through a mechanism of plugging and squeezing [62]. In this mechanism, the emerging tip of the dispersed phase blocks the downstream channel to the flow of the continuous phase; this causes the pressure to rise in the continuous phase which, in turn, squeezes on the dispersed phase and pinches off a drop. In this mechanism pressure fluctuations are generated in the continuous and dispersed phases and the drops that are formed are always larger than the downstream channel. For the majority of cases in which T-junctions are used, plugging and squeezing is the primary mechanism of drop formation.

Another drop formation geometry is the flow focus device [63]. In this geometry, the dispersed phase is introduced from one channel and the continuous phase from channels on either side. The fluids are focused through an "orifice," where droplets are formed. There are several variations on this geometry, including one in which a small constriction is added at the orifice, as pictured in figure 2.2 (c), and in which the constriction is omitted, yielding a straight "throat." Both variations tend to form droplets with comparable properties for the majority of flow rates. Like the T-junction, the mechanism of drop formation in the flow focus geometry depends on the

Ca of the flow: At low Ca the drops form through a process of plugging and squeezing while at high Ca, they form through a process that depends primarily on viscous drag and interfacial tension [64].

At very high flow rates all three drop makers exhibit "jetting," in which a long tube of the dispersed phase jets through the drop maker and breaks up downstream due to the Rayleigh-Plateau instability [59,65,66], yielding somewhat polydisperse emulsions. The transition to jetting thus sets an upper limit to the rate at which monodisperse droplets can be formed. While this rate can exceed kilohertz for these drop makers, in some instances it is desirable to form drops even faster and, thus, several strategies have been invented to increase drop rates. One strategy is to form large drops at kilohertz rates that are then split into small drops using geometrically-mediated breakup [67]. This increases the droplet production rate by a factor equal to the number of daughter drops formed from each large drop, and has been used to increase net throughput significantly [68]. Another strategy is to exploit the periodic formation of air bubbles to trigger the periodic breakup of an otherwise stable jet [69]. This allows greatly increased drop formation rates because air bubbles, due to their low viscosity and mass, can be formed at rates much faster than droplets of most liquids and, thus, can trigger the breakup of the jet at rates much faster than it would break up spontaneously. To increase the production rate further, drop makers can also be parallelized. Rather than operating one drop maker at a time, several can be operated simultaneously to increase the drop production rate by many times [70–72]. For a thorough review of rapid emulsion techniques, see the following reference [55]. Other useful techniques are valve-based flow focusing, which allows drop size and frequency to be adjusted without changing flow rates [73], and step emulsification, which allows the formation of very small droplets [74,75].

2.4.2 Encapsulating cells and biomolecules

Perhaps the greatest impact of droplet-based microfluidic techniques will be in their ability to perform massively-parallel analysis on populations of single cells. A critical step in this analysis is achieving controlled, efficient encapsulation of the cells in microdroplets. The simplest and most common way to achieve this is limiting dilution, in which a dilute suspension of cells is emulsified such that several drops are formed for every cell in the solution. Under such conditions, the cells are loaded randomly in a process governed by Poisson statistics [76]. This allows one to guarantee that an acceptably small fraction of the droplets contain more than a single cell, at the cost that the majority are empty and unusable, and with a small fraction containing single cells. This tradeoff, however, is often agreeable due to the simplicity of the method, its robustness in use, and the enormous quantity with which droplets can be formed [77]. When this inefficiency is unacceptable, other methods can be implemented to greatly increase single-cell encapsulation efficiency.

One strategy for increasing encapsulation efficiency is to organize the cells prior to encapsulating them. This can be accomplished using inertial microfluidics to order the cells into a periodically-spaced line that travels into the droplet maker at constant velocity; by matching the periodicity of the cells to that of the drop formation, it is possible to encapsulate a controlled number of cells in every drop [77,78], as illustrated in figure 2.3. The ordering of the cells is achieved passively by flowing the cells at high velocity through a long, narrow channel, making it suitable for ultrahigh-throughput applications. However, the high flow rates make this strategy difficult to integrate into complex microfluidic networks, which often contain components that require much lower flow rates. Another challenge is that in many biological assays the amount of reagent available is limited, making it difficult to achieve steady encapsulation before the regents are exhausted.

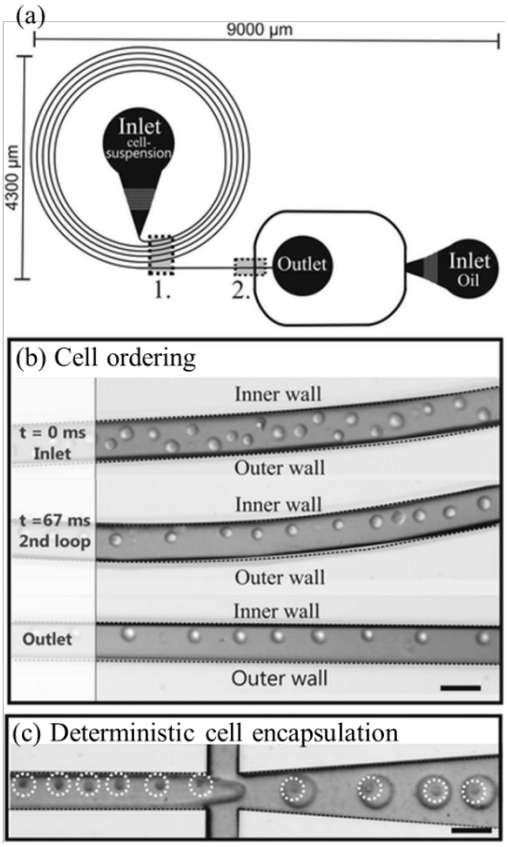

Figure 2.3 Cell encapsulation in droplet-based microfluidics is most often achieved using limiting dilution, so that some drops contain single cells but most are empty. Newer methods are allowing much greater encapsulation efficiency by exploiting inertial microfluidics (a). A spiral geometry couples Dean forces with inertial lift to order the cells prior to encapsulation, as illustrated by images in (b). The periodicity of the regularly-spaced cells can be matched to that of the drop formation, to fill most drops with single cells (c). Reproduced from [78] with permission of The Royal Chemical Society.

An alternative ordering strategy that circumvents some of these issues is close-packed encapsulation [79]: When regularly-sized particles are packed together, they spontaneously organize into a lattice that minimizes packing forces. The periodicity of the lattice can be used to generate periodic particle flow into a drop maker, to achieve high encapsulation efficiency. Because this approach does not require inertial effects, it can be used over a flexible range of flow rates, making it easier to integrate into devices incorporating multiple microfluidic components.

However, it is yet to be demonstrated with cells, which may be difficult to pack and prone to aggregation.

Another strategy for achieving high encapsulation efficiency is cell-triggered jet breakup [80]. In this approach, cells are introduced into a drop maker randomly and used to trigger the breakup of a jet. When no cell is present, very small drops bud from the end of the jet, but when a cell flows into the jet it perturbs the jet, triggering the formation of a larger-than-average drop with the cell encapsulated inside. The result is a bi-disperse emulsion consisting of small, empty drops and large drops containing single cells. The cell-containing drops can then be selectively recovered from the emulsion using passive methods like pinched flow fractionation [81]. This encapsulation approach may potentially be the most valuable for biological applications, because it does not require high flow rates or close packing of the cells. However, it is yet to be widely adopted, possibly due to the complexity of integrating the cell triggering and sorting devices into a microfluidic system, which may not be worth the gain of the increasing the fraction of usable drops.

The encapsulation of biomolecules into drops is achieved exclusively using limiting dilution because molecules are too small to passively organize with inertial or packing methods and to trigger the breakup of a jet. By tuning concentration and drop size, it is possible to precisely set the fraction of drops containing single molecules [82–84].

2.5 Further processing of droplets

After the droplets have been formed and loaded with the cells or biomolecules to be analyzed, several additional operations may be needed to complete the analysis, such as adding reagents to them, incubating them at controlled temperature, or sorting them to recover the ones

most interesting for further study. In this section, we describe the techniques that have been developed for processing drops that are most suitable for ultrahigh-throughput biological studies.

2.5.1 Adding reagents to surfactant-stabilized drops

Next to droplet generation, reagent addition is perhaps the most important operation for ultrahigh-throughput applications. Fundamentally, reagent addition allows the execution of multistep reactions in drops, allowing the drops to be loaded with specific reagents in one step, incubated, and then the conditions in the drops changed by adding another set of reagents.

The challenge with reagent addition is that the drops are almost always stabilized by surfactants, essential for preventing them from coalescing upon contact and thus retaining their integrity as separate microreactors. Reagent addition techniques temporarily destabilize the drops so that the reagents can be added. The techniques that are available can be grouped into two categories, passive and active reagent addition. Whereas passive methods allow reagents to be added without the use of external forces, active methods use external forces like electric fields and focused laser beams, to temporarily and controllably destabilize the drops.

One passive method uses a “push-pull” chamber that expands and then contracts; when two drops flow into the chamber, they merge as they exit through the contracting region [85]. This study demonstrated that, unexpectedly, droplet coalescence is favored by pulling the drops apart rather than squeezing them together. Alternatively, surfactant stabilized drops can also be fused with drops that are not stabilized by flowing them through a zigzag geometry. This strategy enables efficient one-to-one, two-to-one, and three-to-one droplet fusions [86,87]. These passive techniques have the advantage of being exceptionally simple to implement, requiring no specialized electrodes or laser beams to be integrated into the device, as is needed in active methods. However, a disadvantage of these methods is that the fusion depends sensitively on the

chemical properties of the droplets and the dimensions and flow conditions in the microfluidic device; this can make achieving efficient fusion for all biological reagents challenging, particularly when surface-active compounds, like detergents, are present in the drops.

A passive method that overcomes this issue is wettability patterning, in which a hydrophilic strip is patterned into a microfluidic channel [88]. When pairs of droplets flow over the strip, they wet the wall and coalesce with each other and eventually re-form into a single droplet that travels downstream. This method is more robust with respect to the kinds of droplets that can be fused, but has a tendency to transfer material between successive pairs of drops, since material left behind by one pair can be absorbed by a later pair.

Active methods are more difficult to implement because they require the integration of specialized components into the device, like electrodes, but are also more robust in operation and can be applied to a wider variety of reagents [89]. Active methods employ external forces, such as an electrical field, to induce droplet merger. Heat and light have been used for droplet merger [90] but electrical methods have the best potential for ultrahigh-throughput applications because they can merge droplets very quickly and, thus, be applied to drops moving at high velocities past the electrode region. One approach uses electrodes submerged in the reagents to create pairs of drops with opposite charge, forcing them to coalesce [91]. A more robust method uses electric fields not in contact with the reagents to create an electric field that the drops must flow through as they move through the microfluidic device. The electric field causes the conductive drops to temporarily polarize, leading to drop-drop interactions that induce coalescence [89,92,93], as shown in figure 2.4 (a).

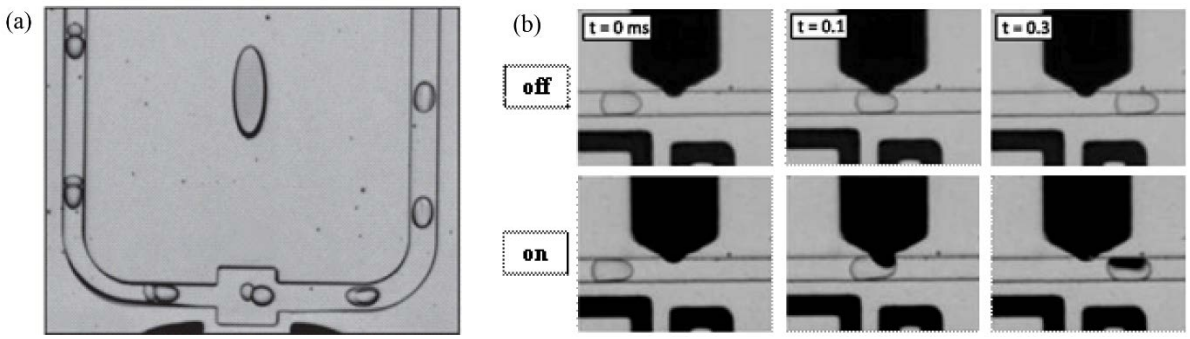

Figure 2.4 The addition of reagents to already-formed droplets is essential when performing most biological assays, since most assays require the addition of different reagents to the drops at different times. The most common techniques for doing this are to coalesce the target drop with a drop of the reagent to be added, (a), or to inject the reagent using picoinjection, (b). Both strategies exploit electric fields to temporarily destabilize the droplets so that the target drops merge with the reagent to be added. (a) Adapted with permission from Macmillan Publishers Ltd: Nature Biotechnology [92], copyright 2009, and (b) reproduced with permission from [100].

In both passive and active droplet merger techniques, it is imperative to synchronize the trains of drops to be merged so that one of each type of drop is paired together and the pair merged. This is often achieved by making one of the drops smaller than the other. In Poiseuille flow, the parabolic profile in the channel causes the small drops to flow faster than the large drops so that they tend to catch up to the larger drops, forming pairs, at which point they can be fused [92,94–96]. For pairs of similarly sized droplets synchronization can be achieved by incorporating expansion chambers to slow down the leading drop [85,97] or electric fields [98,99] to trap the leading drop, allowing the lagging drop to catch up so that the pairs fuse.

A method that bypasses the need for synchronization is picoinjection. In this approach, the droplets to be injected are flowed past a channel containing the reagent to be added. As they pass the channel, an electric field is applied rupturing the surfactant-stabilized interfaces and allowing the reagent to enter the drop, as shown in figure 2.4 (b). This approach allows injection of surfactant-stabilized drops and can perform single and combinatorial injections at kilohertz rates [100].

2.5.2 Rapidly mixing the contents of drops

Due to the small dimensions and relatively low flow rates utilized in most microfluidic studies, the conditions in the channels are laminar; turbulence is absent and streamlines follow paths dictated by the channel geometry. A consequence of laminar flow is that mixing is slow compared to the convective motion of the fluids, which often necessitates the implementation of strategies to enhance mixing. Droplet-based microfluidics is an exception in which mixing is not normally a concern. Even though droplet-based systems operate under laminar flow conditions, mixing is rapid due to the natural generation of recirculating flows in the drops, a result of the drag of the channel walls on the edges of the drops. The recirculating flows decrease the striation length – the average distance for which mixing occurs via diffusion between two materials – so that mixing via diffusion happens much more rapidly than in single-phase fluidic systems [101,102]. Mixing can be enhanced further by flowing droplets through a zigzag geometry, which causes the recirculating flows to change directions, increasing the exchange of fluids between the two halves of the drop and greatly accelerating mixing (figure 2.5) [103,104]. This geometry can mix drops in milliseconds, fast enough for most ultrahigh-throughput applications [105,106].

2.5.3 Recovering the contents of drops

In some implementations of droplet-based microfluidics, the final operation is to optically scan the drops to characterize the outcomes of the reactions. However, there are other instances in which the material in the drops must be recovered for further analysis. The simplest way to achieve this is to coalesce all the drops to form a single aqueous pool. Several methods have been developed to coalesce drops, including flash freezing [107] or by adding a chemical destabilizer to the emulsion [83,92,108].

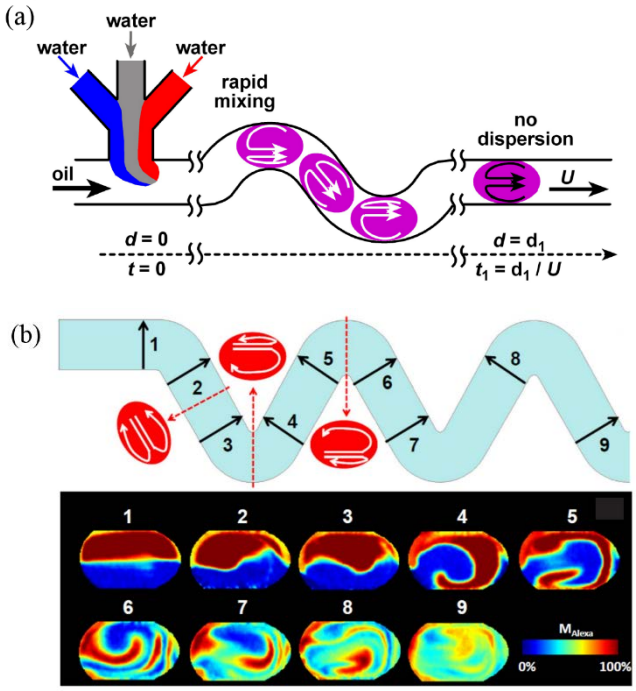

Figure 2.5 Mixing in droplets can be accelerated significantly by flowing the droplets through curving channels. (a) Illustration of streamlines within droplets passing through a curving channel. (Reproduced with permission from [105]). (b) Images of two dyes mixing in a serpentine channel with droplet positions in channel indicated by numbers (Reprinted with permission from [104]. Copyright 2012, American Institute of Physics).

In other instances, in addition to coalescing the drops, it is desirable to ensure that the drop contents remain distinct after coalescence. This can be accomplished by solidifying the interior of the drops prior to coalescence using a gelling agent, such as alginate or agarose. After the drops coalesce, the gelled interiors remain distinct and can be collected and suspended into an aqueous carrier solution. This has been used, for instance, to perform PCR analysis on single cells [109,110]. Functionalized beads can also be used to selectively capture specific analytes from the drops, such as a target protein or DNA molecule [111–114,83]. The beads can be recovered by breaking the emulsion and using a separation technique, like magnetic separation or centrifugation [113].

The droplet contents can also be recovered by selectively fusing them with an aqueous stream using a microfluidic device, figure 2.6. The droplets pass an opening containing a flowing stream of aqueous fluid. Due to surfactants in the oil phase, in the absence of other forces the droplets do not merge with the stream and exit the device intact. However, when an electric field is applied the droplets fuse with the stream, releasing their contents into it for collection [96,115]. This process is very high throughput and has demonstrated the capability of selectively fusing drops at kilohertz rates.

Another strategy for recovering material from drops that does not require the extraction of the entire drop is geometrically-mediated splitting [116]. In this approach, the drops are flowed into a channel that bifurcates into two channels; as the drops flow through the bifurcation, they are divided into two portions, one traveling down each arm of the split. The volumes of the two portions and, thus, of fluid that is sampled from each drop, can be adjusted by controlling the flow rates through the two arms, either by pressurizing the outlets or tuning hydrodynamic resistances [67]. The different portions of the droplets can then be analyzed by optically scanning them or merging them with droplets containing other reagents [117–119].

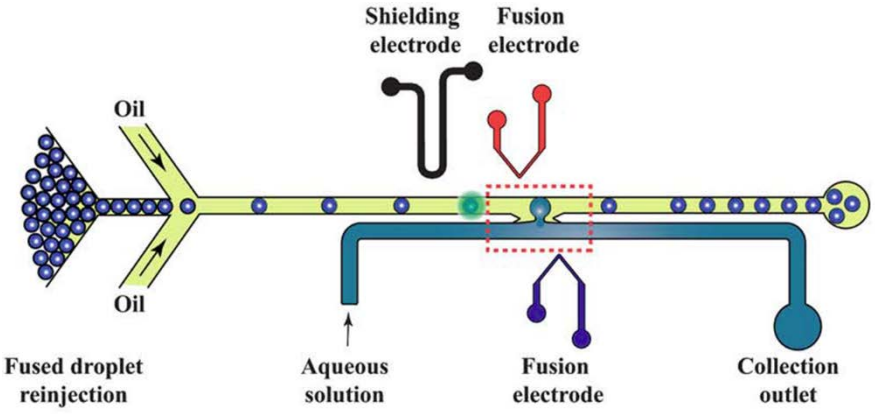

Figure 2.6 Electrocoalescence of drops with an aqueous stream for recovering target drops. Reproduced in part from [96] with permission of The Royal Society of Chemistry.

2.5.4 Incubation and storage of drops

In nearly all biological assays, steps of thermally-controlled incubation are required, such as to stimulate the growth of bacteria or perform PCR amplification of nucleic acids. In droplet-based microfluidics, droplets can be incubated off the microfluidic device, for example, in an incubator or PCR machine, or on the microfluidic device, using integrated thermoelectrics and temperature controllers [120,121].

On-chip incubation is normally achieved by flowing the drops through channels or trapping them in static arrays. With channel incubation, there are different options depending on the duration of incubation required. For example, for very short incubations (seconds), the drops can be flowed single-file through a channel of controlled length [122]. This has the benefit of keeping the drops in order, but is limited in the duration of incubation it can achieve because long incubations require long channels, which have high hydrodynamic resistances and require impossibly large input pressures to drive the flow. This can be avoided by stopping the flow so that the drops are static in the channel but, due to the small volume of even a relatively long microchannel, this strategy is only applicable to storing thousands of drops [123].

When longer delays are required, the most common strategy is to use a delay line, which is a wide and tall channel that is able to store a large number of drops. Due to the large diameter of the delay line, the pressure required to pump the drops through it is small, making it appropriate for hours of incubation. The drawback to this approach, however, is that the drops pack into the delay line in three dimensions and, consequently, lose their original order. The drops can also move with respect to one another, resulting in dispersion of the incubation time – that is, in which the duration that each drop spends in the delay line varies. Time dispersion can be overcome using several strategies, including by packing the drops densely so that the drops jam and are prevented

from changing positions, as shown in figure 2.7 (a) [124]. Another strategy is to include periodic constrictions into the line, which cause the drops to repeatedly shuffle; this averages out variations in droplet velocity, causing the incubation time of each drop to converge to the average value, as shown in figure 2.7 (b) [124].

Reservoirs are very large channels (millimeters in width) that can store millions of droplets for hours of incubation. Once droplets are packed into the reservoir, the flow can be stopped and the device can be incubated under the desired conditions [33,51,24]. The drops can be packed as a monolayer to allow each droplet to be directly visualized [125]. In addition, if stored in a gas-permeable PDMS device, gas exchange through the channel walls can be used to enhance the survival or cells compared to storage in an air-tight syringe [76].

An alternative strategy for storing drops in a chamber is to use microfabricated features to position the drops at defined locations; this can aid visualization and prevent the drops from moving over the course of the experiment [39,45,126], as shown in figure 2.8. A limitation of static arrays, however, is that they are difficult to fabricate with the capacity needed to make them valuable for ultrahigh-throughput applications: While the largest demonstrated array held 1 million drops [127], most have only been able to hold tens of thousands [39,45,120,126,128–132].

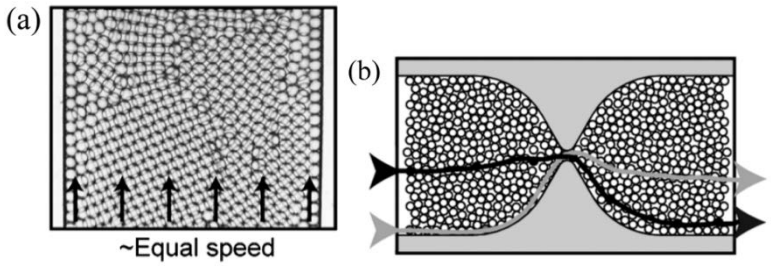

Figure 2.7 Strategies for preventing dispersion of incubation time in delay lines include (a) densely packing drops or (b) implementing repeated constrictions to average out positional-dependent differences in droplet velocity, yielding equal incubation time for all drops. Reproduced in part from [124] with permission of The Royal Society of Chemistry.

When there is not an explicit need to incubate droplets on the microfluidic device, off-chip incubation is often the easiest strategy. Off-chip incubation is often accomplished by transferring the droplets from the microfluidic device into a syringe or centrifugal tube, and then storing the tube at the desired temperature and atmospheric conditions in a cell incubator, thermal cycler, or other controlled environment [34,35,42,95,133–135]. Off-chip storage is appropriate for hours to weeks of incubation and the emulsion can be re-injected into a microfluidic device for analysis and further manipulation [34]. Long-term off-chip storage of droplets for screening applications has also been proposed using microfluidic cartridges [136,137]. Ultimately, the limit to the duration over which the emulsion can be stored depends on the stability of the emulsion and viability of the reagents or living organisms contained within the drops.

2.5.5 Sorting

The sorting of an emulsion, the selective retrieval from an emulsion of a population of drops, is critical for a number of especially important ultrahigh-throughput studies. It is needed, for instance, when performing directed evolution, in which a large library of drops is prepared, each containing a distinct mutant of a cell or protein, and a small fraction of which are desirable for further study. To perform the experiment, all droplets must be scanned and the ones with desirable

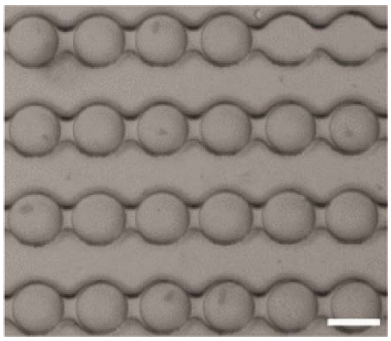

Figure 2.8 Drops stored in a static array of microfabricated chambers. Adapted from [39] with permission of The Royal Society of Chemistry.

mutants must be recovered. Because ultrahigh-throughput biological systems typically operate at droplet rates in the kilohertz, exceptionally fast sorting methods are required.

Ultrahigh-throughput sorting of droplets can be achieved using passive and active means [96,138], although the active method is generally the most useful because it is versatile and can be used to sort droplets based on a complex logical decision. Active droplet sorting has been demonstrated using magnetic [139,140], mechanical [141], acoustic [142], electrophoretic [91] and dielectrophoretic [143–145] forces to separate the drops. The general approach involves flowing the drops single file into a junction with two or more outlet channels. The junction is designed so that, by default, all droplets flow into one of the outlet channels, termed the "waste," due to differences of the channels in hydrodynamic resistance. Select drops can then be sorted into the other channel by applying one of the abovementioned forces. Of the techniques developed, pressure-based, acoustic, and dielectrophoretic sorting have proven to be the fastest, capable of sorting droplets at rates faster than 200 Hz. Dielectrophoretic droplet sorting has been used to screen a large library of enzymes at rates greater than 1 kHz [144,145], as illustrated in figure 2.9. An alternative approach to microfluidic sorters is to perform the reactions in water/oil/water double emulsion droplets which can then be scanned and sorted using flow cytometry [146,147]; however, the lower stability of the double emulsions, coupled with a larger solubility of encapsulated

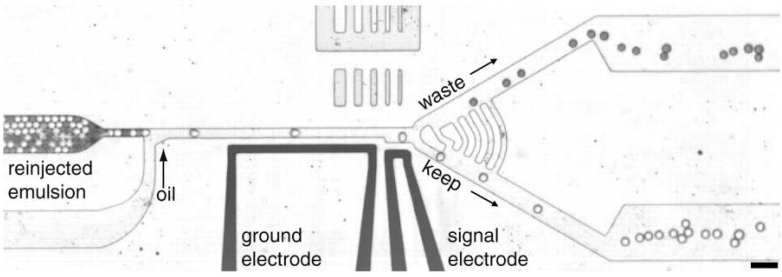

Figure 2.9 Dielectrophoretic sorting of drops at kilohertz rates. Reproduced with permission from [145].

molecules in the aqueous carrier phase, can limit the utility of this approach for certain applications [144,147].

2.5.6 Device integration

The components we have described can be integrated together to form complex devices capable of performing multiple tasks, such as forming the drops in one part of the device, incubating them in another, and optically scanning and sorting the drops [127,148,149]. Integration is made possible by the precision with which the individual components operate, making their behavior predictable and reproducible: Drop makers can form drops with less than 1% variation in the drop diameter, while picoinjectors can inject controlled volumes of reagents into drops with near 100% efficiency, and sorters can sort drops with less than 0.01% sorting errors [54,100,145]. Nevertheless, when integrating multiple components together, special care must be taken to ensure that all components operate under similar flow and pressure conditions. If a drop maker is to be combined with a sorter, for example, then the drop maker must form drops of the size and rate required by the sorter. Such optimization can be tedious and require significant investments of time [150]. One way to avoid these difficulties is to use each component individually as its own device [92,96,145]. For example, to form and then sort drops, the fluids for drop formation can be injected into a drop making device at the flow rates needed to form drops of the desired size. The drops can then be collected into a syringe and, after they have all been formed, injected into the sorting device at the flow rates needed for this device. In this way, many operations can be performed in sequence, without having to engineer the components to operate simultaneously, at the same flow rates, on a single chip.

2.6 Labeling and detecting droplets

2.6.1 Labeling strategies

Labeling refers to marking the droplets in an emulsion so that the identity of each droplet can be determined by reading the label at a later time, for instance, to know which reaction is being performed in a given droplet. Methods to label droplets utilize spatial and chemical encoding. In spatial encoding, the identity of the droplet is linked to its location [151], for instance, by positioning drops on an array such that the position of each drop on the array relates its identity [152]. Single-file positioning is limited in the number of drops that can be stored by the length of the channel. Two dimensional arrays allow much larger numbers of drops to be stored and are generally more useful for ultrahigh-throughput studies [127,153].

Another way to label droplets is to add fluorescent dyes to them. Dyes are can be used to determine which drops have successfully been encapsulated with cells [77,128], cellular components [154], and beads [155]. Dyes can also be used to indicate the concentration of compounds [40,156,157]. Multiple dyes can be used to create “virtual arrays” in which the x-y position of a given droplet on the array is determined by measuring the concentrations of two differently-colored dyes in the drop [40]. Other labeling strategies that are not as widely used include the use of DNA sequences [158,159], quantum dots [160–164], and suspension array technologies [165].

2.6.2 Interrogating drops

Droplets can be interrogated using serial scanning or parallel scanning. Serial scanning interrogates droplets individually as they flow through a specific location in the microfluidic channel. For ultrahigh-throughput applications, this necessitates very high speed interrogation to keep pace with the kilohertz droplet rates. Parallel detection, on the other hand, can utilize slower measurement strategies, such as CCD imaging, because a large number of droplets can be

interrogated simultaneously, yielding a net high throughput. A variety of optical, chemical, and electrical detection methods have been reported for microfluidic biological assays, but few are appropriate for ultrahigh-throughput applications because of their inability to precisely interrogate the drops on the timescales needed to keep pace with the microfluidic devices. Examples of methods with high potential value that have, as yet, not been shown capable of ultrahigh-throughput interrogation of drops are mass spectrometry [136,166,167] electrochemical detection [168,169], Raman spectroscopy [170], surface enhanced Raman scattering (SERS) [171–174], surface enhanced resonance Raman scattering (SERRS) [175], and fluorescence polarization [176].

The most widely used interrogation methods for ultrahigh-throughput applications utilize fluorescence and brightfield microscopy [121,132,149]. Fluorescence enables measurements with high signal-to-noise and spatial resolution, and it can be coupled to a wide variety of existing biochemical assays for which fluorescent readouts already exist. The fluorescence readings can be obtained using high speed, high sensitivity single-point detectors, such as photomultiplier tubes (PMTs) [95,100,107,128,133,135,144,145,148] or avalanche photodoides (APDs) [77,155,178–184]. The sensitivity and versatility of fluorescence has made this approach useful for a variety of ultrahigh-throughput applications, including cell and protein screening [144,177,184], DNA and protein detection [77,133,155,178], quantitative PCR [107] and dose-response screening [148]. A representative schematic of ultrahigh-throughput fluorescence drop interrogation is shown in figure 2.10. Fluorescence has also been used to image arrays of droplets for real-time monitoring of large numbers of drops [126]. Fluorescence resonance energy transfer (FRET), another technique that affords information about molecular-scale conformations, has been used to measure binding kinetics [155,183,185], enzyme kinetics [179], and protein-protein interactions [180] at

kilohertz rates. Fluorescence lifetime imaging (FLIM) has also been demonstrated with microsecond temporal resolution for reconstructing mixing patterns within droplets [181,186]. The main challenge with fluorescence-based detection methods is their dependence on a suitable fluorescent marker that can be attached to the molecule of interest. Such tags are not readily available for all molecules and the properties of small molecules can be significantly altered by the presence of an extrinsic marker. Indeed, the primary challenge when performing reactions in microdroplets is identifying a suitable fluorescent marker.

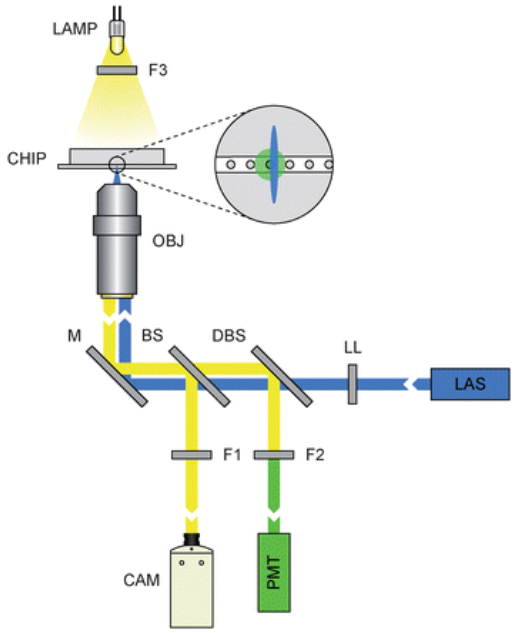

Figure 2.10 Schematic of fluorescence activated droplet detection. Laser light (LAS) is used to excite droplets. The fluorescent emission from each drop is detected with a photomuliplier tube (PMT). Filtered light from a halogen lamp (CAM) allows droplets to be monitored with

2.7 From Tubes to Drops: applications of droplet-based microfluidics in biology

There are numerous examples in biological research in which the major bottleneck is screening massive libraries of reactions. For example, directed evolution of enzymes, which generate enzymes for a host of biotechnology and industrial applications, often require the screening of libraries of enzymes numbering in the billions of mutants [187]. Small molecule

screens for drug discovery often require the analysis of millions of compounds, each of which must be tested in a separate reaction chamber [172]. Such screens are currently conducted using conventional high-throughput methods with pipetting robots in 384 or 1536 well plate formats. With a maximal screening rate of ~1 Hz and a minimal sample volume of 100 nL, screening a million compounds would require weeks of continuous runtime and litres of total reagent, making it impractical for all but the best-funded operations and, even then, for only the most valuable targets [172].

Droplet-based microfluidics affords an exciting and potentially vastly superior methodology for making large library screening accessible by significantly reducing the volume and increasing the throughput of the screening. With this approach, it is possible to screen reactions at a rate of ~1 kilohertz using ~1 pL per reaction, allowing millions of reactions to be screened in minutes using microlitres of total reagents [188]. The barrier to implementing this approach, and realizing its enormous potential for future screening needs, is integrating all of the necessary capabilities into onto one microfluidic workflow. In this section, we describe the first forays into this arena and the use of these techniques to perform novel screens with unprecedented reductions in screening time and cost.

2.7.1 Biological operations in droplet-based microfluidic screening

Most biological protocols involve the repeated transfer of reagents into and out of a reaction vessel, combined with incubation and separation of reactants and products. In theory, these operations can all be performed in microdroplets using microfluidic devices to perform the various needed operations of reagent transfer, incubation, and sorting.

In addition to these common microfluidic operations, many screening applications also require executing a recurring set of biological operations. One such operation often needed in cell-

based studies is to culture cells in drops. Mammalian, algae, and fungal cells have all been cultured in drops for several days [41,42,189]. Another important operation is to transfect cells to induce the expression of a protein of interest or to knock out a gene of interest, which has been achieved in drops using chemical agents [35], electroporation [190], and viral infection [42] at efficiencies comparable to bench top methods. DNA can be extracted by lysing cells in drops [110], and purified from lysate by repeated washing of DNA binding magnetic beads co-encapsulated in the drops [116]. Another valuable operation is to perform entirely *in vitro*, cell-free expression and characterization of enzymes in drops [24]. This is valuable because existing ultrahigh-throughput screening methods utilizing FACS require a cell that can both synthesize the enzyme and be used to characterize its activity. Host cells may not survive screens that involve the use of toxic substrates or products, or require extreme conditions of temperature or pH.

Early work into the kinetics of enzymes demonstrated that microdroplet encapsulation affords the sensitivity needed to measure the activity of single molecules of □-galactosidase [191]. Similarly, digital emulsion PCR, in which individual molecules of DNA are encapsulated in drops and amplified, has now become a standard biological protocol used in many applications, including as an alternative to quantitative PCR and to prepare DNA libraries for next generation sequencing [114,192]. Other amplification strategies have also been demonstrated with DNA and RNA in drops, including RT-PCR [193] and rolling circle amplification for diagnostic and directed evolution applications [134].

One of the challenges of performing complex biological operations in microdroplets is if the protocol requires a large number of steps, it can be challenging to build a fully integrated microfluidic platform to do this. In these instances, a possible solution is to solidify the drops using a gelling agent, such as agarose [110], so that the emulsion can be broken and the microgels re-

dispersed into an aqueous carrier phase. This allows the numerous steps of the protocol to be performed off microfluidic device using standard bench-top methods, while partially maintaining the compartmentalization of the drops. This approach, which has enormous potential for single-cell analysis, has already been demonstrated for performing PCR analysis on large numbers of single cells [72]. However, molecules smaller than the pore size of the gels can exit the gels via diffusion, making this approach only applicable to molecules larger than the pore size or that can be chemically bonded to the gel matrix.

2.7.2 Ultrahigh-throughput studies utilizing co-flowing stream encapsulation

Co-flowing stream encapsulation allows multiple reagents to be combined immediately before being encapsulated in microdroplets. Due to laminar flow conditions in the channels, the reagents in the different streams do not mix until after they are in the drops. This is useful for a variety of applications of ultrahigh-throughput studies. For example, this approach has been used to profile a population of bacteria for sensitivity to different antibiotics. The different antibiotics were first loaded into the channel as long plugs separated by plugs of an inert spacer fluid. The plugs were then merged with reagents needed for the assay and the bacteria and immediately encapsulated in drops using a T-junction drop maker, as shown in figure 2.11. This approach allowed multiple antibiotics at several concentrations to be rapidly screened [194]. The same principle was applied to screen the effects of varying salt, protein concentration, and precipitants to identify optimal parameters for protein crystallization [149,195]. This principle was further applied to generate high-resolution drug dose-response curves [148].

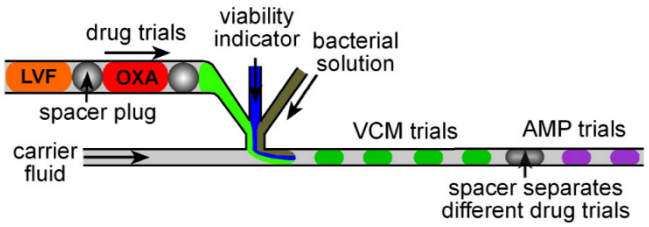

Figure 2.11 Co-flow drop formation used to assay drug susceptibility of bacteria. Figure adapted from [194].

2.7.3 Ultrahigh-throughput screens using combinatorial droplet merger

Co-flowing stream encapsulation is suitable for screening a small number of reagents at different concentrations and, combined with a reagent-plug technique like the one described above, can also be used to screen moderately large sets of compounds, numbering in the tens-to-hundreds. However, for larger numbers of compounds, it becomes impractical because it requires very long tubes of plugs or large numbers of inlets on the microfluidic device. In these cases, a superior approach is combinatorial droplet merger. The basic strategy of combinatorial droplet merger is to use an automated method to create a "droplet library" of the different compounds to be screened, as shown in figure 2.12 (a); the droplet library consist of an emulsion of monodisperse droplets in which each droplet contains a different reagent or concentration of reagent. The droplets library can then be merged with other droplets using electrocoalescence, as illustrated in figure 2.12 (b). This can be useful for protein crystallography, where screening for optimal crystallization conditions is a bottleneck [196,197].

A key consideration when using combinatorial droplet merger to screen a library of compounds is indexing each drop to keep track of which compound is being tested. One way to do this is to label the droplets with fluorescent dyes, as described in the previous section of droplet labeling, in which fluorescent dyes of different color are loaded into the droplets at different concentrations. Each colored dye can be used to represent a digit in a multi-digit number, where

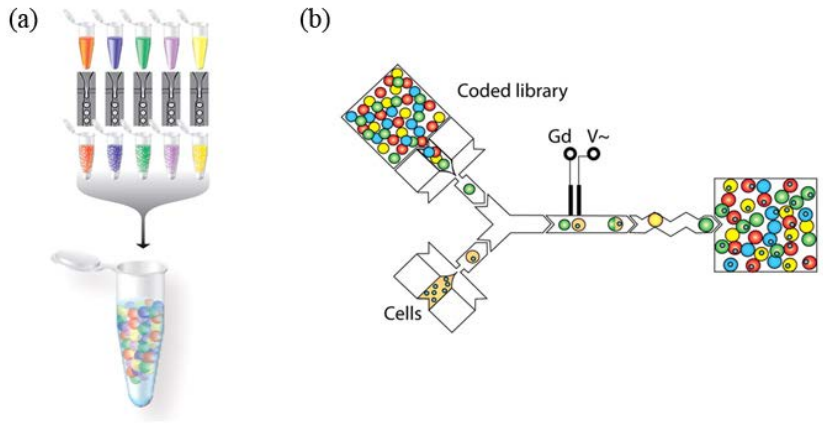

Figure 2.12 Creation and use of a drop library for combinatorial screening. (a) Multiple reagents are emulsified and pooled, forming a droplet library. (b) The library of reagents are randomly paired and merged with the assay drops. Adapted with permission from [40].

the concentration of the dye sets the value of the digit. An approach like this was used to screen a drug library of mitomycin C at different concentrations to characterize cytotoxicity [40]. However, optical labeling of drops with fluorescent dyes is limited by the finite spectrum of visible light and the precision with which dye concentrations can be measured in the drops.

Another important application of combinatorial droplet merger is to perform highly multiplexed targeted PCR amplification of genomes. The genomes of organisms are often massive, containing millions or billions of base pairs of information, but the information that is the most relevant for study may be localized in specific regions. The challenge is to target these regions for sequencing and discard the vast “background” of genomic DNA in the other regions. One way to do this is to use multiplexed PCR, in which primer sets are designed that target each of the desired regions for amplification. This allows, in principle, only these regions to be copied, discarding the rest of the genomic DNA. However, in practice it can be extremely challenging to optimize multiplexed amplification of so many regions, limiting the total number of regions that can be simultaneously interrogated. In these cases emulsion PCR with combinatorial droplet merger affords an excellent solution [92] where each of the PCR amplifications for the different primer

sets are performed in a separate microdroplet. Because the primer sets are isolated from one another, they do not interact or compete for binding to the genomic DNA. This yields much cleaner PCR products and allows more uniform amplification of all regions. A technology based on this approach is in fact already being commercialized by RainDance Technologies as a pre-sequencing front-end to enrich for genomic regions of interest.

2.7.4 Ultrahigh-throughput applications utilizing droplet sorting

Droplet sorting is essential in applications where specific droplets must be recovered from a large population of other drops. To date, the majority of microfluidic studies utilizing droplet sorting have been focused on performing protein engineering through directed evolution, a technique in which proteins are evolved to enhance a desired property by processing them through successive rounds of mutagenesis and screening. Droplet-based methods of directed evolution are used because the drops can encapsulate products that are secreted from cells as well as provide encapsulation for cell-free systems. This is particularly important for evolving enzymes, which typically catalyze reactions in the liquid phase and generally release products into solution. Methods utilizing FACS cannot easily accomplish this because FACS requires that that the product of the enzyme be localized within the cell. While certain enzymes can be screened inside cells, for many enzymes this is not possible.

Droplet-based microfluidic screening thus holds enormous potential as a general platform for evolving enzymes that, presently, can only be evolved using low throughput methods, like screening on a well plate array. At a screening rate of 2 kHz, more than 10^8 droplets can be sorted per day, matching the library size that can be expressed using yeast. Compared to 384 well plates, droplet screening achieves 3-4 orders of magnitude greater throughput and ~6 orders of magnitude reductions in reagent costs [145].

The principle strategy in directed evolution with microdroplets is to isolate each variant of the protein in a different droplet, screen all variants, and recover the best by sorting. The precise mechanism by which the protein is synthesized from the gene varies and can be accomplished using bacteria, yeast, or even cell-free expression methods. Directed evolution with droplets has already been used to improve the catalytic rate of horseradish peroxidase [145], to screen a retrovirus display library for active tissue plasminogen activator [177], and with an *in vitro* transcription-translation system to select for highly active □-galactosidase from a mixed population [96].

Beyond directed evolution, droplet sorting has also been used as a post-enrichment screen for aptamer libraries, to replace the costly sequencing and re-synthesizing steps of the SELEX workflow for aptamer discovery [198]. The secretion of IL-10 by immune-suppressing cell populations in the bloodstream was detected using antibody functionalized beads co-encapsulated with the cells in drops. Sorting based on IL-10 secretion can be used to enrich for rare cells previously isolated [199].

2.7.5 Digital assays on single molecules or cells

For a fixed number of molecules, reducing the volume of the reaction vessel effectively increases the concentration of the molecules. By shrinking the reactor to the size of a microdroplet, the effective concentration of a single molecule per drop can be comparable to the concentrations used in bench top assays. This concept was employed in the early 1960s to measure the activity of individual molecules of □-galactosidase encapsulated in drops, as shown in figure 2.13 (a) [191].

Microdroplet encapsulation is thus one way to significantly increase the sensitivity of an assay. Another major advantage is that it can isolate molecules in a complex mixture so that they can be interrogated individually. For example, single molecule encapsulation has been combined

with multiplexed PCR to identify and quantify multiple DNA targets in an originally mixed population [200]. Microdroplet “digital” quantification of encapsulated molecules affords an alternative strategy to quantitative PCR that provides absolute molecule counts without the need for normalization or calibration (figure 2.13 (b)) [201]. Digital PCR can achieve higher sensitivity and dynamic range than standard quantitative PCR methods [202,203]. Digital PCR has been used to detect aneuploidy with precision that exceeds what is possible with other methods and has been successfully implemented into a commercial laboratory instrument for DNA quantification [134,203,204]. Using a similar approach to digital detection of nucleic acids, rare cells can also be detected “digitally” with microdroplet encapsulation [72]. For further information on digital PCR in droplets, we refer the interested reader to this recent comprehensive review [205].

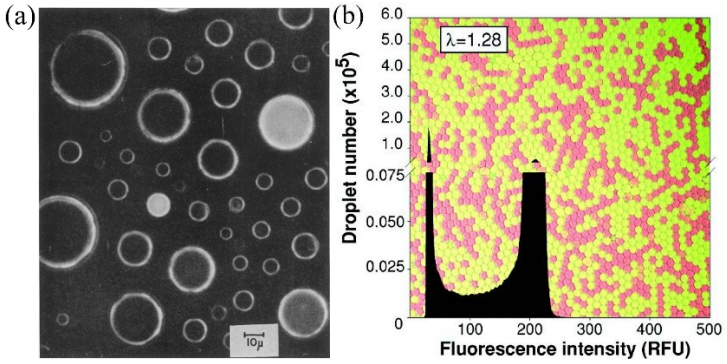

Figure 2.13 Single molecule analysis in drops. (a) The activity of single molecules of β-galactosidase can be measured using microdroplets, as illustrated by the fluorescently bright drops (Reproduced with permission from [191]. Copyright 2005 National Academy of Sciences, U.S.A.). (b) Amplification of single DNA molecules in microdroplets using a DNA intercalating green fluorescent dye and dextran-Texas red as a reference. Adapted with

2.8 Conclusions

The field of droplet-based microfluidics is exploding and has yielded numerous technologies that are enabling for applications throughout biology. The next critical steps in the development of this field are for microfluidic research labs to continue to develop robust and widely applicable tools and to demonstrate the power of these tools through proof-of-principle

experiments that biologists will recognize. In addition, collaborations with industry will be crucial, because like all high technologies, droplet-based microfluidics will only be adopted widely when systems are built that are easy to use, cost effective, and robust in operation, even with operators that are not familiar with the underlying microfluidic technology. This is a tall order but it has been achieved before, as evidenced by the numerous high technologies commonly use in biological research labs, like next generation sequencing platforms, mass spectrometers, and FACS machines. Indeed, FACS, in many ways, is the predecessor of droplet-based microfluidics and affords an excellent example of what we, as a field, should strive for in the translation of our technology: Like droplet-based systems, FACS utilizes microfluidic channels, high-speed optical detectors, and high speed computational analysis for data capture and logic-based sorting. We envision a time in the near future when FACS machines will be upgraded with droplet-based systems to yield a much more general screening platform – one that is not limited to the screening of cells alone, but can conduct, with full automation, and screen any variety of liquid-phase reactions, involving cells, biomolecules, and other reagents. In addition, while in this Review we have focused on the biological applications of this technology, the same capabilities of high efficiency, ultrahigh throughput, and precision of measurement will make it valuable for screens in other fields too, particularly in the chemical sciences.

2.9 Acknowledgements

This work was supported by startup funds from the University of California San Francisco Department of Bioengineering and Therapeutic Sciences, a Research Award from the California Institute for Quantitative Biosciences (QB3), the Bridging the Gap Award from the Rogers Family Foundation, and the UCSF/Sandler Foundation Program for Breakthrough Biomedical Research.

References

1. Wang W, Walker J R, Wang X, Tremblay M S, Lee J W, Wu X and Schultz P G 2009 Proc Natl Acad Sci U S A 106 1427–32
2. Burbaum J J 1998 Drug Discovery Today 3 313–22
3. Major J 1998 J Biomol Screen 3 13–7
4. Aharoni A, Griffiths A D and Tawfik D S 2005 Curr Opin Chem Biol 9 210–6
5. Dalby P A 2003 Curr Opon Struct Biol 13 500–5
6. Wittrup K D 2001 Curr Opin Biotechnol 12 395–9
7. Liebeton K, Zonta A, Schimossek K, Nardini M, Lang D, Dijkstra B W, Reetz M T and Jaeger K-E 2000 Chemistry & Biology 7 709–18
8. Daugherty P S, Iverson B L and Georgiou G 2000 J Immunol Methods 243 211–27
9. Aebersold R, Mann M 2003 Nature 422 198–207
10. Boder E T and Wittrup K D 1997 Nat Biotechnol 15 553–7
11. Fernandez-Gacio A, Uguen M and Fastrez J 2003 Trends Biotechnol 21 408–14
12. Forrer P, Jung S and Plückthun A 1999 Curr Opon Struct Biol 9 514–20
13. Amstutz P, Forrer P, Zahnd C and Plückthun A 2001 Curr Opin Biotechnol 12 400–5
14. Glieder A, Farinas E T and Arnold F H 2002 Nat Biotechnol 20 1135–9
15. Jaeger K-E and Eggert T 2002 Curr Opin Biotechnol 13 390–7
16. Turner N J 2003 Trends Biotechnol 21 474–8
17. Williams G J, Zhang C and Thorson J S 2007 Nat Chem Biol 3 657–62
18. Otten L G, Schaffer M L, Villiers B R M, Stachelhaus T and Hollfelder F 2007 Biotechnol J 2 232–40
19. Polizzi K M, Parikh M, Spencer C U, Matsumura I, Lee J H, Realff M J and Bommarius A S 2006 Biotechnol Progr 22 961–7
20. Tee K L and Schwaneberg U 2006 Angew. Chem. Int. Ed. 45 5380–3
21. Teh S-Y, Lin R, Hung L-H and Lee A P 2008 Lab Chip 8 198–220
22. Mukhopadhyay R 2007 Anal. Chem. 79 3248–53
23. Zeng Y, Novak R, Shuga J, Smith M T and Mathies R A 2010 Anal. Chem. 82 3183–90

24. Wu N, Zhu Y, Brown S, Oakeshott J, Peat T S, Surjadi R, Easton C, Leech P W and Sexton B A 2009 Lab Chip 9 3391– 8

25. Lorenz H D 1997 J Micromech Microeng 7 121–4

26. McDonald J C, Duffy D C, Anderson J R, Chiu D T, Wu H, Schueller O J A and Whitesides G M 2000 Electrophoresis 21 27–40

27. Rotem A, Abate A R, Utada A S, Steijn V V and Weitz D A 2012 Lab Chip 12 4263–8

28. Haubert K, Drier T and Beebe D 2006 Lab Chip 6 1548–9

29. Fritz J L and Owen M J 1995 J Adhes 54 33–45

30. Dangla R, Gallaire F and Baroud C N 2010 Lab Chip 10 2972

31. He M, Edgar J S, Jeffries G D M, Lorenz R M, Shelby J P and Chiu D T 2005 Anal. Chem. 77 1539–44

32. Lee J N, Park C and Whitesides G M 2003 Anal. Chem. 75 6544–54

33. Courtois F, Olguin L F, Whyte G, Bratton D, Huck W T S, Abell C and Hollfelder F 2008 ChemBioChem 9 439–46

34. Kumaresan P, Yang C J, Cronier S A, Blazej R G and Mathies R A 2008 Anal. Chem. 80 3522–9

35. Chen F, Zhan Y, Geng T, Lian H, Xu P and Lu C 2011 Anal. Chem. 83 8816–20

36. Studer A 1997 Science 275 823–6

37. Curran D P 1998 Angew. Chem. Int. Ed 37 1174–96

38. Lowe K C, Davey M R and Power J B 1998 Trends Biotechnol 16 272–7

39. Schmitz C H J, Rowat A C, Köster S and Weitz D A 2009 Lab Chip 9 44

40. Brouzes E, Medkova M, Savenelli N, Marran D, Twardowski M, Hutchison J B, Rothberg J M, Link D R, Perrimon N and Samuels M L 2009 Proc Natl Acad Sci U S A 106 14195–200

41. Pan J, Stephenson A L, Kazamia E, Huck W T, Dennis J S, Smith A G and Abell C 2011 Integr Biol (Camb) 3 1043–51

42. Clausell-Tormos J, et al 2008 Chem Biol 15 427–37

43. Sadtler V M, Krafft M P and Riess J G 1996 Angew. Chem. Int. Ed in English 35 1976–8

44. Guo M T, Rotem A, Heyman J A and Weitz D A 2012 Lab Chip 12 2146

45. Bai Y, He X, Liu D, Patil S N, Bratton D, Huebner A, Hollfelder F, Abell C and Huck W T S 2010 Lab Chip 10 1281

46. Baret J-C 2012 Lab Chip 12 422

47. Holtze C, et al 2008 Lab Chip 8 1632

48. Roach L S, Song H and Ismagilov R F 2005 Anal. Chem 77 785–96

49. Sadtler V M, Jeanneaux F, Pierre Krafft M, Rábai J and Riess J G 1998 New J Chem 22 609–13

50. Liau A, Karnik R, Majumdar A and Cate J H D 2005 Anal. Chem 77 7618–25

51. Courtois F, Olguin L F, Whyte G, Theberge A B, Huck W T S, Hollfelder F and Abell C 2009 Anal. Chem 81 3008–16

52. Kaltenbach M, Devenish S R A and Hollfelder F 2012 Lab Chip 12 4185

53. Paegel B M and Joyce G F 2010 Chem Biol 17 717–24

54. Christopher G F and Anna S L 2007 J Phys D 40 R319–R336

55. Vladisavljević G, Kobayashi I and Nakajima M 2012 Microfluid Nanofluid 13 151–78

56. Seemann R, Brinkmann M, Pfohl T and Herminghaus S 2012 Rep Prog Phys 75 016601

57. Utada A S, Fernandez-Nieves A, Stone H A and Weitz D A 2007 Phys. Rev. Lett. 99 094502

58. Utada A S, Fernandez-Nieves A, Gordillo J M and Weitz D A 2008 Phys. Rev. Lett. 100 014502

59. Cramer C, Fischer P and Windhab E J 2004 Chem Eng Sci 59 3045–58

60. Guillot P, Colin A and Ajdari A 2008 Phys. Rev. E 78 016307

61. Thorsen T, Roberts R W, Arnold F H and Quake S R 2001 Phys. Rev. Lett. 86 4163–6

62. Garstecki P, Fuerstman M J, Stone H A and Whitesides G M 2006 Lab Chip 6 437

63. Anna S L, Bontoux N and Stone H A 2003 Appl. Phys. Lett. 82 364

64. Abate A R, Poitzsch A, Hwang Y, Lee J, Czerwinska J and Weitz D A 2009 Phys. Rev. E 80 026310

65. De Menech M, Garstecki P, Jousse F and Stone H A 2008 J Fluid Mech 595

66. Nie Z, Seo M, Xu S, Lewis P, Mok M, Kumacheva E, Whitesides G, Garstecki P and Stone H 2008 Microfluid Nanofluid 5 585–94

67. Link D R, Anna S L, Weitz D A and Stone H A 2004 Phys. Rev. Lett. 92 054503

68. Abate A R and Weitz D A 2011 Lab Chip 11 1911

69. Abate A R and Weitz D A 2011 Lab Chip 11 1713

70. Nisisako T, Torii T, Takahashi T and Takizawa Y 2006 Adv Mater 18 1152–6

71. Nisisako T and Torii T 2008 Lab Chip 8 287

72. Zeng Y, Novak R, Shuga J, Smith M T and Mathies R A 2010 Anal. Chem. 82 3183–90

73. Abate A R, Romanowsky M B, Agresti J J and Weitz D A 2009 Appl. Phys. Lett. 94 023503

74. Priest C, Herminghaus S and Seemann R 2006 Appl. Phys. Lett. 88 024106 –024106–3

75. Chokkalingam V, Herminghaus S and Seemann R 2008 Appl. Phys. Lett. 93 254101

76. Köster S, et al 2008 Lab Chip 8 1110

77. Huebner A, Srisa-Art M, Holt D, Abell C, Hollfelder F, deMello A J and Edel J B 2007 ChemComm1218

78. Kemna E W M, Schoeman R M, Wolbers F, Vermes I, Weitz D A and Berg A van den 2012 Lab Chip 12 2881–7

79. Abate A R, Chen C-H, Agresti J J and Weitz D A 2009 Lab Chip 9 2628

80. Chabert M and Viovy J-L 2008 PNAS 105 3191–6

81. Um E, Lee S-G and Park J-K 2010 Appl. Phys. Lett. 97 153703

82. Tawfik D S and Griffiths A D 1998 Nat Biotechnol 16 652–6

83. Dressman D, Yan H, Traverso G, Kinzler K W and Vogelstein B 2003 PNAS 100 8817–22

84. Nakano M, Komatsu J, Matsuura S, Takashima K, Katsura S and Mizuno A 2003 J Biotechnol 102 117–24

85. Bremond N, Thiam A R and Bibette J 2008 Phys. Rev. Lett. 100 024501

86. Mazutis L, Baret J-C and Griffiths A D 2009 Lab Chip 9 2665

87. Mazutis L and Griffiths A D 2012 Lab Chip 12 1800

88. Fidalgo L M, Abell C and Huck W T S 2007 Lab Chip 7 984

89. Chabert M, Dorfman K D and Viovy J-L 2005 Electrophoresis 26 3706–15

90. Baroud C N, Robert de Saint Vincent M and Delville J-P 2007 Lab Chip 7 1029

91. Link D R, Grasland-Mongrain E, Duri A, Sarrazin F, Cheng Z, Cristobal G, Marquez M and Weitz D A 2006 Angew. Chem. Int. Ed 45 2556–60

92. Tewhey R, et al 2009 Nat Biotechnol 27 1025–31

93. Thiam A R, Bremond N and Bibette J 2009 Phys. Rev. Lett. 102 188304

94. Ahn K, Agresti J, Chong H, Marquez M and Weitz D A 2006 Appl. Phys. Lett. 88 264105

95. Mary P, Chen A, Chen I, Abate A R and Weitz D A 2011 Lab Chip 11 2066

96. Fallah-Araghi A, Baret J-C, Ryckelynck M and Griffiths A D 2012 Lab Chip 12 882

97. Tan W-H and Takeuchi S 2006 Lab Chip 6 757

98. Zagnoni M and Cooper J M 2009 Lab Chip 9 2652

99. Zagnoni M, Le Lain G and Cooper J M 2010 Langmuir 26 14443–9

100. Abate A R, Hung T, Mary P, Agresti J J and Weitz D A 2010 PNAS 107 19163–6

101. Handique K and Burns M A 2001 J Micromech Microeng 11 548–54

102. Tice J D, Song H, Lyon A D and Ismagilov R F 2003 Langmuir 19 9127–33

103. Bringer M R, Gerdts C J, Song H, Tice J D and Ismagilov R F 2004 Phil. Trans. R. Soc. Lond. A 362 1087–104

104. Jiang L, Zeng Y, Zhou H, Qu J Y and Yao S 2012 Biomicrofluidics 6 012810–012810–12

105. Song H, Tice J D and Ismagilov R F 2003 Angew Chem Int Ed 115 792–6

106. Liau A, Karnik R, Majumdar A and Cate J H D 2005 Anal. Chem. 77 7618–25

107. Kiss M M, Ortoleva-Donnelly L, Beer N R, Warner J, Bailey C G, Colston B W, Rothberg J M, Link D R and Leamon J H 2008 Anal. Chem. 80 8975–81

108. Theberge A B, Mayot E, El Harrak A, Kleinschmidt F, Huck W T S and Griffiths A D 2012 Lab Chip 12 1320

109. Leng X, Zhang W, Wang C, Cui L and Yang C J 2010 Lab Chip 10 2841

110. Novak R, Zeng Y, Shuga J, Venugopalan G, Fletcher D A, Smith M T and Mathies R A 2011 Angew Chem Int Ed 123 410–5

111. Sepp A, Tawfik D S and Griffiths A D 2002 FEBS Letters 532 455–8

112. Levy M, Griswold K E and Ellington A D 2005 RNA 11 1555–62

113. Diehl F, Li M, He Y, Kinzler K W, Vogelstein B and Dressman D 2006 Nat Methods 3 551–9

114. Margulies M, et al 2005 Nature 437 376–80

115. Fidalgo L M, Whyte G, Bratton D, Kaminski C F, Abell C and Huck W T S 2008 Angew. Chem. Int. Ed 47 2042–5

116. Pan X, Zeng S, Zhang Q, Lin B and Qin J 2011 Electrophoresis 32 3399–405

117. Adamson D N, Mustafi D, Zhang J X J, Zheng B and Ismagilov R F 2006 Lab Chip 6 1178

118. Liu W, Kim H J, Lucchetta E M, Du W and Ismagilov R F 2009 Lab Chip 9 2153

119. Clausell-Tormos J, Griffiths A D and Merten C A 2010 Lab Chip 10 1302

120. Sgro A E, Allen P B and Chiu D T 2007 Anal. Chem. 79 4845–51

121. Stan C A, Schneider G F, Shevkoplyas S S, Hashimoto M, Ibanescu M, Wiley B J and Whitesides G M 2009 Lab Chip 9 2293

122. Song H and Ismagilov R F 2003 J Am Chem Soc 125 14613–9

123. Chanasakulniyom M, Martino C, Paterson D, Horsfall L, Rosser S and Cooper J M 2012 The Analyst 137 2939

124. Frenz L, Blank K, Brouzes E and Griffiths A D 2009 Lab Chip 9 1344

125. Hofmann T W, Hänselmann S, Janiesch J-W, Rademacher A and Böhm C H J 2012 Lab Chip 12 916

126. Edd J F, Humphry K J, Irimia D, Weitz D A and Toner M 2009 Lab Chip 9 1859

127. Hatch A C, Fisher J S, Tovar A R, Hsieh A T, Lin R, Pentoney S L, Yang D L and Lee A P 2011 Lab Chip 11 3838

128. Huebner A, Bratton D, Whyte G, Yang M, deMello A J, Abell C and Hollfelder F 2009 Lab Chip 9 692

129. Laval P, Lisai N, Salmon J-B and Joanicot M 2007 Lab Chip 7 829

130. Um E, Rha E, Choi S-L, Lee S-G and Park J-K 2012 Lab Chip 12 1594

131. Boukellal H, Selimović Š, Jia Y, Cristobal G and Fraden S 2009 Lab Chip 9 331

132. Lau B T C, Baitz C A, Dong X P and Hansen C L 2007 J. Am. Chem. Soc. 129 454–5

133. Joensson H N, Samuels M L, Brouzes E R, Medkova M, Uhlén M, Link D R and Andersson-Svahn H 2009 Angew Chem Int Ed 121 2556–9

134. Pekin D, et al 2011 Lab Chip 11 2156–66

135. Mazutis L, Baret J-C, Treacy P, Skhiri Y, Araghi A F, Ryckelynck M, Taly V and Griffiths A D 2009 Lab Chip 9 2902

136. Hatakeyama T, Chen D L and Ismagilov R F 2006 J. Am. Chem. Soc.128 2518–9

137. Zheng B and Ismagilov R F 2005 Angew. Chem. Int. Ed 44 2520–3

138. Mazutis L and Griffiths A D 2009 Appl. Phys. Lett. 95 204103 –204103–3

139. Zhang K, Liang Q, Ma S, Mu X, Hu P, Wang Y and Luo G 2009 Lab Chip 9 2992

140. Al-Hetlani E, Hatt O J, Vojtíšek M, Tarn M D, and Pamme N, 2010 in 14th International Conference on Miniaturized Systems for Chemistry and Life Sciences, Groningen, The Netherlands, pp. 167–75

141. Abate A R, Agresti J J and Weitz D A 2010 Appl. Phys. Lett. 96 203509

142. Franke T, Abate A R, Weitz D A and Wixforth A 2009 Lab Chip 9 2625

143. Ahn K, Kerbage C, Hunt T P, Westervelt R M, Link D R and Weitz D A 2006 Appl. Phys. Lett. 88 024104

144. Baret J-C, et al 2009 Lab Chip 9 1850

145. Agresti J J, Antipov E, Abate A R, Ahn K, Rowat A C, Baret J-C, Marquez M, Klibanov A M, Griffiths A D and Weitz D A 2010 PNAS 107 4004–9

146. Bernath K, Hai M, Mastrobattista E, Griffiths A D, Magdassi S and Tawfik D S 2004 Anal. Biochem. 325 151–7

147. Mastrobattista E, Taly V, Chanudet E, Treacy P, Kelly B T and Griffiths A D 2005 Chemistry & Biology 12 1291–300

148. Miller O J, El Harrak A, Mangeat T, Baret J C, Frenz L, El Debs B, Mayot E, Samuels M L, Rooney E K, Dieu P, Galvan M, Link D R and Griffiths A D 2011 Proc Natl Acad Sci U S A 109 378–83

149. Zheng B, Roach L S and Ismagilov R F 2003 J. Am. Chem. Soc.125 11170–1

150. Kintses B, van Vliet L D, Devenish S R A, and Hollfelder F 2010 Curr Opin Chem Biol 14 548-55

151. Pompano R R, Liu W, Du W and Ismagilov R F 2011 Annu Rev Anal Chem 4 59–81

152. Chen D L and Ismagilov R F 2006 Curr Opin Chem Biol 10 226–31

153. Schonbrun E, Abate A R, Steinvurzel P E, Weitz D A and Crozier K B 2010 Lab Chip 10 852

154. He M, Edgar J S, Jeffries G D M, Lorenz R M, Shelby J P and Chiu D T 2005 Anal. Chem. 77 1539–44

155. Srisa-Art M, deMello A J and Edel J B 2007 Anal. Chem.79 6682–9

156. Zheng B, Tice J D and Ismagilov R F 2004 Anal. Chem.76 4977–82

157. Baret J-C, Beck Y, Billas-Massobrio I, Moras D and Griffiths A D 2010 Chem Biol 17 528–36

158. Melkko S, Zhang Y, Dumelin C E, Scheuermann J and Neri D 2007 Angew. Chem. Int. Ed 46 4671–4

159. Portney N G, Wu Y, Quezada L K, Lonardi S and Ozkan M 2008 Langmuir 24 1613–6

160. Lorenceau E, Utada A S, Link D R, Cristobal G, Joanicot M and Weitz D A 2005 Langmuir 21 9183–6

161. Shah R K, Kim J-W, Agresti J J, Weitz D A and Chu L-Y 2008 Soft Matter 4 2303

162. Ji X-H, Zhang N-G, Cheng W, Guo F, Liu W, Guo S-S, He Z-K and Zhao X-Z 2011 J Mater Chem 21 13380

163. Theilacker N, Roller E E, Barbee K D, Franzreb M and Huang X 2011 J. R. Soc. Interface 8 1104–13

164. Zhang P, He Y, Ruan Z, Chen F F and Yang J 2012 J Colloid Interface Sci 385 8–14

165. Miller M B and Tang Y-W 2009 Clin. Microbiol. Rev. 22 611–33

166. Niu X Z, Zhang B, Marszalek R T, Ces O, Edel J B, Klug D R and deMello A J 2009 ChemComm 6159-61

167. Ji J, Nie L, Qiao L, Li Y, Guo L, Liu B, Yang P and Girault H H 2012 Lab Chip 12 2625

168. Liu S, Gu Y, Le Roux R B, Matthews S M, Bratton D, Yunus K, Fisher A C and Huck W T S 2008 Lab Chip 8 1937

169. Luo C, Yang X, Fu Q, Sun M, Ouyang Q, Chen Y and Ji H 2006 Electrophoresis 27 1977–83

170. Cristobal G, Arbouet L, Sarrazin F, Talaga D, Bruneel J-L, Joanicot M and Servant L 2006 Lab Chip 6 1140

171. Strehle K R, Cialla D, Rösch P, Henkel T, Köhler M and Popp J 2007 Anal. Chem.79 1542–7

172. Wang G, Lim C, Chen L, Chon H, Choo J, Hong J and deMello A J 2009 Anal Bioanal Chem 394 1827–32

173. Ackermann K R, Henkel T and Popp J 2007 ChemPhysChem 8 2665–70

174. März A, Ackermann K R, Malsch D, Bocklitz T, Henkel T and Popp J 2009 J Biophotonics 2 232–42

175. Cecchini M P, Hong J, Lim C, Choo J, Albrecht T, deMello A J and Edel J B 2011 Anal. Chem. 83 3076–81

176. Choi J-W, Kang D-K, Park H, deMello A J and Chang S-I 2012 Anal. Chem. 84 3849–54

177. Granieri L, Baret J C, Griffiths A D and Merten C A 2010 Chem Biol 17 229–35

178. Nguyen N-T, Lassemono S and Chollet F A 2006 Sens Actuators, B 117 431–6

179. Srisa-Art M, Dyson E C, deMello A J and Edel J B 2008 Anal. Chem. 80 7063–7

180. Srisa-Art M, Kang D-K, Hong J, Park H, Leatherbarrow R J, Edel J B, Chang S-I and deMello A J 2009 ChemBioChem 10 1605–11

181. Srisa-Art M, deMello A and Edel J 2008 Phys.Rev. Lett. 101 014502

182. Srisa-Art M, deMello A J and Edel J B 2009 ChemComm6548

183. Niu X, Gielen F, Edel J B and deMello A J 2011 Nat Chem 3 437–42

184. Srisa-Art M, Bonzani I C, Williams A, Stevens M M, deMello A J and Edel J B 2009 Analyst 134 2239

185. Wang J, Jiang P, Han Z, Qiu L, Wang C, Zheng B and Xia J 2012 Langmuir 28 7962–6

186. Casadevall i Solvas X, Srisa-Art M, deMello A J and Edel J B 2010 Anal. Chem. 82 3950–6

187. Cherry J R and Fidantsef A L 2003 Curr Opin Biotechnol 14 438–43

188. Dove A 1999 Nat Biotechnol 17 859–63

189. Gong Z, Zhao H, Zhang T, Nie F, Pathak P, Cui K, Wang Z, Wong S and Que L 2011 Biomed Microdevices 13 215–9

190. Zhan Y, Wang J, Bao N and Lu C 2009 Anal. Chem. 81 2027–31

191. Rotman B 1961 Proc. Natl. Acad. Sci. USA 47 1981–91

192. Hindson B J, et al 2011 Anal. Chem. 83 8604–10

193. Zhang H, Jenkins G, Zou Y, Zhu Z and Yang C J 2012 Anal. Chem. 84 3599–606

194. Boedicker J Q, Li L, Kline T R and Ismagilov R F 2008 Lab Chip 8 1265–72

195. Chao W C, Collins J, Wang S W, Li G P, Bachman M and Lee A P 2004 Conf Proc IEEE Eng Med Biol Soc 4 2623–6

196. Maeki M, Yoshizuka S, Yamaguchi H, Kawamoto M, Yamashita K, Nakamura H, Miyazaki M and Maeda H 2012 Anal Sci 28 65

197. Chayen N E and Saridakis E 2008 Nat Methods 5 147–53

198. Zhang W Y, Zhang W, Liu Z, Li C, Zhu Z and Yang C J 2011 Anal. Chem. 84 350–5

199. Konry T, Dominguez-Villar M, Baecher-Allan C, Hafler D A and Yarmush M L 2011 Biosens Bioelectron 26 2707–10

200. Zhong Q, Bhattacharya S, Kotsopoulos S, Olson J, Taly V, Griffiths A D, Link D R and Larson J W 2011 Lab Chip 11 2167–74

201. Mazutis L, et al 2009 Anal. Chem. 81 4813–21

202. Whale A S, Huggett J F, Cowen S, Speirs V, Shaw J, Ellison S, Foy C A and Scott D J 2012 Nucleic Acids Res 40 e82

203. Heyries K A, Tropini C, Vaninsberghe M, Doolin C, Petriv O I, Singhal A, Leung K, Hughesman C B and Hansen C L 2011 Nat Methods 8 649–51

204. Hussein S M, et al 2011 Nature 471 58–62

205. Zhu Z, Jenkins G, Zhang W, Zhang M, Guan Z and Yang C J 2012 Anal. Bioanal. Chem. 403 2127–43

Chapter 3: Coaxial flow focusing in PDMS microfluidic devices

The following section is reprinted from "Coaxial flow focusing in PDMS microfluidic devices" by Tuan M. Tran, Sean Cater, and Adam R. Abate. The article was published as a research article in Biomicrofluidics on January 8 2014. Tuan Tran and Adam R. Abate wrote the manuscript. Sean Cater performed the experiments.

3.1 Abstract

We have developed a coaxial flow focusing geometry that can be fabricated using soft lithography in poly(dimethylsiloxane) (PDMS). Like coaxial flow focusing in glass capillary microfluidics, our geometry can form double emulsions in channels with uniform wettability and of a size much smaller than the channel dimensions. However, In contrast to glass capillary coaxial flow focusing, our geometry can be fabricated using lithographic techniques, allowing it to be integrated as the drop making unit in parallel drop maker arrays. Our geometry enables scalable formation of emulsions down 7 μm in diameter, in large channels that are robust against fouling and clogging.

3.2 Introduction

Double emulsions consist of droplets that contain smaller droplets in their bulk, and have many applications for research and industry. For example, in research, double emulsions serve as templates for polymer capsules, core-shell particles, and non-spherical particles.[1] In industry, double emulsions are being developed as delivery vehicles for active compounds, like pesticides, cosmetic agents, and drugs. By encapsulating active compounds in double emulsions, they can be dispersed into environments in which they are poorly soluble, protected from degradation and controllably released to achieve uniform dosing.[2–7]

Controlling the performance characteristics of double emulsions requires precise control of their structural properties. The best method for forming double emulsions with controlled structure is coaxial flow focusing, a technique pioneered in glass capillary microfluidics.[8] In this technique, the inner and middle phases of the double emulsion are sheared into monodisperse droplets by focusing them though a small orifice. By adjusting flow conditions and orifice dimensions, it is possible to form double emulsions over a broad range of dimensions and morphologies.[9] Coaxial flow focusing also has benefits for industrial applications: Because the inner and middle phases are centered in the orifice and protected from the channel walls by the encapsulating sheath fluid, fouling by dissolved compounds is minimized, allowing the device to operate for long periods without interruption. In addition, coaxial flow focusing can generate droplets much smaller than the focusing orifice. Without coaxial flow focusing, forming drops <10 μm in diameter requires channels smaller than this size.[10,11] Thus, coaxial flow focusing is valuable for forming emulsions < 10 μm in diameter, because the large channels it uses are easier to fabricate and more robust against clogging.[12]

The primary disadvantage of coaxial flow focusing is that it requires the fabrication of microfluidic devices with channels that constrict in the horizontal and vertical planes. While methods to make multilayer droplet generation devices in PDMS have been developed for both emulsification and laminar flow mixing, such devices do not employ coaxial flow focusing to generate emulsions smaller than the nozzle size.[10,13–15] To date, coaxial flow focusing geometries have only been fabricated with glass capillaries or multiple layers of SU-8.[16,17] While these devices are capable of forming double emulsions with controlled properties, they are difficult to replicate. Glass capillary devices require manual tip shaping and alignment of each device, while multilayer SU-8 devices require long cycles of spin coating, baking, exposure, and

alignment.[17,18] In addition, both methods yield one device per fabrication, whereas with soft lithography a single master can be used to replicate hundreds of exact copies, making the approach scalable. To enable the generation of double emulsions of the desired size and in a format that is scalable, a new approach is needed that combines the optimal flow characterisitics of coaxial flow focusing with the scalability of devices fabricated using soft lithography.

In this paper, we introduce coaxial flow focusing in lithographically-fabricated PDMS devices. Just as in glass capillary microfluidics, our geometry focuses the fluids through a constriction that narrows in the horizontal and vertical planes. As such, our device shares many of the advantages of capillary coaxial flow focusing: Because the walls are protected by the sheath flow of the carrier phase, channel wettability is unimportant with respect to the kinds of emulsions that can be formed, allowing us to form o/w single emulsions and w/o/w double emulsions in channels that are uniformly hydrophobic. The sheath flow also minimizes contact of the phases with the channel walls, reducing fouling. Moreover, just like coaxial flow focusing in glass capillaries, our geometry forms double emulsions smaller than the orifice, allowing droplets < 10 μm in diameter to be generated in channels 50 μm in size. Lastly, and perhaps most importantly, our geometry is fabricated in PDMS using an entirely lithographic process, and thus can be integrated as the drop making unit in parallel drop maker arrays. PDMS is the dominant polymer used in microfluidics, allowing our method to be widely adopted. In addition, the same molding technique used to fabricate our coaxial flow focusing geometry in PDMS can also be extended to other materials, like photopolymerizable epoxies or plastic devices constructed with hot embossing or injection molding. Combined, these properties should allow the scalable production of double emulsions of the desired small size in device arrays that are robust against fouling and clogging.

3.3 Experimental

3.3.1 Preparation of devices

To fabricate our coaxial flow focusing geometry, we use multi-level photolithography [19,20], which allows us to create channels with constrictions in the x-y and y-z planes. To fabricate these devices, we use two masters (Figure 3.S1)[21]. One master contains the 50 μm tall features for the first cross junction and constriction and 185 μm tall features for the large channels of the second junction. The second master contains a 135 μm mirror-image of just the 185 μm channels.

To construct the finished drop maker, the two masters are used to mold separate PDMS devices. The PDMS devices are sliced and peeled from the masters and the inlet ports are punched into them. The PDMS devices are washed with isopropanol and plasma oxidized to ready them for alignment and bonding. To bond the devices, a droplet of water is placed onto the PDMS slab containing 135 μm channels, with the channels face-up. The slab containing the 50 and 185 μm layers is then placed onto the first slab face down, so that the 135 μm and 185 μm channels align as mirror images. To align the slabs with high precision, we implement mechanical alignment "frames" consisting of 50 μm protruding ridges on the upper slab and 50 μm recessed channels on the lower slab, which lock into place when the two slabs are precisely aligned. The water droplet lubricates the slabs, allowing them to slide until the mechanical alignment lock is achieved. We use water because it is an effective lubricant for the hydrophilic plasma treated surfaces and also because it does not reduce the strength of the plasma bond. To evaporate the water and allow the two surfaces to fully bond, the aligned devices are baked for two days at 60°C. During this time, the channels revert to their native hydrophobic state, which is necessary for our device to form water-in-oil-in-water double emulsions. While PDMS is

optically transparent, the thickness of the lower layer of the device may limit high resolution imaging in the channels for certain applications.[22]

3.3.2 Preparation of emulsions

To generate double emulsions, we use distilled water for the inner phase, Novec 7500 fluorinated oil with 1 wt% biocompatible surfactant for the middle phase[23] , and a 10 wt% polyethylene glycol (PEG) solution containing 1 wt% Tween 20 and 1 wt% sodium dodecyl sulfate (SDS) for the continuous phase. The viscosities of the solutions are: 7.7×10^{-7} m^2 s^{-1} for Novec 7500, 1.01×10^{-6} m^2 s^{-1} for water and $\geq6\times10^{-6}$ m^2 s^{-1} for the PEG solution.[24] The surface tension between the water phases and the oil is estimated to be between 0.002-0.005 N m^{-1}.[25] The PEG increases the viscosity of the continuous phase, allowing us to achieve higher shears in the second junction with lower flow rates, making it easier to form the emulsions.

3.3.3 Flow rate estimation for single emulsions

To achieve the wide range of single emulsion drop sizes, we wanted a low flow rate of the inner phase. At low flow rates, syringe pumps tend to have lower accuracy. Therefore our desired inner phase flow rate of 20 µL/hr on our control software did not match the actual inner phase flow rate. To determine the actual flow rate of single emulsions, we used the double emulsion images to obtain an equation relating flow rate to the measured jet diameter:

$$Q_{sum} = \frac{Q_C}{\frac{16WH}{9\pi D_{jet}} + 1} \quad (1)$$

where D_{jet} is the diameter of the jet, Q_{sum} is the sum of the inner and middle phase flow rates, Q_C is the continuous phase flow rate, and W and H are the width and height of the constriction, respectively. Equation 1 is derived from assuming a parabolic flow profile in a rectangular

channel and is an approximation of the flow profile since the two jets may not form a continuous parabola. However, we can still obtain an accurate prediction of flow rate by adjusting H to match our double emulsion flow rate data. We then use equation 1 to calculate the flow rate of Q_{sum} for single emulsions and obtain an average value of Q_{sum}=118 µL/hr, which we use for the remainder of our analysis.

3.4 Results and Discussion

3.4.1 Microfluidic design and operation

Our coaxial flow focusing geometry employs a 3-dimensional channel layout (Figure 3.1). The inner phase is first combined with the middle phase in a 10 × 50 µm cross junction. Due to the hydrophobicity of the channels, the oil phase lifts the aqueous phase off of the channels and surrounds it, forming a long jet that flows into the second junction. In the second junction the channels abruptly increase in height to 320 µm, and a second aqueous phase is injected, as illustrated in Figures 3.1b and 3.1c. The abrupt expansion of the channels and high velocity of the outer aqueous fluid lifts the oil from the channel walls. This creates a double jet consisting of the inner jet of aqueous fluid sheathed in a thin shell of oil, surrounded by the second aqueous phase, as illustrated in Figures 3.1b and 3.1d. The double jet is then focused through a small "orifice" consisting of a 50 × 50 µm channel constriction, as shown from different perspectives in the panels in Figure 3.1. The constriction causes the velocity of the continuous phase to increase, generating high shears that rip droplets from the end of the jet, as

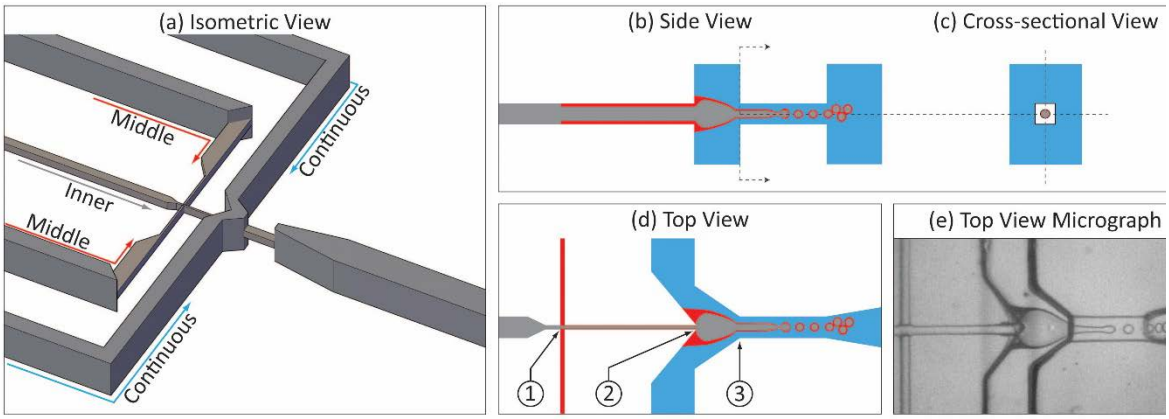

Figure 3.1 a) Isometric view of lithographically-fabricated coaxial flow focusing device, with phases labelled. b) Side view of channels with inner (grey), middle (red), and continuous (blue) phases indicated. c) Cross sectional view showing the square orifice enabling flow focus drop formation. d) Schematic diagram and e) microscope image of top view of device showing flow focus drop formation. At junction (1), the inner and middle phases combine. At junction (2), the channel expands and the inner and middle phases combine with the continuous phase, creating the double jet. At junction (3), the double jet is focused through the orifice, generating double emulsions.

illustrated in Figure 3.1e. This process resembles the generation of double emulsions with coaxial flow focusing in glass capillary devices, except that the channels have rectangular cross sections rather than round ones.

3.4.2 Flow focused formation of single and double emulsions

The coaxial geometry of our device allows us to generate single and double emulsions over a wide range of sizes and flow rates (Figure 3.2). It also allows us to generate drops substantially smaller than the constriction orifice. For the single emulsions, we form drops smaller than the pixel size in our image, which is 2 μm. However, we omitted the resolution limited data from our analysis since an accurate estimate of the error is difficult to obtain (Figure 3.S2).[21] For the double emulsions, we form drops down to 14 μm in diameter. To characterize the uniformity of the emulsions generated by our device, we measure the coefficient of variation

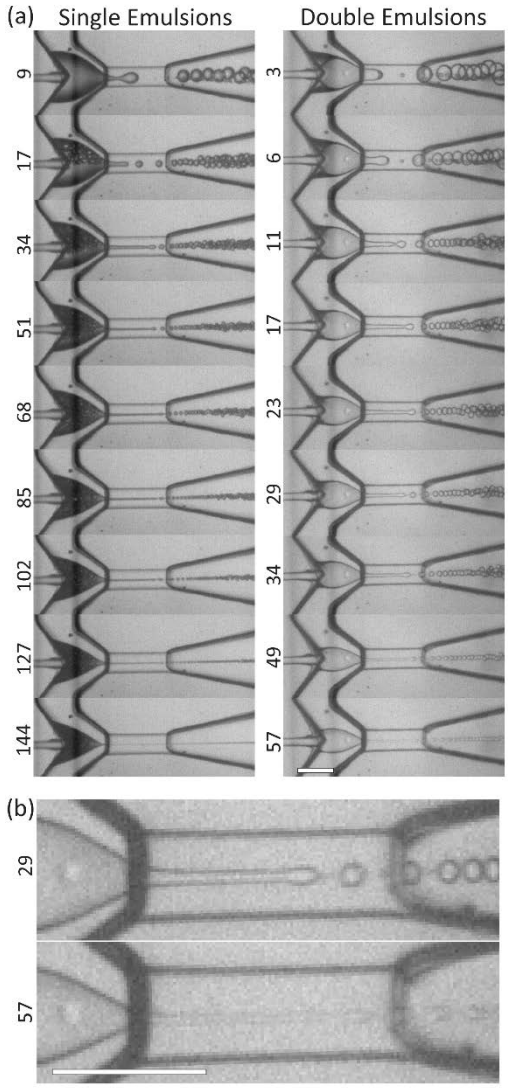

Figure 3.2 Generation of single (left) and double (right) emulsions at different flow rates. The number labels correspond to the Q_C/Q_{sum} values. Q_{sum}=118 and 350 µl/hr for single and double emulsions, respectively. b) Magnified images of double emulsion drop formation with Q_C/Q_{sum} values to the left. The scale bar denotes 100 µm.

(CV) of the droplet diameters. For the double emulsions, we measure a CV of 5.2% and for single emulsions 5.6%.

Our geometry mimics the flow focusing geometry of microcapillary devices, except that rather than a round orifice, the orifice of our device is rectangular. In a round orifice, the velocity

profile is axisymmetric, whereas it is not axisymmetric in a square channel.[26] However previous studies have shown the dripping and jetting regimes of jets in square channels and cylindrical channels generally agree for jets unconfined by the square channel walls, which is the case for our device too.[27,28] In addition, for square channels, the scaling laws for drop size based on inner and outer flow rates are similar for unconfined drops.[29] Therefore, our device should form double emulsions through the same mechanism as microcapillaries. If so, the scaling of drop size as a function of flow rate should be similar. To confirm whether this is the case, we vary flow rates and measure the corresponding change in drop size. We find that, just as in glass capillary devices, increasing the ratio of continuous phase to the inner and middle phases yields smaller drops, Figure 3.3. In glass capillary devices,

$$\frac{D_{drop}}{D_{orifice}} = C\left(\frac{Q_C}{Q_{sum}} + 1\right)^{-\frac{1}{2}} \quad (2)$$

where $D_{orifice}$ is the width of the flow focusing orifice and C is a fitted parameter related to λ, the most unstable perturbation wavelength of the jet.[30] To compare our data with this functional form, we plot the scaled double emulsion drop size as a function of flow rates in Figure 3.4 and fit equation 2 by adjusting C. By fitting our double emulsion data, we obtain C=1.77±.07. This C value agrees with C=1.87 from previous double emulsion results for glass capillary devices.[8] Our data is thus remarkably well described by the equation, suggesting that the mechanism of drop formation in our lithographically-fabricated device is similar to that of glass capillary devices.

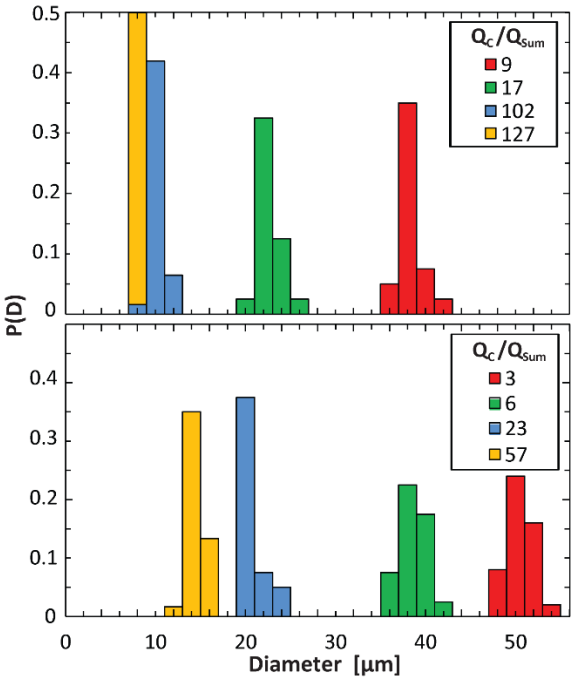

Figure 3.3 Histograms of drop sizes for single (top) and double (bottom) emulsions for different flow rates.

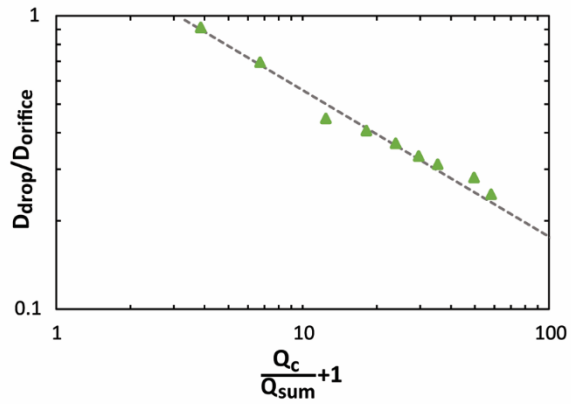

Figure 3.4 Droplet diameter versus flow rate ratio $Q_c/Q_{sum}+1$ for double emulsions. The dotted line correspond to the best fit of Eqn 1 for the double emulsions, which yields C=1.77±.07

3.5 Conclusion

We have demonstrated the generation of single and double emulsions using coaxial flow focusing in a lithographically-fabricated device. Our device combines the ability to form small, monodisperse emulsions of glass capillary flow focusing with the scalability of devices

fabricated lithographically. The devices can be readily parallelized by fabricating them in an array format and using published methods for distributing fluids evenly to the double emulsification junctions. This should allow the droplet generation rates to increase by several orders of magnitude, allowing scalable generation of small, monodisperse double emulsions. In addition, the ability to form small double emulsions in large coaxial flow focusing channels should make the device resistant to fouling and clogging, which is critical when parallelizing the devices intended to run for long durations without intervention.

References

1. C.A. Serra and Z. Chang, Chem. Eng. Technol. 31, 1099 (2008).
2. C. Laugel, A. Baillet, M. P Youenang Piemi, J.P. Marty, and D. Ferrier, Int. J. Pharm. 160, 109 (1998).
3. D. Lee and D.A. Weitz, Adv. Mater. 20, 3498 (2008).
4. M.-H. Lee, S.-G. Oh, S.-K. Moon, and S.-Y. Bae, J. Colloid Interface Sci. 240, 83 (2001).
5. C. Lobato-Calleros, E. Rodriguez, O. Sandoval-Castilla, E.J. Vernon-Carter, and J. Alvarez-Ramirez, Food Res. Int. 39, 678 (2006).
6. D. Vasiljevic, J. Parojcic, M. Primorac, and G. Vuleta, Int. J. Pharm. 309, 171 (2006).
7. J. Weiss, I. Scherze, and G. Muschiolik, Food Hydrocoll. 19, 605 (2005).
8. A.S. Utada, E. Lorenceau, D.R. Link, P.D. Kaplan, H.A. Stone, and D.A. Weitz, Science 308, 537 (2005).
9. L.-Y. Chu, A.S. Utada, R.K. Shah, J.-W. Kim, and D.A. Weitz, Angew. Chem. Int. Ed. 46, 8970 (2007).
10. Rotem, A.R. Abate, A.S. Utada, V. Van Steijn, and D.A. Weitz, Lab. Chip 12, 4263 (2012).
11. Holtze, J. Phys. Appl. Phys. 46, 114008 (2013).
12. R.K. Shah, J.-W. Kim, J.J. Agresti, D.A. Weitz, and L.-Y. Chu, Soft Matter 4, 2303 (2008).
13. M.E. Brennich, J.-F. Nolting, C. Dammann, B. Nöding, S. Bauch, H. Herrmann, T. Pfohl, and S. Köster, Lab. Chip 11, 708 (2011).
14. M.E. Kinahan, E. Filippidi, S. Köster, X. Hu, H.M. Evans, T. Pfohl, D.L. Kaplan, and J. Wong, Biomacromolecules 12, 1504 (2011).
15. H.Y. Park, X. Qiu, E. Rhoades, J. Korlach, L.W. Kwok, W.R. Zipfel, W.W. Webb, and L. Pollack, Anal. Chem. 78, 4465 (2006).
16. R.K. Shah, H.C. Shum, A.C. Rowat, D. Lee, J.J. Agresti, A.S. Utada, L.-Y. Chu, J.-W. Kim, A. Fernandez-Nieves, C.J. Martinez, and D.A. Weitz, Mater. Today 11, 18 (2008).
17. S.-H. Huang, W.-H. Tan, F.-G. Tseng, and S. Takeuchi, J. Micromechanics Microengineering 16, 2336 (2006).
18. A.R. Abate, D. Lee, C. Holtze, A. Krummel, and W.D. Do T, Lab---Chip Technol. Fabr. Microfluid. Caister Acad. Press (2009).
19. F.-C. Chang and Y.-C. Su, J. Micromechanics Microengineering 18, 065018 (2008).

20. M.B. Romanowsky, A.R. Abate, A. Rotem, C. Holtze, and D.A. Weitz, Lab. Chip 12, 802 (2012).

21. See Supplementary Material at [URL Will Be Inserted by AIP] for Figures S1 and S2 (n.d.).

22. Lab. Chip 8, 649 (2008).

23. O'Donovan, D.J. Eastburn, and A.R. Abate, Lab. Chip 12, 4029 (2012).

24. L. Ninni, H. Burd, W.H. Fung, and A.J.A. Meirelles, J. Chem. Eng. Data 48, 324 (2003).

25. A.R. Abate, A. Poitzsch, Y. Hwang, J. Lee, J. Czerwinska, and D.A. Weitz, Phys. Rev. E 80, 026310 (2009).

Chapter 4: Dissecting enzyme function with microfluidic-based deep mutational scanning.

The following section is reprinted from "Dissecting enzyme function with microfluidic-based deep mutational scanning." by Philip Romero, Tuan Tran and Adam Abate. It was published in PNAS on June 9 2015. Philip Romero, Tuan Tran and Adam Abate. designed the experiments; Philip Romero and Tuan Tran performed the experiments. Philip Romero analyzed the data; Philip Romero and Adam Abate wrote the manuscript.

4.1 Abstract

Natural enzymes are incredibly proficient catalysts, but engineering them to have new or improved functions is challenging due to the complexity of how an enzyme's sequence relates to its biochemical properties. High-throughput functional characterization can be paired with next-generation sequencing to generate rich data sets mapping protein sequence to function. These large-scale surveys can be used to explore the molecular basis of protein function in a comprehensive and unbiased manner. However, these methods are currently restricted to proteins that can be analyzed using growth-based selections or binding assays, and thus exclude many important enzymes. Here, we present a method for high-throughput mapping of sequence-function relationships that greatly expands the classes of enzymes that can be analyzed. We apply our method to a glycosidase enzyme, allowing us to identify new sites that play important functional roles and mutations that enhance enzyme thermostability. Our results demonstrate the power of combining droplet microfluidic screening with next generation DNA sequencing for understanding how specific residues and interactions influence enzyme activity.

4.2 Introduction

Enzymes are powerful biological catalysts capable of remarkably accelerating the rates of chemical transformations[1]. The molecular bases of these rate accelerations are often complex,

employing multiple steps, multiple catalytic mechanisms, and relying on numerous molecular interactions, in addition to those provided by the main catalytic groups. This complexity imposes a significant barrier to understanding how an enzyme's sequence impacts its function and, thus, on our ability to rationally design biocatalysts with new or enhanced functions[2–4].

Comprehensive mappings of sequence-function relationships can be used to dissect the molecular basis of protein function in an unbiased manner[5]. Growth selections or *in vitro* binding screens can be combined with next-generation DNA sequencing to generate detailed mappings between a protein's sequence and its biochemical properties[6–9]. These large-scale data sets have been used to study the structure of the protein fitness landscape, discover new functional sites, improve molecular energy functions, and identify beneficial combinations of mutations for protein engineering. However, these methods rely on functional assays coupled to cell growth or protein binding, severely limiting the types of proteins that can be analyzed. For example, most enzymes of biological or industrial relevance cannot be analyzed using existing methods because they do not catalyze a reaction that can be directly coupled to cell growth. Experimental advances are needed to broaden the applicability of sequence-function mapping to the diverse palette of functions performed by enzymes.

In this paper, we present a general method for mapping protein sequence-function relationships that greatly expands the scope of biochemical functions that can be analyzed. Ultrahigh-throughput droplet-based microfluidic screening enables us to characterize the chemical activities of millions of enzyme variants. By sorting the variants based on chemical activity and performing next-generation DNA sequencing of sorted and unsorted libraries, we obtain a detailed mapping of how changes to enzyme sequence impact chemical function. We demonstrate this method using a glycosidase enzyme important in the deconstruction of biomass into fermentable

sugars for biofuel production. Comprehensive mutagenesis and functional characterization allowed unbiased discovery of residues within the enzyme crucial to function and the identification of mutations that enhance activity at elevated temperatures. This “reverse engineering” approach can be applied to any enzyme whose chemical activity can be measured with a fluorogenic assay in microfluidic droplets[10–13]. Our method extends the applicability of sequence-function mapping to a wide range of protein functions and reaction conditions not accessible by other high-throughput methods.

4.3 Results

4.3.1 High-throughput sequence-function mapping

Protein sequence space is vast and an enzyme's functional properties may depend on hundreds to thousands of molecular interactions, most of which have never been characterized. Systematically exploring this space thus necessitates methods capable of characterizing massive numbers of sequence variants. We have developed a general method for performing millions of sequence-function measurements on an enzyme (Figure 4.1a). A library of enzyme variants is expressed in *E. coli* and single cells are encapsulated in microfluidic droplets containing lysis reagents and a fluorogenic enzyme substrate (Supplementary Figure 4.1a). Upon lysis, the expressed enzyme variant is released into the droplet, allowing it to interact with the substrate. The surrounding oil acts as a barrier that keeps reagents contained within the droplets, preventing product molecules generated by one variant from mixing with those of another in a different droplet. Droplets that contain efficient enzyme variants thus rapidly accumulate fluorescent product, while those with inactive variants remain dim. The DNA sequences of the active variants are then recovered using a high-throughput microfluidic droplet sorter[14]. The sorter can analyze more than 100 enzyme

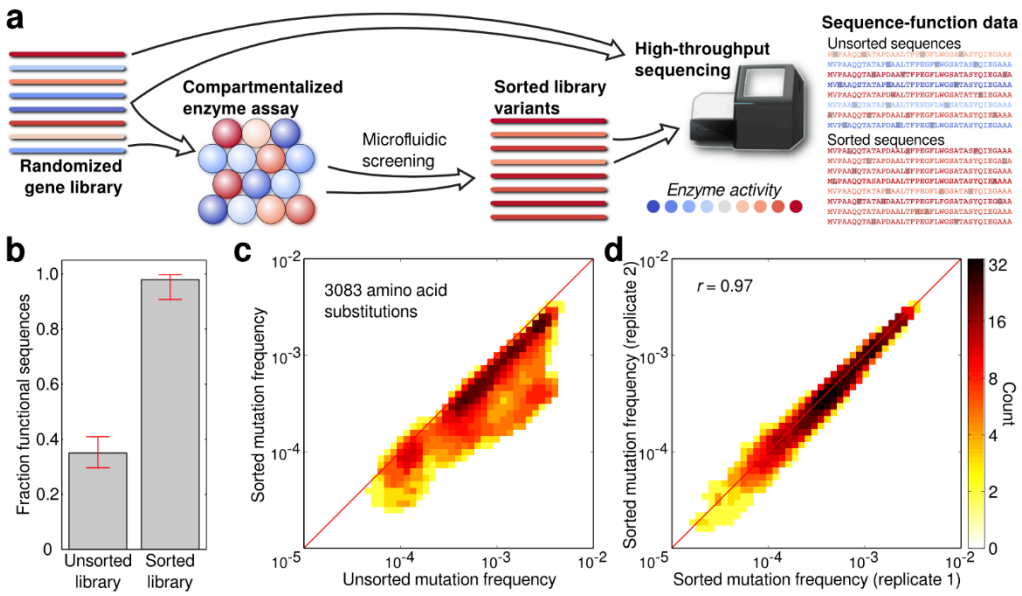

Figure 4.1 High-throughput sequence-function mapping. (a) A conceptual overview of the sequence-function mapping protocol. Individual members of a randomized gene library are assayed in aqueous microdroplets, and microfluidic screening is used to sort out the active variants. The unsorted and sorted variant pools are then analyzed using high-throughput DNA sequencing. The resulting sequence-function data set is used to understand the functional impact of mutations. (b) Droplet-based microfluidic screening recovers functional sequences from the initial random mutagenesis library. Individual clones from the unsorted and sorted libraries were tested in a plate-based assay and were considered functional if their end-point activity was greater than 50% of Bgl3's. Initially, only 35% of the library was functional, but after screening the fraction of functional sequences increased to 98%. (c) The frequency of 3083 amino acid substitutions in the unsorted and sorted libraries. A large fraction of mutations decrease in frequency after sorting, suggesting they are deleterious to

variants per second, reaching one million in just a few hours. The sorted and unsorted gene libraries are then processed using next-generation DNA sequencing and statistical analysis.

As a demonstration of the generality and power of our sequence-function mapping method, we used it to analyze Bgl3, a beta-glucosidase enzyme from *Streptomyces sp*[15]. To enable accurate sorting of active from inactive variants, we developed an emulsion-based beta-glucosidase assay that showed excellent discrimination between wild-type Bgl3 and an inactive mutant (Supplementary Figure 4.1b,c,d). We used error-prone PCR to generate a Bgl3 mutant library with an average of 3.8 amino acid substitutions per gene. We screened this library for a total of 23 hours (four separate runs), analyzing over 10 million variants, 3.4 million of which contained measurable

enzymatic activity and were recovered via microfluidic sorting (Supplementary Figure 4.1e). To confirm enrichment of functional sequences within the sorted population, we tested a random sampling of mutants in a plate assay before and after sorting (Figure 4.1b). Before sorting, ~35% of variants were found to be functional, the remainder inactive due, presumably, to deleterious point mutations. After sorting, the fraction of functional sequences increased to 98%.

We processed the unsorted and sorted gene libraries using the Nextera XT sequencing library prep kit, sequenced using an Illumina MiSeq v3 2x300 run, and mapped the sequence reads to the *bgl3* gene using Bowtie2. The DNA sequencing showed good coverage across the entire *bgl3* gene for both the unsorted and sorted libraries (Supplementary Figure 4.2a). The Bgl3 construct has 500 amino acid positions and therefore a total of 10,000 (500 x 20) possible amino acid substitutions including nonsense mutations. After applying sequencing quality filters, there were sufficient statistics to quantify the frequency of 3083 (31%) of these amino acid substitutions. The remaining 6917 substitutions were difficult to access because they require two or three nucleotide mutations within a single codon, which is a rare occurrence in libraries generated via error-prone PCR (Supplementary Figure 4.2b).

The effect of an amino acid substitution can be estimated by how much its frequency changes in response to functional screening. A majority of mutations decreased in frequency in the sorted library, suggesting they are deleterious to the enzyme's function (Figure 4.1c). This observation is consistent with other studies analyzing the effects of random mutations on protein function[16–19]. To further evaluate the method, we tested the reproducibility of the mapping by comparing amino acid frequencies from two independent sorting experiments (Figure 4.1d). These data sets show excellent agreement (r = 0.97) across all 3083 point mutations.

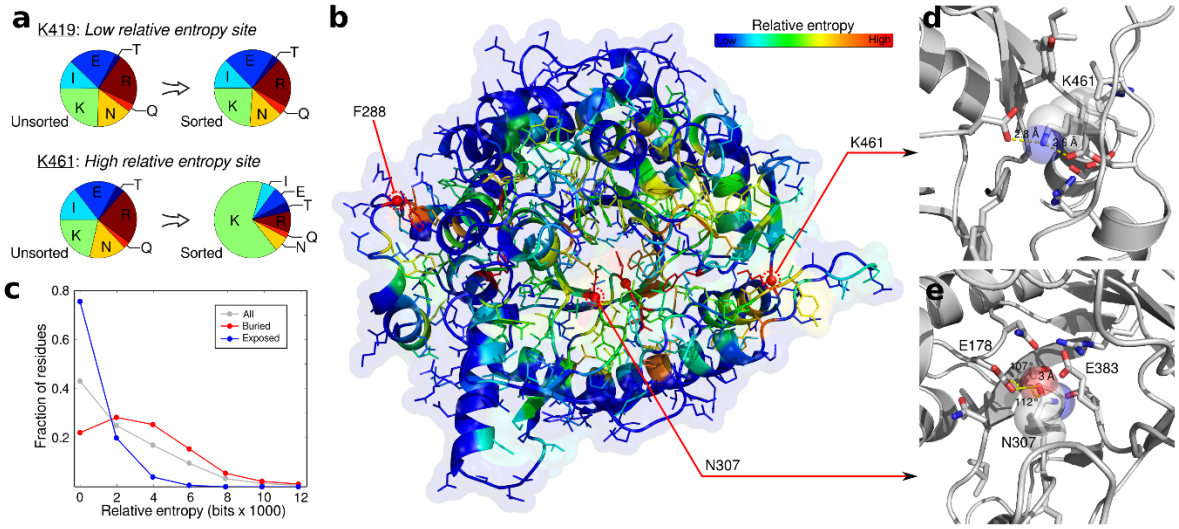

Figure 4.2 Analysis of site-specific mutational tolerance. **(a)** Relative entropy (RE) describes how much the amino acid probability distribution changes in response to functional screening. The amino acid distribution of mutated codons is shown for a low RE site and a high RE site. Only synonymous substitutions are shown for the WT amino acid. The low RE site (K419) shows little change between the unsorted and sorted libraries, suggesting this position can tolerate substitutions to other amino acids. In contrast, the high RE site (K461) shows a strong shift back to the WT residue. **(b)** Structural patterns of mutational tolerance. The relative entropy of each site was mapped onto the Bgl3 crystal structure (PDB ID: 1GNX). Sites with the highest relative entropies (≥ 99th percentile) have a red sphere at their alpha carbon. As expected, known functional sites, such as the catalytic residues, are highly intolerant to mutation. The analysis also reveals previously unannotated positions that are intolerant to mutation and may therefore play an important role in Bgl3 function. Three of these sites (F288, N307, and K461) are labeled in the figure. **(c)** The mutational tolerance of a position depends on its solvent exposure. The distribution of relative entropies for all positions is shown in grey. Buried residues (relative surface area [RSA] < 0.2) tend to have higher relative entropies and are therefore less tolerant to mutations than solvent-exposed residues (RSA ≥ 0.2). **(d)** Detailed view of K461 in Bgl3 structure. K461 (transparent spheres) forms salt bridges with two nearby aspartic acid residues. The short inter-atomic distances and their networked nature, suggests these interactions are strong and may be important for the structural stability of the enzyme. **(e)** Detailed view of N307 in Bgl3 structure. N307 (transparent spheres) is located directly between the enzyme's nucleophile (E383) and the general acid/base (E178). Based on the distance and angles of the residues, N307 appears to hydrogen bond with E178, which may be important for perturbing the pKa of that group and, thus, the catalytic mechanism of the enzyme.

4.3.2 Site-specific mutational tolerance

Data from millions of functional sequence variants can be used to identify residues important for enzyme function. Residues that cannot be mutated to other amino acids are likely to

play a specific role required for enzyme activity. The degree to which a site can tolerate amino acid change is thus an indicator of its functional importance. The relative entropy (RE) can be used to score a residue's mutational tolerance, since it quantifies how much the amino acid probability distribution changes between the unsorted and sorted libraries (Figure 4.2a). A site whose distribution shifts significantly from random has high relative entropy, implying that a specific amino acid must reside at that position for the enzyme to remain functional.

The mutational tolerance of a site should be related to its position in the protein's three-dimensional structure, since this determines the other residues with which it interacts. To investigate this, we mapped the relative entropy of each position onto the Bgl3 crystal structure (Figure 4.2b). As expected, the catalytic nucleophile (E383) and general acid/base (E178) are both highly intolerant to mutation, falling at the 99th and 95th percentiles, respectively. We also expect core residues to be less tolerant to mutation than surface residues because the protein core tends to be well packed, forming many inter-residue interactions. To support this, the alpha helices that compose the TIM-barrel wall display an alternating pattern, where the interior helix face is less tolerant to mutation than the exterior face (Figure 4.2b). Overall, buried residues are less tolerant to mutation than solvent-exposed residues (Figure 4.2c).

The analysis of mutational tolerance reveals sites that play an important functional role, several of which have never been described in the literature. For example, lysine 461 has the highest relative entropy of any residue (100th percentile) though, oddly, it is far from the active site (Figure 4.2b). Targeted mutagenesis shows no other amino acid can be accepted at this location, validating the mutational tolerance findings (Supplementary Figure 4.3c). In the crystal structure, K461 is involved in networked salt bridges with two aspartic acid residues (Figure 4.2d).

The short distance of these interactions indicates they are strong and suggests that K461 may be important for the structural stability of the enzyme.

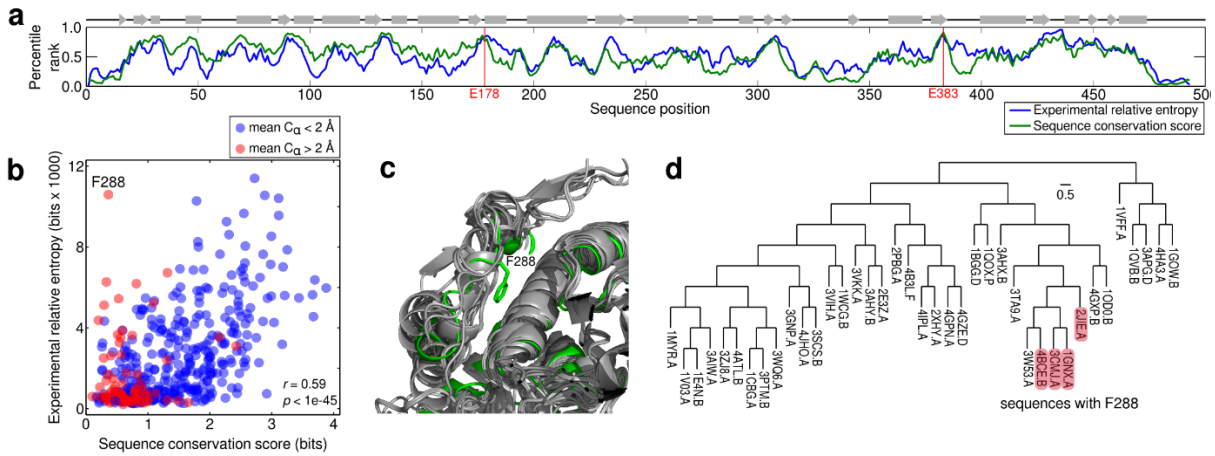

Figure 4.3 Comparison to natural sequence variation. (a) Gene-scale patterns of Bgl3's mutational tolerance and the observed GH1 sequence conservation. A moving average (5 site window) of the experimental relative entropy and sequence conservation scores is plotted over sequence positions. Percentile ranks are used to plot the two scores on the same axis. The overall patterns of Bgl3 mutational tolerance and GH1 conservation are very similar and tend to correspond with secondary structure elements (displayed across the top). (b) The relationship between a site's mutational tolerance and sequence conservation. A scatter plot of the experimental relative entropy and sequence conservation scores displays a strong correlation ($r = 0.59$, $p < 1E\text{-}45$), indicating that sites important for Bgl3 function are also important throughout the GH1 family. Outlying sites, such as F288, can be explained by structural diversity within the enzyme family. Structural diversity (mean Cα displacement) was quantified by aligning all related structures to Bgl3, calculating each structure's Cα displacement from Bgl3 at each position, and averaging over all structures. Positions with a high experimental relative entropy, but low sequence conservation score (top, left corner) tend to come from regions with more structural diversity (red points). (c) Structural diversity may explain outlying sites. Position 288 is highly intolerant to mutation in Bgl3 (99th percentile for RE) but has little conservation in the GH1 alignment (11th percentile for sequence conservation score). An alignment of GH1 structures reveals that position 288 occurs in a structurally diverse loop. We hypothesize that F288 is important for Bgl3 function, but its interactions are not conserved throughout the GH1 family. (d) Sequence-function mapping provides a local view of sequence space. A phylogenetic tree of GH1 structures shows that the few sequences that do contain F288 are closely related.

Asparagine 307 is another residue with high relative entropy (99th percentile) that, again, has not been described previously. N307 is located in the enzyme's active site and appears to be hydrogen bonding with the general acid/base E178 in the crystal structure (Figure 4.2e). Targeted

mutagenesis at this position also shows no other amino acid is tolerated, again validating the results of the mutational tolerance map obtained with our approach (Supplementary Figure 4.3b). We hypothesize that N307 may act to shift the pKa of the general acid/base, which is crucial for the pKa-cycling mechanism of most retaining glycosidases[20]. These results demonstrate the power of comprehensive and unbiased sequence-function mapping for investigating enzyme function and identifying important residues.

4.3.3 Comparison to the natural sequence record

Bgl3 is a member of glycoside hydrolase family 1 (GH1), a large enzyme family accepting a broad range of glycosylated substrates[21,22]. The sequences within the GH1 family typically differ by hundreds of mutations, providing a diverse sampling of the sequence space explored by natural evolution. By contrast, our experimental sequence-function mapping densely samples the local space of sequences within a few mutations of Bgl3. Comparing the global versus local view of sequence space may provide insight into the evolutionary constraints imposed on members of the GH1 family.

To investigate how our results compare to the natural sequence record, we used a large GH1 multiple sequence alignment to calculate a relative entropy sequence conservation score[23,24]. Bgl3's mutational tolerance shows a strong correspondence with the observed GH1 sequence conservation. Gene-scale patterns can be visualized by taking a moving average (5 site window) of the relative entropy and sequence conservation scores across sequence positions (Figure 4.3a). The experimental mutational tolerance and GH1 conservation are strikingly similar, and their patterns tend to correspond with secondary structure elements. Overall, the experimental relative entropy and the sequence conservation score display a strong, statistically significant correlation

(r = 0.59, p < 1E-45, Figure 4.3b), suggesting that most sites important for Bgl3 function are also important throughout the GH1 family.

There are, however, unexpected and interesting exceptions to this correspondence. The most extreme is position 288, which is highly intolerant to mutation in Bgl3 (99th percentile for RE) but has little conservation in the GH1 alignment (11th percentile for sequence conservation). Targeted mutagenesis at this location again validates the sequence-function mapping results, confirming that Bgl3 can only tolerate 21% of all amino acid substitutions at position 288 (Supplementary Figure 4.3a). The fact that other GH1 members can accept mutations at position 288 suggests that Bgl3 evolution may be constrained by mutational epistasis at this site.

A closer look at GH1 structures reveals that position 288 occurs within a loop region that displays high diversity in the family (Figure 4.3c). In fact, the most outlying positions (high experimental RE and low sequence conservation) occur in regions with high structural variation within the GH1 family (Figure 4.3b, *red points*). We hypothesize that through the course of natural evolution, Bgl3 may have evolved unique structural motifs that constrain its mutational tolerance relative to the GH1 family. We expect closely related sequences to also share these motifs and therefore to have similar residue preferences. Indeed, the phylogenetic tree of GH1 structures shows the few members that do contain F288 are closely related (Figure 4.3d). Similar idiosyncrasies may be present in all family members, but get blurred when looking at the entire family alignment.

These results highlight how sequence-function mapping provides a detailed local view of sequence space, whereas large multiple sequence alignments provide a global perspective. A local sequence space mapping is important for applications such as protein engineering or the prediction

of disease-associated mutations, because they focus on the mutational properties of the specific family member under investigation.

4.3.4 High-temperature screening enriches for stabilizing mutations

Previous work in enzyme sequence-function mapping has used *in vivo* assays coupling an enzyme's function to cellular growth[7,25–27]. These *in vivo* selections are limited not only in the types of enzyme functions that can be analyzed, but also by the range of experimental conditions compatible with the intracellular environment. An advantage of droplet-based microfluidics is the ability to precisely control screening conditions, such as time, temperature, and concentration. Screening under altered conditions allows for enrichment of variants with enhanced unnatural properties.

To investigate this capability, we modified the microfluidic screening protocol to include a heat challenge directly after droplet formation (Supplementary Figure 4.4). We hypothesized that this should enrich for mutations that increase Bgl3's thermostability. We screened a total of 10 million enzyme variants, 2 million (20%) of which were determined to remain active and recovered via sorting. In this experiment, the heat challenge inactivated approximately half of the variants active in the original room temperature screen.

To observe the effects of the heat-challenge on the functional space of enzyme sequences, we plotted the enrichment value for every observed amino acid substitution along the length of the enzyme (Figure 4.4a). Overall, most mutations (97%) decreased in frequency (blue), but a small number showed positive enrichment values (red, Figure 4.4b). The mutation with the greatest enrichment was S325C, located in an unresolved loop of the Bgl3 structure. This mutant was constructed and characterized and, indeed, yields a 5.3 °C increase in thermostability (Figure 4.4c).

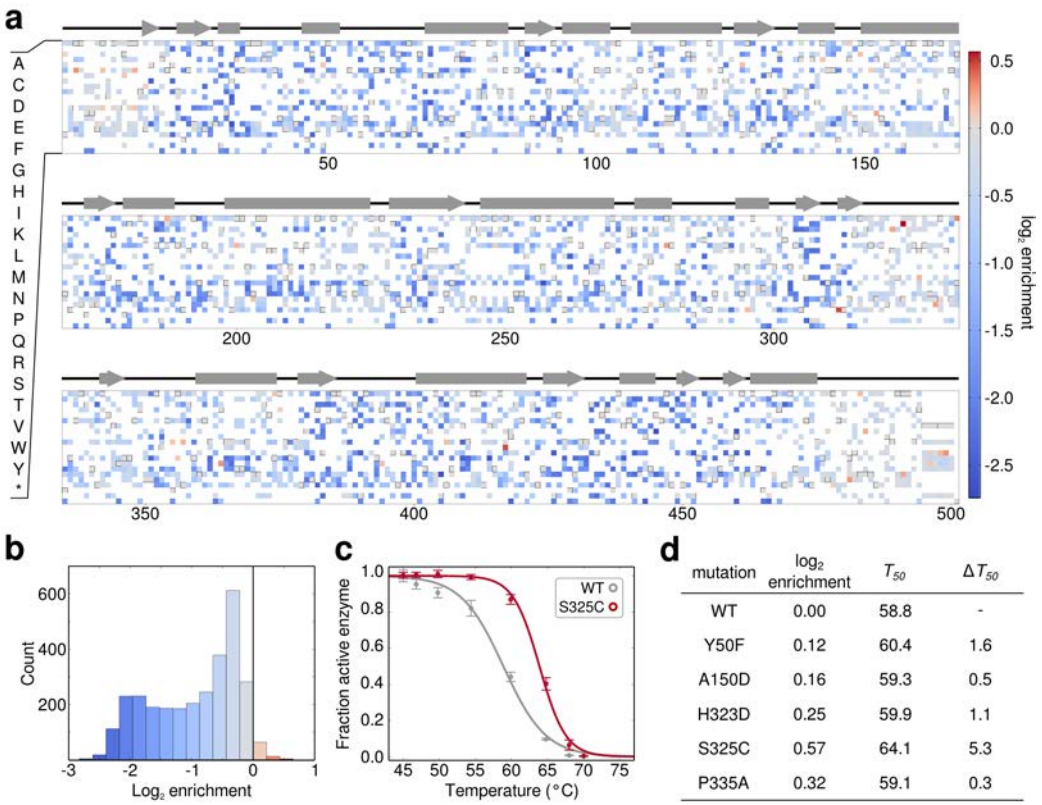

mutation	$\log_2$ enrichment	T_{50}	ΔT_{50}
WT	0.00	58.8	-
Y50F	0.12	60.4	1.6
A150D	0.16	59.3	0.5
H323D	0.25	59.9	1.1
S325C	0.57	64.1	5.3
P335A	0.32	59.1	0.3

Figure 4.4 Identification of stabilizing point mutations. (a) High-temperature screening enriches for stabilizing mutations. The enrichment value of 2956 amino acid substitutions plotted over sequence positions. Amino acids that weren't observed are colored as white and the wild-type residue is colored grey with a box around it. (b) The overall distribution of enrichment values. Only 3% of substitutions have a positive enrichment value. (c) Thermal inactivation curves for WT Bgl3 and the mutant with the highest enrichment value. S325C increases the T50 of the enzyme by 5.3 °C. (d) Enriched mutations confer enhanced thermostability. A panel of five enriched mutations was characterized, and all showed moderate to large increases in thermostability. The magnitudes of the stability increases depend on the assay conditions and tend to be lower when tested under conditions different from the screen (Supplementary Figure 6).

Stability increases of this magnitude are very hard to achieve with other protein engineering methods. Other substitutions with positive enrichment values also increase the enzyme's thermostability (Figure 4.4d, Supplementary Figure 4.5). This simple protocol allows the identification of thermostabilizing mutations and can be adapted to enrich for a variety of additional properties by screening under different conditions.

4.4 Discussion

High-throughput sequence-function mapping is a powerful tool for exploring the molecular basis of protein function[7,16,26,27]. However, restrictions on functional assays have limited its general applicability, particularly for enzymes. We have presented a method for characterizing millions of enzyme variants by compartmentalizing reactions in aqueous microdroplets. The assays utilize an optical readout and can therefore be readily adapted to the numerous classes of enzymes with fluorescence-based activity assays.

Our experimental protocol enabled the analysis of over one million Bgl3 variants, and we used the resulting sequence-function map to evaluate the enzyme's tolerance to mutation. This unbiased analysis discovered sites within the enzyme that cannot tolerate mutations, and are therefore likely to play an important role in Bgl3 function. Alternately, sites with a high tolerance to mutation are important for protein evolution and engineering because they can accept diversification while still maintaining catalytic function; this provides the protein engineer with flexibility in enhancing certain properties while maintaining others. The sequence-function mapping approach provides a local view of protein sequence space that can identify important interactions overlooked by large alignments of homologous sequences.

Droplet-based microfluidic screening provides a flexible platform for assaying enzyme activity over a broad range of reaction conditions[10–13]. We adapted our screening protocol to include a heat challenge and enriched for mutations that increase the enzyme's thermostability. Similar approaches could be used to identify variants with enhanced properties including increased k_{cat} (reduced reaction time), decreased K_m (reduced substrate concentration), increased tolerance to biomass pretreatments (increased ionic liquid concentration), and reduced product inhibition

(increased glucose concentration). Systematically mapping multiple enzyme properties will allow us to evaluate the trade-offs between properties and enable multi-objective protein engineering.

Experimentally mapping protein sequence space requires high-throughput library synthesis, screening, and sequencing, any of which could be a bottleneck. From this work, we found library construction and sequencing to be more limiting than microfluidic screening. Our random mutagenesis library contained 6 million unique variants (CFUs), and the transformation efficiency limited the size of this library. The microfluidic sorter analyzed over 10 million enzyme variants in 23 hours, and the throughput of more recent sorter designs is more than an order of magnitude faster[28]—enabling the screening of libraries beyond 10^8 variants. While Illumina DNA sequencers can provide a large number of sequencing reads, read length is currently limited to ~600 bp, about one third of the Bgl3 gene. With implementation of longer read lengths, it will be possible to perform pairwise analysis by correlating the effects of mutations at distant sequence positions.

Our method relies on a microfluidic droplet sorter that requires specialized instrumentation not typically found in a biochemistry laboratory. However, an alternative to screening enzyme variants in water-in-oil droplets is to screen them water-in-oil-in-water (W/O/W) double emulsions[29]. Double emulsion droplets also provide microcompartments with which to test individual enzyme variants but can be generated using commercially available microfluidic systems (Dolomite Microfluidics) and sorted using standard cell sorters[30,31]. This should provide an easily adoptable and widely available solution for implementing our sequence-function mapping method.

The ability to rationally engineer enzymes will have a far-reaching impact on areas that range from medicine and agriculture to environmental protection and industrial chemistry.

However, enzyme function involves an extraordinarily complex balance of numerous physical interactions, which has limited the design of tailor-made enzymes. Large sequence-function data sets will provide an increasingly detailed view of the determinants of enzyme function. When combined with methods from statistics and machine learning, protein design rules can be extracted and applied in an automated manner. Given the rapid pace of advances in high-throughput experimentation, data-driven protein engineering may be able to outpace more traditional physics-based methods.

4.5 Methods

4.5.1 Fabrication of microfluidic devices

All microfluidic devices were fabricated in-house using standard soft lithography techniques[32]. Photomasks were used to pattern layers of photoresist (SU-8 3025) on a silicon wafer, and uncured PDMS (11:1 polymer to cross-linker ratio) was poured over the mold. The PDMS was cured at 80 °C for 1 hour, extracted from the mold with a scalpel, and access holes were punched using a 0.75 mm biopsy core. The devices were then bonded to glass slides after a plasma surface treatment. The device channels were made hydrophobic by flushing with Aquapel (Pittsburgh Glass Works) and then baking for an additional 10 minutes at 80 °C.

4.5.2 Construction of Bgl3 random mutagenesis library

The Bgl3 gene was cloned into the pET-22b (Novagen) expression vector and used as a template for error-prone PCR. Error-prone PCR was performed following a protocol where $MnCl_2$ is used to tune the mutation rate of *Taq* polymerase[33]. We determined that a final concentration of 100 uM $MnCl_2$ yielded ~4 amino acid substitutions per gene. After fifteen PCR cycles, the reaction was treated with DpnI overnight and purified with a DNA spin column (Zymo research).

The mutagenized Bgl3 insert was cloned back into pET-22b using circular polymerase extension cloning (CPEC)[34]. The CPEC reaction was purified and concentrated using a DNA spin column (Zymo research) and used to transform electrocompetent BL21(DE3) *E. coli* cells (Lucigen). The transformed cells were recovered in expression recovery media (Lucigen) at 37 °C for one hour. Several dilutions of the transformation were plated to determine the total library size and the remainder used to inoculate a 50 ml LB-carbenicillin culture. Once the culture reached a measurable OD600, freezer stocks were made by combining with 50% glycerol and the library was stored at -80 °C until use. The final library contained 6 million unique transformants. Ten individual clones were sequenced to determine the library's mutation rate of 3.8 amino acid substitutions per gene.

4.5.3 Microfluidic screening of Bgl3 library

A glycerol stock of the Bgl3 library was used to inoculate a 5 ml MagicMedia (Invitrogen) expression culture. This library was expressed overnight, pelleted, and resuspended in assay buffer (100 mM potassium phosphate, pH 7). A 2x cell solution was made by diluting the cell suspension to an OD600 of 0.05 in assay buffer. Assay reagents at 2x concentration were combined to a final concentration of 0.6x BugBuster (Novagen), 60 KU/ml rLysozyme (Novagen), 200 uM fluorescein di-(β-D-glucopyranoside) (Sigma) in 100 mM potassium phosphate, pH 7.

Microdroplets containing expressed enzyme variants were generated using a co-flow droplet maker device (Supplementary Figure 4.7a). Equal volumes of 2x cells and 2x assay reagents were combined by the device and emulsions generated using fluorinated oil (HFE 7500) containing 2% (w/w) PEG-PFPE amphiphilic block copolymer surfactant (RAN Technologies) in a flow focus droplet maker. Both aqueous inlets were injected at 150 μl/h and the fluorinated oil at 700 μl/h. At these flow rates, each droplet has a volume of ~2 pL and, on average, one in ten

contains a single *E. coli* cell. The droplets were collected into a syringe and incubated at 37 °C for 1 hour.

After incubation, the droplets were sorted using selective electrocoalescence with an aqueous collection stream (Supplementary Figure 4.7b). A 473 nm laser was focused onto the channel just upstream of the sorting junction, each droplet was individually excited, and its fluorescence emission measured using a spectrally-filtered PMT (Hamamatsu Photonics) at 520 nm (Supplementary Figure 4.8). An FPGA card controlled by custom LabVIEW code analyzed the droplet signal at 200 KHz, and if it detected sufficient fluorescence (Supplementary Figure 4.1d,e), a train of seven 100 V, 40 kHz pulses was applied by a high-voltage amplifier (Trek). This pulse destabilized the interface between the droplet and the adjacent aqueous stream, causing the droplet to merge with the steam via a thin-film instability, after which the volume of the droplet was injected into the collection stream via its surface[14]. The contents of the sorted droplets were collected in a microcentrifuge tube for further processing. Droplets were analyzed at 1,300/second and, since one in ten droplets contained a cell, cells were analyzed at ~130/second.

The Bgl3 library was sorted on four separate days for about 6 hours each day. During each of these runs, we analyzed ~27 million droplets containing ~2.7 million cells. Approximately 900,000 individual droplets containing active cells were sorted during each run. In total, we analyzed over ~10 million cells and recovered ~3.4 million active variants, which fed into the sequence-function mapping pipeline.

For the screen containing a heat challenge, a PID-controlled heating element was added inline directly after droplet formation (Supplementary Figure 4.4). This allowed us to heat the droplets at 65 °C for ~10 minutes. Using this protocol we analyzed 100 million droplets containing ~10 million cells, and recovered ~2 million active variants.

4.5.4 Recovery of sorted DNA

The contents of the sorted droplets were collected from the microfluidic chip and DNA was recovered using a DNA spin column (Zymo research). The eluted DNA was transformed into high efficiency competent *E. coli* cells (Lucigen), and transformed cells were cultured in expression recovery media (Lucigen) at 37 °C for one hour. Several dilutions of the transformation were plated to determine the total number of transformants and the remainder used to inoculate a 50 ml LB-carbenicillin culture. Once the culture reached a measurable OD600, freezer stocks were made by combining the culture with 50% glycerol and were stored at -80 °C. For these transformations, we typically obtained 1-10 times more transformants (CFUs) than sorted droplets that entered the protocol, suggesting good sampling of the genetic diversity within sorted population.

4.5.5 Illumina library preparation and sequencing

The gene libraries before and after sorting were used to prepare an Illumina sequencing library. Individual sorting runs were prepared as separate sequencing libraries to allow for internal validation of the method's reproducibility. A library's glycerol stock was used to inoculate an overnight LB culture and the plasmid DNA was mini-prepped. The gene insert was cut out of the pET-22b vector using the SgrAI and DraIII sites and gel extracted.

The gel extracted inserts were used as inputs to the Nextera XT DNA Sample Prep Kit (Illumina). Each sample was barcoded using a different index primer. A low SPRI bead ratio (0.4x) was used to select for longer sequence fragments. The resulting libraries were quantified using a high sensitivity Bioanalyzer chip (Agilent), a Qubit Assay Kit (Invitrogen), and finally quantitative PCR (Kapa Biosystems). The average sequence fragment was ~1,400 bp. All libraries were pooled in equimolar proportions and sequenced using a MiSeq v3 2x300 run with a 5% PhiX control spike-in.

4.5.6 Analysis of Illumina sequencing data

Paired-end DNA sequencing reads were mapped to the Bgl3 gene using Bowtie2's very-sensitive-local alignment setting[35]. Typically, 80-90% of the paired-end reads aligned concordantly exactly one time. The resulting SAM files were parsed to count the amino acids observed at each Bgl3 position. Reads with a Phred quality score (Q-score) of less than 30 were excluded from the analysis.

The frequency of each amino acid at each position was calculated by dividing the number of times the amino acid was observed by the total number of observations at that position. Amino acids with less than 10 total observations at a given position were considered insignificant and excluded from the analysis. After this filter, there were good statistics on the 500 WT amino acids plus 3083 amino acid substitutions. The frequency of WT amino acids was significantly larger than the substitutions because mutations only occur ~1% of the time.

The relative entropy of a specific site is given by

$$RE = \sum_{a} f_{sort,a} \log_2 \frac{f_{sort,a}}{f_{unsort,a}}$$

where the sum is over all 20 amino acids, and $f_{sort,a}$ and $f_{unsort,a}$ are the frequencies of amino acid a. If either $f_{sort,a}$ or $f_{unsort,a}$ are equal to zero, then amino acid a is excluded from the summation in order to prevent infinite values.

The enrichment of a substitution to amino acid a is given by

$$E = \log_2 \frac{f_{sort,a}}{f_{unsort,a}}$$

where $f_{sort,a}$ and $f_{unsort,a}$ are the frequencies of amino acid a in the sorted and unsorted libraries, respectively.

4.5.7 Analysis of natural glycoside hydrolase family 1 sequences

The sequences of other glycoside hydrolase family 1 members were downloaded from the NCBI Protein database using GenBank accession numbers from the Carbohydrate Active Enzymes (CAZY) GH1 database[36]. Sequences containing less than 30% sequence identity with Bgl3 were removed, and the remaining 1,300 sequences were aligned using the MUSCLE multiple sequence alignment program[37]. The frequency of each amino acid at each Bgl3 site was calculated by dividing the number of times the amino acid was observed by the total number of observations at that position. Gaps in the alignment were excluded from the analysis.

The sequence conservation score describes how much the amino acid distribution at a given site in the multiple sequence alignment (MSA) differs from a general, background amino acid distribution. This is quantified using the multiple sequence alignment (MSA) relative entropy[23,24]

$$RE_{MSA} = \sum_{a} f_{msa,a} \log_2 \frac{f_{msa,a}}{f_{bg,a}}$$

where the sum is over all 20 amino acids, $f_{msa,a}$ is the frequency of amino acid a at a particular position in the multiple sequence alignment, and $f_{bg,a}$ is the background amino acid frequency of amino acid a taken from all positions in the MSA. If $f_{msa,a}$ is equal to zero, then amino acid a is excluded from the summation to prevent infinite values. The MSA relative entropy (RE_{MSA}) is different from the relative entropy used to analyze the experimental mutational data because it describes how the MSA's amino acid distribution differs from a fixed background amino acid distribution.

We generated the glycoside hydrolase family 1 phylogenetic tree (Figure 4.3d) by taking the sequences of all GH1 entries in the Protein Data Bank. Redundant sequences containing

greater than 90% sequence identity were removed. The remaining 39 sequences were then processed using the Phylogeny.fr web server[38].

4.5.8 Cloning of individual mutations

Individual mutations for follow-up analyses were cloned using the QuikChange Lightning kit (Agilent) and transformed into Bl21 (DE3) (Lucigen). A single colony was grown overnight, mini-prepped, and gene sequence was verified using Sanger sequencing with the T7 promoter and T7 terminator primers.

4.5.9 Plate-based functional assay

The fraction of functional sequences was determined for the initial library, the sorted library, and the site-specific libraries using a plate-based functional assay. Single colonies were picked into a 96 deep well plate containing 500 μl MagicMedia (Invitrogen), and these cultures were expressed overnight, shaking at 37 °C. The next day the cells from the expression culture were pelleted and resuspended in 200 μl of assay buffer (100 mM potassium phosphate, pH 7). 2x assay reagents were combined to a final concentration of 0.6x BugBuster (Novagen), 60 KU/ml rLysozyme (Novagen), 2 mM 4-Methylumbelliferyl-β-D-glucopyranoside (Sigma) in 100 mM potassium phosphate, pH 7. 75 μl of the cell suspension was combined with 75 μl of the 2x assay reagents and allowed to react for 15 minutes at room temperature. Then 100 μl of 1M Tris pH 9.5 was added to each reaction, and the fluorescence was measured with an excitation of 380 nm and an emission of 450 nm. A sequence was considered functional if its end-point activity was at least 50% of Bgl3's.

4.5.10 Thermostability measurements

A Bgl3 variant was expressed overnight, shaking at 37 °C in a 5 ml MagicMedia (Invitrogen) culture. The cells from the expression culture were pelleted and frozen. The cell pellets were resuspended in lysis buffer [0.3x BugBuster (Novagen), 30 KU/ml rLysozyme (Novagen), and 50 U/ml DNase I (New England Biolabs) in 100 mM potassium phosphate, pH 7]. Serial dilutions of the lysate were performed to determine the linear range of the enzyme assay, and all samples were diluted in lysis buffer to be within the linear range and have similar end-point activities.

The diluted cell extracts were arrayed into 96-well PCR plates. Using a gradient thermocycler, the samples were heated over multiple temperatures (typically 45-70°C) for 10 minutes. After the heat step, the remaining functional enzyme was quantified by adding the substrate 4-Methylumbelliferyl-β-D-glucopyranoside (Sigma) to a final concentration of 1 mM. After reacting for 15 minutes, the fluorescence was measured with an excitation and emission of 380 nm and 450 nm, respectively. The T_{50} (temperature where 50% of the protein is inactivated in 10 minutes) was determined by fitting a shifted sigmoid function to the thermal inactivation curves. All measurements were performed in at least triplicate and the median T_{50} values are reported.

4.6 Supplementary figures

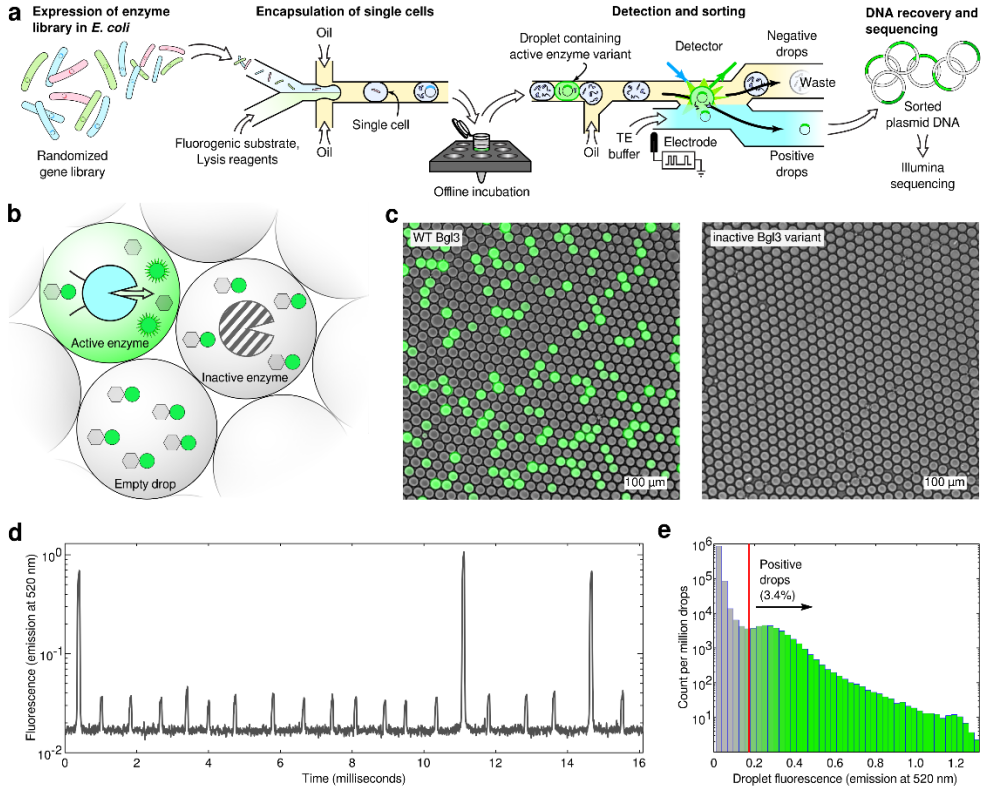

Figure S 4.1 Microfluidic beta-glucosidase assay. (a) An overview of the microfluidic screening workflow. A library of enzyme variants is expressed in E. coli, and single cells are encapsulated in microdroplets that contain lysis reagents and a fluorogenic substrate. The droplets are incubated offline at 37 °C and reinjected onto a microfluidic sorting device. The florescence of each droplet is analyzed. If a droplet's fluorescence meets the specified criteria, an electric pulse is used to merge its contents with the aqueous collection stream. The sorted DNA is then recovered for downstream processing. (b) The fluorogenic substrate produces a strong green fluorescence signal upon hydrolysis by a beta-glucosidase. Bright droplets contain an active enzyme variant, while dark droplets could be empty (no E. coli) or contain an inactive enzyme variant. (c) Microscopy images of the emulsion-based enzyme assay. Both panels show an overlay of bright-field and fluorescence (FITC channel) images with the same exposure and image settings. The left panel shows droplets containing WT Bgl3, while the right panel shows the results using an inactive (truncated) Bgl3 variant. (d) A time trace from the photomultiplier tube (PMT) fluorescence detection system (Supplementary Figure 8). The three large peaks correspond to droplets containing WT Bgl3, while the remaining peaks are empty droplets. Droplets are analyzed at 1.3 kHz. (e) A histogram showing the fluorescence intensities of the Bgl3 random mutagenesis library. The red line indicates the threshold that was used for the sorting experiments.

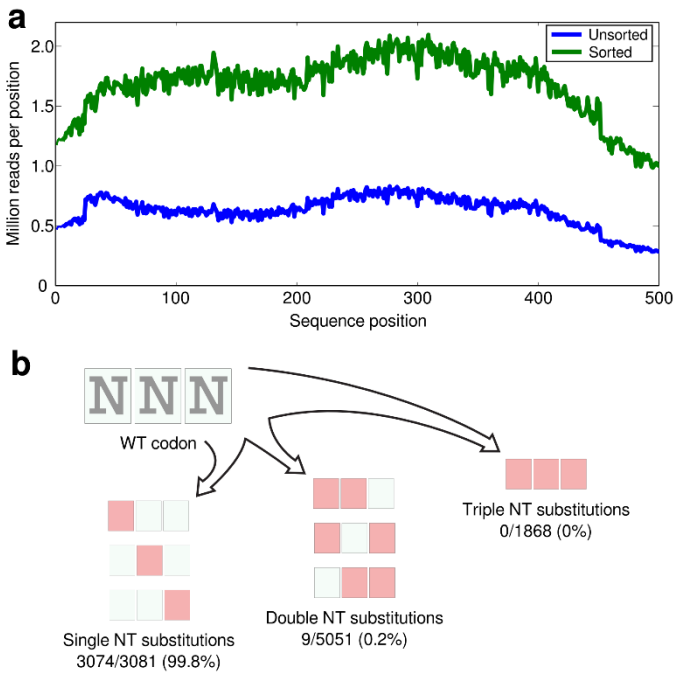

Figure S 4.2 Sequencing and mutational coverage. (a) The sequencing coverage for the unsorted and sorted libraries. The Nextera XT kit gave roughly uniform coverage across the Bgl3 gene. We observed at least one million reads for every position in the sorted library. (b) There are 500 positions in the Bgl3 construct and each of these positions can be mutated to 20 other amino acids (including the stop codon), for a total of 10,000 possible substitutions. Of these 10,000 amino acid substitutions, 3018 can be reached by a single nucleotide substitution, 5051 require two nucleotide substitutions within a single codon, while the remaining 1868 require all three nucleotides to be mutated. With the random mutagenesis library, we are analyzing nearly all (99.8%) of the amino acid substitutions that can be reached by a single nucleotide substitution. As expected, the coverage of amino acid substitutions requiring two or three nucleotide changes within a single codon is much lower.

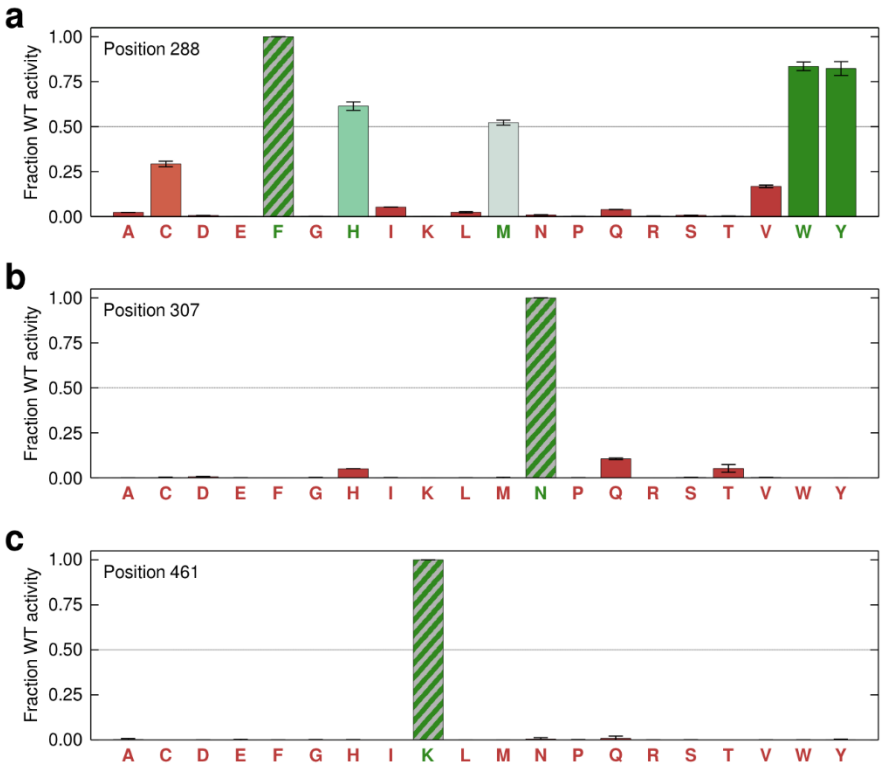

Figure S 4.3 Further validation of site-specific mutational tolerance. Sites of interest were investigated by constructing all possible amino acid substitutions and testing each mutant's end-point activity. Activity values are shown relative to wild type (striped bar). (a) Mutagenesis of position 288 showed that only 4/19 (21%) of amino acid substitutions are tolerated. Based on the fact that other tolerated amino acids include His, Trp, and Tyr, we hypothesize that F288 could be involved in cation-π interactions with two structurally adjacent arginine residues. (b,c) Positions 307 and 461 cannot accept any mutations.

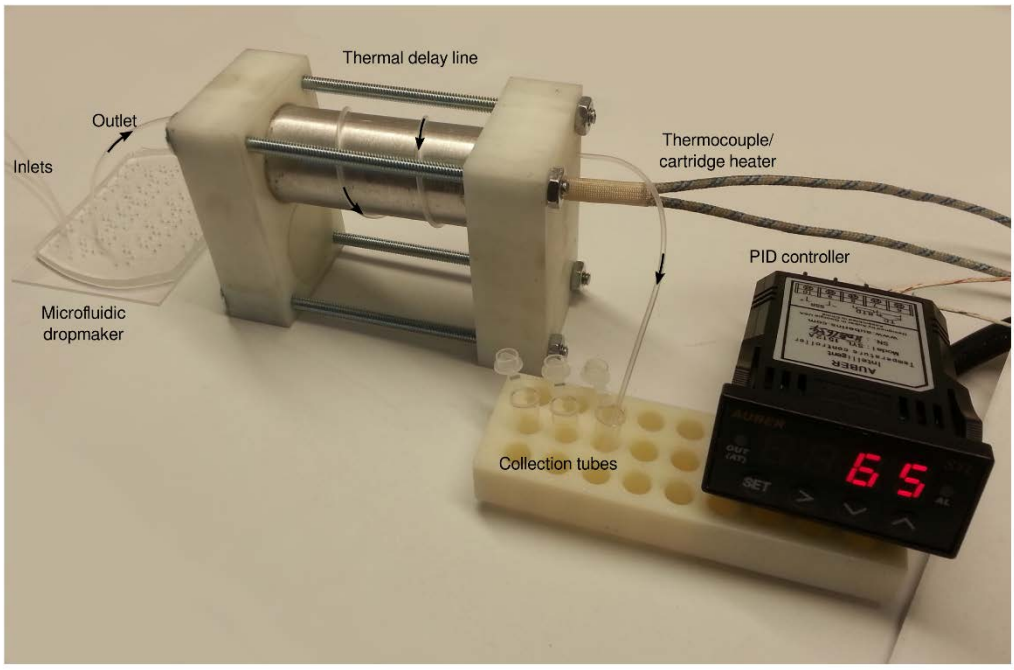

Figure S 4.4 Thermal inactivation device used for high-temperature screening. An aluminum cylinder was interfaced with a thermocouple and a cartridge heater, and a PID controller was used to hold the cylinder at 65 °C. The microemulsions were made using a microfluidic droplet maker and immediately flowed through a thermal delay line coiled around the heated cylinder. The length of polyethylene tubing was adjusted to incubate the droplets for approximately 10 minutes. After the heat challenge, the emulsions were collected and processed using the standard workflow.

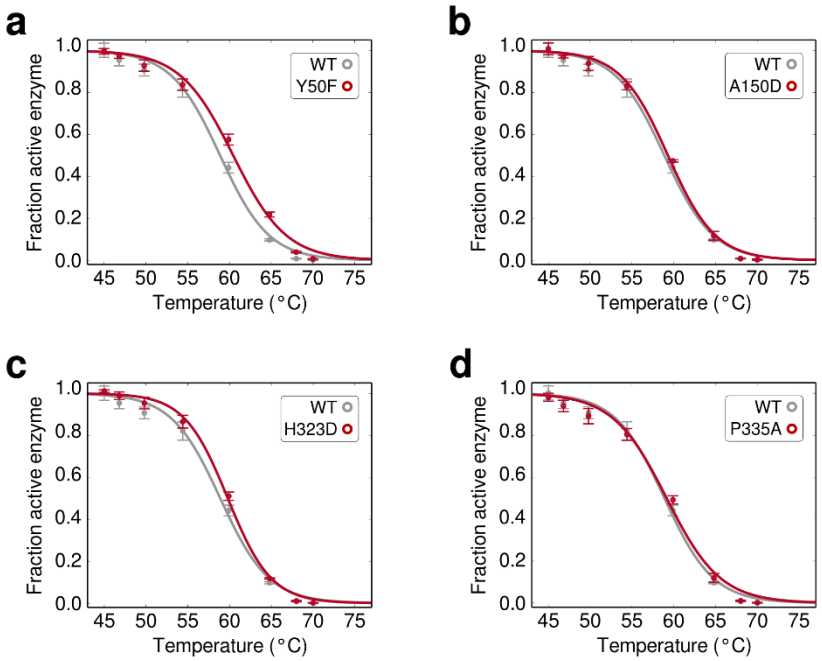

Figure S 4.5 Thermal inactivation curves for enriched Bgl3 mutants. All mutants were assayed in conditions that matched the original microfluidic screening protocol.

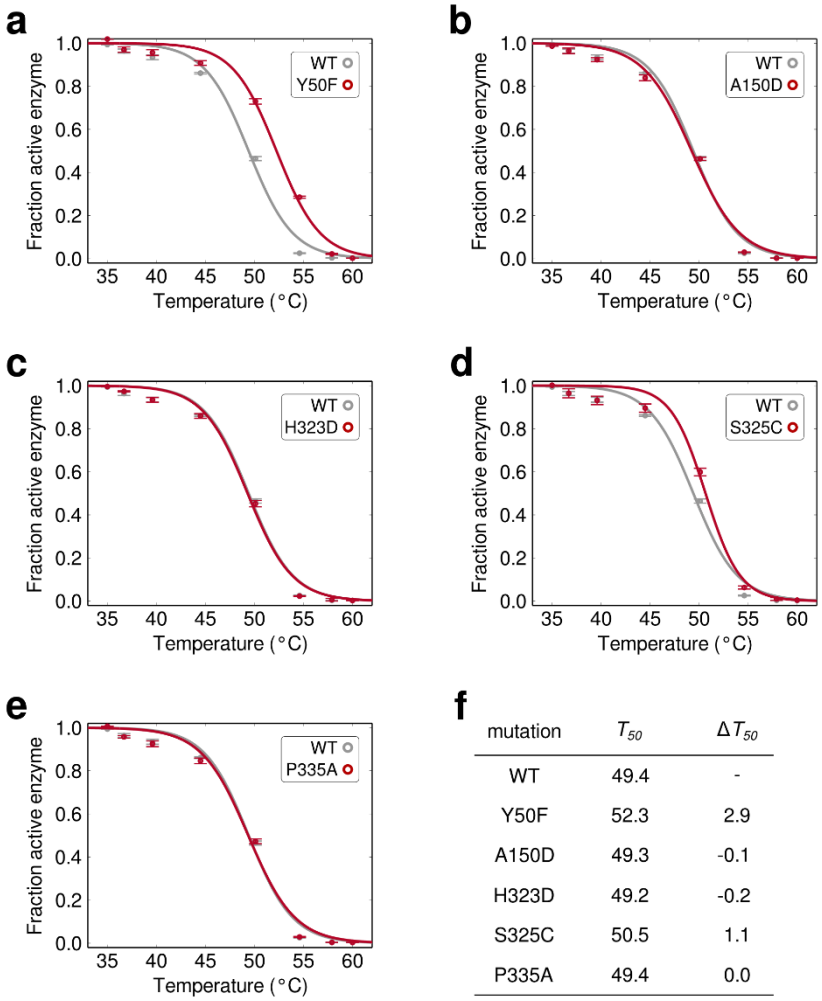

f

mutation	T_{50}	ΔT_{50}
WT	49.4	-
Y50F	52.3	2.9
A150D	49.3	-0.1
H323D	49.2	-0.2
S325C	50.5	1.1
P335A	49.4	0.0

Figure S 4.6 Thermostability of Bgl3 mutants in 100 mM potassium phosphate, pH 7. Cells were lysed using sonication rather than detergents and lysozyme. (a-e) Thermal inactivation curves for enriched Bgl3 mutants. (f) Summary of thermostability measurements in 100 mM potassium phosphate, pH 7. All measurements were performed in at least triplicate and the median T50 values are reported. The absolute T50 values decrease when assayed in pure buffer, which we attribute to a stabilizing effect caused by the lysis detergents used in the microfluidic screen. In addition, the magnitudes of the stability increases (ΔT50) tend to be lower when tested under conditions different from the original screening conditions.

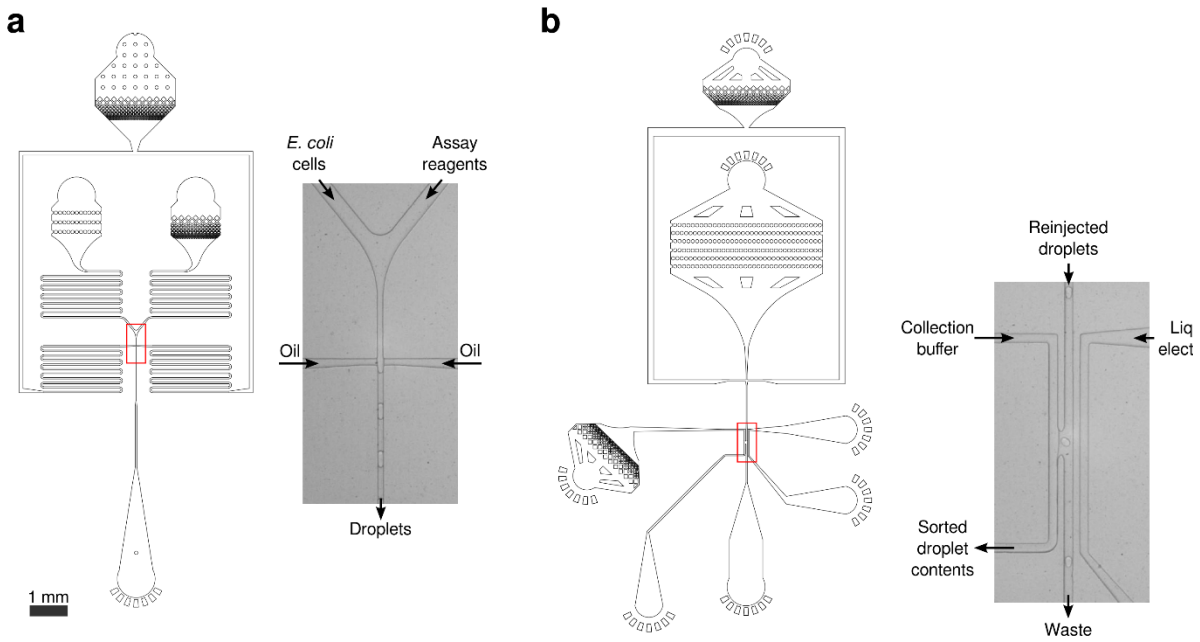

Figure S 4.7 Illustrations and microscopy images of the microfluidic devices used in this work. Both devices had channels 20 μm tall. (a) Droplet maker device with a microscopy image of the device in operation. The droplet making junction is a cross 15 μm wide on all edges. The cell suspension enters the left inlet and the assay reagents the right inlet. Immediately after these two aqueous streams combine, the oil pinches off monodisperse droplets. The serpentine channels act as flow resistors that dampen pressure fluctuations. (b) Sorting device with microscopy image of device in operation. Close-packed droplets are reinjected onto the chip and spaced with addition of oil. If a droplet meets the desired fluorescence criteria, then a series of electric pulses is applied to the collection buffer. The applied electric field destabilizes the interface between the droplet and the adjacent aqueous stream, and surface tension pulls the sorted droplet into the aqueous collection stream. The liquid electrode serves as a ground and an electrostatic shield.

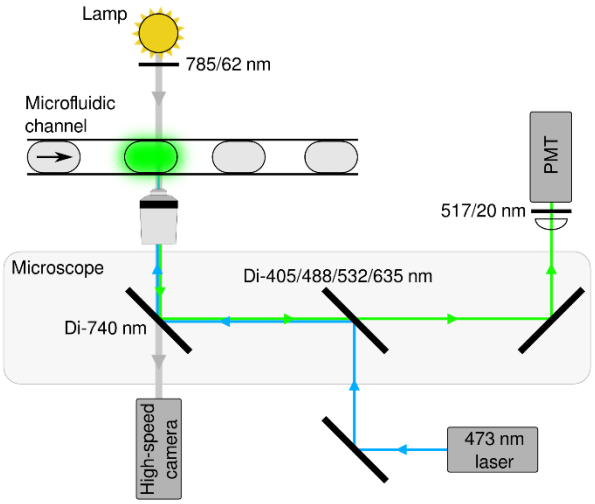

Figure S 4.8 Fluorescence detection system. The fluorescence of each droplet is analyzed using an epifluorescence microscope. A 473 nm laser is used to excite each droplet, and the fluorescence emission is measured using a photomultiplier tube (PMT) with a 517 nm bandpass filter. Simultaneously, an incandescent lamp is used for high-speed, bright-field imaging of the microfluidic channel.

References

1. Wolfenden, R. & Snider, M. J. The depth of chemical time and the power of enzymes as catalysts. *Acc. Chem. Res.* **34,** 938–945 (2001).
2. Baker, D. An exciting but challenging road ahead for computational enzyme design. *Protein Sci.* **19,** 1817–1819 (2010).
3. Lassila, J. K., Baker, D. & Herschlag, D. Origins of catalysis by computationally designed retroaldolase enzymes. *Proc. Natl. Acad. Sci. U. S. A.* **107,** 4937–4942 (2010).
4. Frushicheva, M. P., Cao, J., Chu, Z. T. & Warshel, A. Exploring challenges in rational enzyme design by simulating the catalysis in artificial kemp eliminase. *Proc. Natl. Acad. Sci. U. S. A.* **107,** 16869–16874 (2010).
5. Fowler, D. M. & Fields, S. Deep mutational scanning: a new style of protein science. *Nat. Methods* **11,** 801–807 (2014).
6. Fowler, D. M. *et al.* High-resolution mapping of protein sequence-function relationships. *Nat. Methods* **7,** 741–746 (2010).
7. Hietpas, R. T., Jensen, J. D. & Bolon, D. N. A. Experimental illumination of a fitness landscape. *Proc. Natl. Acad. Sci. U. S. A.* **108,** 7896–7901 (2011).
8. Whitehead, T. A. *et al.* Optimization of affinity, specificity and function of designed influenza inhibitors using deep sequencing. *Nat. Biotechnol.* **30,** 1–9 (2012).
9. McLaughlin Jr, R. N., Poelwijk, F. J., Raman, A., Gosal, W. S. & Ranganathan, R. The spatial architecture of protein function and adaptation. *Nature* **491,** 138–142 (2012).
10. Agresti, J. J. *et al.* Ultrahigh-throughput screening in drop-based microfluidics for directed evolution. *Proc. Natl. Acad. Sci. U. S. A.* **107,** 4004–9 (2010).

11. Kintses, B. *et al.* Picoliter cell lysate assays in microfluidic droplet compartments for directed enzyme evolution. *Chem. Biol.* **19,** 1001–1009 (2012).

12. Granieri, L., Baret, J. C., Griffiths, A. D. & Merten, C. A. High-Throughput Screening of Enzymes by Retroviral Display Using Droplet-Based Microfluidics. *Chem. Biol.* **17,** 229–235 (2010).

13. Fallah-Araghi, A., Baret, J.-C., Ryckelynck, M. & Griffiths, A. D. A completely in vitro ultrahigh-throughput droplet-based microfluidic screening system for protein engineering and directed evolution. *Lab Chip* **12,** 882–91 (2012).

14. Fidalgo, L. M. *et al.* From microdroplets to microfluidics: Selective emulsion separation in microfluidic devices. *Angew. Chemie Int. Ed.* **47,** 2042–2045 (2008).

15. Perez-Pons, J. A. *et al.* A beta-glucosidase gene (bgl3) from Streptomyces sp. strain QM-B814. Molecular cloning, nucleotide sequence, purification and characterization of the encoded enzyme, a new member of family 1 glycosyl hydrolases. *Eur. J. Biochem.* **223,** 557–565 (1994).

16. Jacquier, H. *et al.* Capturing the mutational landscape of the beta-lactamase TEM-1. *Proc. Natl. Acad. Sci. U. S. A.* **110,** 13067–13072 (2013).

17. Guo, H. H., Choe, J. & Loeb, L. A. Protein tolerance to random amino acid change. *Proc. Natl. Acad. Sci. U. S. A.* **101,** 9205–9210 (2004).

18. Bloom, J. D. *et al.* Thermodynamic prediction of protein neutrality. *Proc. Natl. Acad. Sci. U. S. A.* **102,** 606–611 (2005).

19. Bershtein, S., Segal, M., Bekerman, R., Tokuriki, N. & Tawfik, D. S. Robustness-epistasis link shapes the fitness landscape of a randomly drifting protein. *Nature* **444,** 929–932 (2006).

20. Zechel, D. L. & Withers, S. G. Glycosidase mechanisms: Anatomy of a finely tuned catalyst. *Acc. Chem. Res.* **33,** 11–18 (2000).

21. Davies, G. & Henrissat, B. Structures and mechanisms of glycosyl hydrolases. *Structure* **3,** 853–859 (1995).

22. Marana, S. R. Molecular basis of substrate specificity in family 1 glycoside hydrolases. *IUBMB Life* **58,** 63–73 (2006).

23. Halabi, N., Rivoire, O., Leibler, S. & Ranganathan, R. Protein sectors: evolutionary units of three-dimensional structure. *Cell* **138,** 774–786 (2009).

24. Sullivan, B. J. *et al.* Stabilizing proteins from sequence statistics: The interplay of conservation and correlation in triosephosphate isomerase stability. *J. Mol. Biol.* **420,** 384–399 (2012).

25. Adkar, B. V *et al.* Protein model discrimination using mutational sensitivity derived from deep sequencing. *Structure* **20,** 371–381 (2012).

26. Wu, N. C. *et al.* Systematic Identification of H274Y Compensatory Mutations in Influenza A Virus Neuraminidase by High-Throughput Screening. *J. Virol.* **87,** 1193–1199 (2013).

27. Wagenaar, T. R. *et al.* Resistance to vemurafenib resulting from a novel mutation in the BRAFV600E kinase domain. *Pigment Cell Melanoma Res.* **27,** 124–133 (2014).

28. Sciambi, A. & Abate, A. R. Accurate, Chip-Based Sorting of Microfluidic Drops at 29kHz. *Prep.* (2014).

29. Aharoni, A., Griffiths, A. D. & Tawfik, D. S. High-throughput screens and selections of enzyme-encoding genes. *Curr. Opin. Chem. Biol.* **9,** 210–216 (2005).

30. Lim, S. W. & Abate, A. R. Ultrahigh-throughput sorting of microfluidic drops with flow cytometry. *Lab Chip* **13,** 4563–72 (2013).

31. Zinchenko, A. *et al.* One in a million: Flow cytometric sorting of single cell-lysate assays in monodisperse picolitre double emulsion droplets for directed evolution. *Anal. Chem.* **86,** 2526–2533 (2014).

32. Sia, S. K. & Whitesides, G. M. Microfluidic devices fabricated in poly(dimethylsiloxane) for biological studies. *Electrophoresis* **24,** 3563–3576 (2003).

33. Bloom, J. D. *et al.* Evolution favors protein mutational robustness in sufficiently large populations. *BMC Biol.* **5,** 29 (2007).

34. Quan, J. & Tian, J. Circular polymerase extension cloning for high-throughput cloning of complex and combinatorial DNA libraries. *Nat. Protoc.* **6,** 242–251 (2011).

35. Langmead, B. & Salzberg, S. L. Fast gapped-read alignment with Bowtie 2. *Nat. Methods* **9,** 357–359 (2012).

36. Lombard, V., Golaconda Ramulu, H., Drula, E., Coutinho, P. M. & Henrissat, B. The carbohydrate-active enzymes database (CAZy) in 2013. *Nucleic Acids Res.* **42,** 490–495 (2014).

37. Edgar, R. C. MUSCLE: multiple sequence alignment with high accuracy and high throughput. *Nucleic Acids Res.* **32,** 1792–1797 (2004).

38. Dereeper, A. *et al.* Phylogeny.fr: robust phylogenetic analysis for the non-specialist. *Nucleic Acids Res.* **36,** (2008).

Chapter 5: Electrical lysis of cells for detergent-free droplet assays

The following section is reprinted from "Electrical lysis of cells for detergent-free droplet assays" by Niek de Lange, Tuan Tran and Adam Abate. It was published in Biomicrofluidics on March 22 2016. Niek de Lange, Tuan Tran and Adam Abate. designed the experiments; Tuan Tran and Niek de Lange performed the experiments and analyzed the data; Niek de Lange Tuan Tran and Adam Abate wrote the manuscript.

5.1 Abstract

Efficient lysis is critical when analyzing single cells in microfluidic droplets, but existing methods utilize detergents that can interfere with the assays to be performed. We demonstrate robust cell lysis without the use of detergents or other chemicals. In our method, cells are exposed to electric field immediately before encapsulation in droplets, resulting in cell lysis. We characterize lysis efficiency as a function of control parameters and demonstrate compatibility with enzymatic assays by measuring the catalysis of ß-glucosidase, an important cellulase used in the conversion of biomass to biofuel. Our method enables assays in microfluidic droplets that are incompatible with detergents.

5.2 Introduction

Cellular heterogeneity is important in a variety of biological systems, from providing robustness to evolutionary stresses to enabling effective immune responses against diverse threats (1-3). Because the heterogeneity exists at the level of single cells, studying these systems requires methods for high-throughput single cell analysis. Flow cytometry enables the detection, characterization, and sorting of single cells at throughputs of >1,000 per second (4) allowing large populations to be screened in hours; however, it is limited by its dependence on affinity reagents

that specifically label the target cell so that it can be detected within a mixed population. Droplet microfluidics breaks through this barrier by allowing single cells to be analyzed using soluble assays, such as enzyme catalysis,(5) detection of secreted products, (6-8) or presence of unique nucleic acid sequences.(9, 10) The devices achieve this using tools for rapidly generating,(11) merging,(12) injecting,(13) and sorting droplets (14) for applications including single-cell sequencing,(15, 16) directed evolution,(17, 18) and drug screening.(19)

When using droplet microfluidics for high-throughput single cell analysis, cellular lysis is essential to provide access to cell contents, such as specific small molecules, proteins, or nucleic acids.(10, 20-22) Lysis of cells can be achieved using chemical (e.g. detergents) (9, 10), optical (e.g. pulsed laser) (23), mechanical (e.g. nanoknives) (24), acoustic (e.g. sonication) (25) or electrical (26) techniques. In droplet microfluidics robust lysis is most commonly achieved using proteases and detergents that digest proteins and solubilize cellular lipids.(9, 10) However, proteases can digest the enzymes necessary for assays, while detergents are difficult to remove from droplets once added and can interfere with important interactions between molecules. Consequently, when using these components to lyse cells, compatible assays must be carefully selected and, even then, the assay may be influenced by their presence. For example, detergents commonly used for lysing cells can perturb the stability and activity of enzymes so that measurements performed with detergents often do not agree with ones performed detergent-free.(27) To enable greater flexibility when choosing assays with which to analyze single cells in microfluidic droplets, new, chemical-free methods are needed for lysing cells.

In this paper, we present a simple, chemical-free method for lysing cells compatible with nearly any droplet assay. Previous work has demonstrated the ability to generate pores in cell membranes by applying electric fields, a method known as electroporation.(28) This is often used

to introduce components into cells that cannot normally pass the membrane, such as nucleic acids and certain small molecules, and can be performed with microfluidics.(29-37) Here, we extend this concept to lyse cells by applying an electric field immediately before merging the cell stream with lysozyme and encapsulating the mixture in droplets. Pulses above the electroporation threshold have been shown to generate pores in the cell membrane that persist for seconds to minutes after the field is removed, providing ample time for lysosome to diffuse into the cell and inter-membrane space and digest the cell wall, ultimately culminating in lysis. As we demonstrate, with lysozyme alone, lysis is poor, whereas when the electric field pulse is added, lysis efficiencies >90% can be achieved. We characterize the dependence of lysis efficiency on multiple parameters and use the method to measure the activity of ß-glucosidase, a cellulase used in biomass deconstruction. Our lysis approach broadens the types of assays that can be used in droplet microfluidics without sacrificing lysis efficiency.

5.3 Materials and methods

5.3.1 A. Microfluidic Fabrication

Photoresist (SU-8 3010) is spin coated onto silicon wafers and cross-linked in the pattern of the microfluidic device using photo-masks and ultra-violet light exposure, followed by development of the master and baking. Poly(dimethylsiloxane) (PDMS) replicas of the device (38) are cast by pouring 11:1 ratio of base to curing agent (Sylgard 184, Dow Chemical, MI, USA) and baking at 80 °C for 1 hour. The replicas are extracted from the wafer with a scalpel and access holes are punched with a 0.75 mm biopsy punch. The device is rinsed with isopropanol and bonded to a glass slide using oxygen plasma treatment. All devices are treated with Aquapel (PPG Industries)

and baked for 30 minutes at 80 °C to render them hydrophobic for water-in-fluorinated oil emulsification. The height of the fabricated channels are 20 µm.

5.3.2 GFP Assay

GFP is cloned into the pET-22b vector and transformed into electrocompetent BL21(DE3) *E. coli* (Lucigen). Expression recovery media (Lucigen) is used to recover transformed cells by incubating at 37 ºC for 1 hour. A glycerol stock of the library is made by combining cell media with 50% glycerol, and stored at -80 ºC until use. 5 ml MagicMedia (Invitrogen) expression culture is inoculated using the glycerol stock library and incubated overnight at 37 ºC, followed by pelleting and re-suspension in the assay buffer (100 mM tris(hydroxymethyl)aminomethane (Tris), pH 7.5). The cell solution is further diluted in the assay buffer to achieve an OD600 of 0.025. The lysozyme solution is produced by diluting rLysozyme (Novagen) to a final concentration of 60 KU/ml in 100 mM Tris, pH 7.5. In the experiments, multiple parameters are varied including aqueous flow rates (50 and 100 µl/h), oil flow rates (200, 300, 400, 600 µl/h), salt concentrations in the assay buffers (0, 50, 100, 200, 500 mM NaCl), electroporation channel dimensions (30x5000, 60x2500; 120x1250; 240x625 µm) and the presence of lysozyme.

5.3.3 ß-Glucosidase Assay

A *BGL3* gene insert is cloned into the pET-22b vector and transformed into electrocompetent BL21(DE3) *E. coli* (Lucigen). Expression recovery media (Lucigen) is used to recover the transformed cells by incubating at 37 ºC for one hour and cell plating. Once colonies have developed, they are stored at 4 ºC until use. A single colony is used to inoculate a 5 ml MagicMedia (Invitrogen) expression culture. The culture is incubated 37 ºC overnight, pelleted, and re-

suspended in the assay buffer (100 mM potassium phosphate, pH 7.2). The cell solution is further diluted in assay buffer to a final cell suspension of OD600 of 0.025 in combination with 1 µg/ml DAPI (4',6-Diamidino-2-Phenylindole, Dihydrochloride) (Life Technologies). The lysis buffer for detergent based lysis consists of 0.6x BugBuster (Novagen), 60 KU/ml rLysozyme (Novagen) and 200 µM fluorescein di-(β-D-glucopyranoside) (Sigma) in 100 mM potassium phosphate, pH 7.

5.3.4 Microfluidic Device Operation

Microdroplets are generated using a co-flow electroporation droplet maker (Figure 5.1) consisting of an inlet for the cell suspension and a co-flow inlet for the lysis buffer, followed by a cross-junction into which oil is introduced (HFE-7500 fluorinated oil with 2 wt% fluorinated surfactant, RAN Technologies) to generate the droplets. Cell densities are controlled to yield ~1 cell per 10 drops. The generated Droplets (~27-29 µm in diameter) are collected into 1.5 ml Eppendorf tubes and incubated at room temperature for 5-10 minutes prior to imaging. The cell stream flows

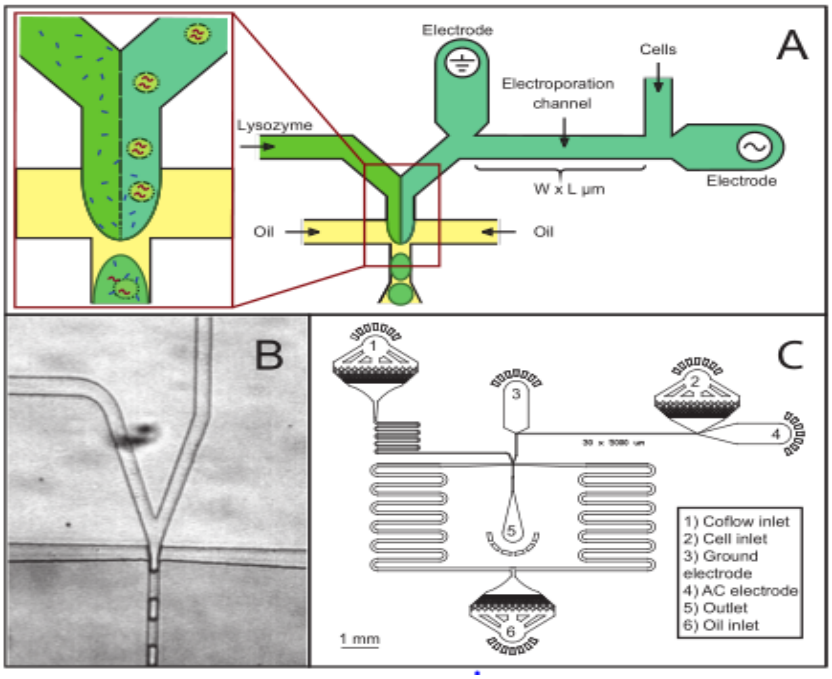

Figure 5.1 Schematic representation of electrical lysis for droplet screening. (A) Schematic of the electrical lysis part and co-flow droplet generation part of the microfluidic device. (B) Actual image of the droplet generation part. (C) A to-scale view of the whole electrical lysis device with electroporation channel dimensions of 30 µm by 5000 µm.

through an electrified channel to initiate electrically-induced cell lysis before merging with the lysis buffer stream. To generate an electric field in the electroporation channel, electrodes consisting of lead-free solder material (Super Solder, 0.8 mm alloy no. 60) are connected to an AC amplifier (JKL Components Corp., 289-1170-ND) powered by a DC supply. The voltage is applied as a 34 KHz sine wave with amplitude 0 to 1300 V, from which we calculate the field applied to the cells by modeling the electrical resistivity of the conducting electrolyte-filled channels through which the cells pass as they enter the droplet generator (29, 30). We estimate the maximum amplitude of the currents to be ~12 mA. Since the electrodes are in contact with the aqueous phase carrying the cells, it is possible that electrochemical products generated by the flow of current may end up in the encapsulating droplets; however, we do not directly observe any such products nor do the assays we perform seem to be perturbed.

5.3.5 Lysis quantification

Droplets are loaded into Countess cell counting chamber slides (Life Technologies) and single layers are imaged using an inverted fluorescence microscope (EVOS® FL Auto Imaging System, life technologies) in bright field and fluorescence modes with 470/22 nm wavelength excitation and 510/42 nm emission (GFP channel). Droplets for the ß-glucosidase experiment are additionally imaged with 357/44 nm excitation and 447/60 nm emission to visualize DAPI, a DNA stain which we used to identify drops containing cells.

5.3.6 Image Analysis

Bright field and fluorescence images are analyzed using ImageJ by selecting a threshold such that droplets or cells appear as disconnected areas on a dark background. Areas of 18-400 μm^2 correspond to small, unlysed cells with localized fluorescence, while ones with 400-1000 μm^2 correspond to lysed cells in which the cell lysate diffuses into the encapsulating droplet, making the droplet diffusely fluorescent. Lysis efficiency is calculated as the number of lysed cells divided by the sum of lysed and unlysed cells.

5.4 Results and discussion

A principal advantage of droplet microfluidics is the extremely high throughput with which individual cells can be analyzed using soluble assays. Leveraging this advantage requires a robust method for lysing cells that minimally interferes with the assays to be performed. Our method for accomplishing this is to flow the cells through a channel with high electric field before encapsulating them in droplets. This pulses the cells with electric field, where the duration of the pulse is determined by flow rate and the amplitude by channel geometry and voltage. We also

include lysozyme, an enzyme that digests bacterial cell walls but minimally interferes with most assays, via a second channel that intersects with the cell-containing channel at the droplet maker, as shown in Figure 5.1A. An image of the droplet generator is provided in Figure 5.1B and a to-scale schematic of the entire device in Figure 5.1C. As a cell passes through the device, it first flows through the electric field channel; the electric field is sufficient to electroporate the cells, but they remain intact as cell bodies. In addition, the Péclet number relating the ratio of advective to diffusive transport is ~10,000, indicating that as the cells travel through the electrification channel, they remain localized in their streamlines; this ensures that each cell's lysate is encapsulated into a single droplet.

To investigate the ability of this technique to lyse bacterial cells, we test the approach with *E. coli* engineered to express green fluorescent protein (GFP). We flow the cells into the device at 100 µl/h using a 30 µm x 5000 µm x 20 µm electroporation channel, exposing them to the electric

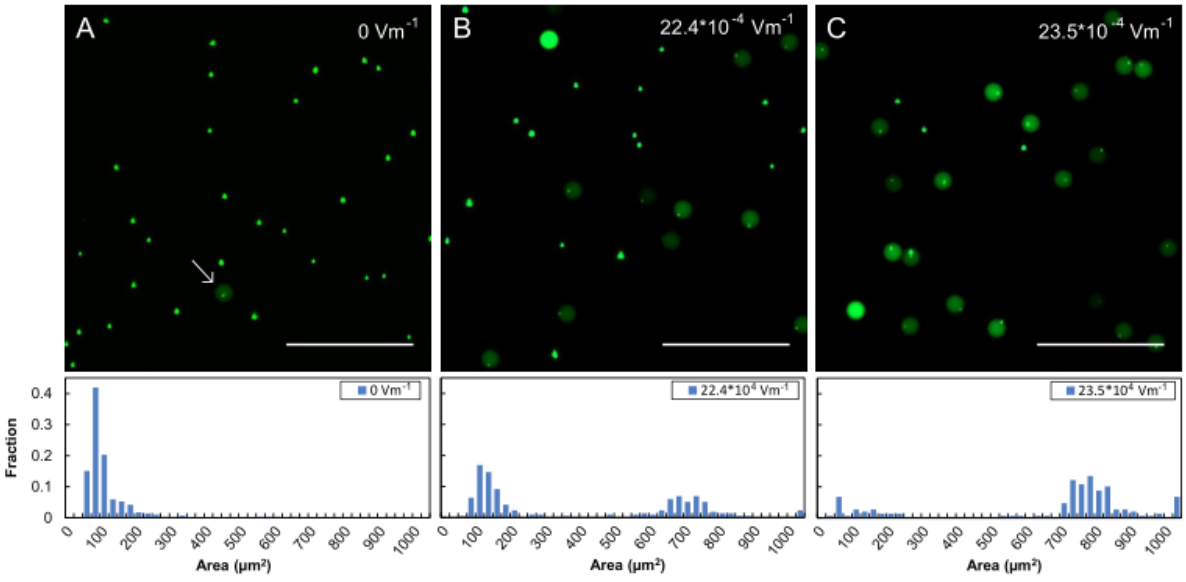

Figure 5.2 Example of the effects of electrical lysis on encapsulated E. coli cells expressing GFP. Green fluorescence pictures of the cells taken when A) no electric field was applied, B) $22.4*10^4$ Vm^{-1} was applied and C) $23.5*10^4$ Vm^{-1} was applied. As the electric field increases, the fraction of lysed cells increases which is quantitatively shown in the histogram below the picture. The scale bar in the pictures represents 100 µm.

field for ~100 ms prior to encapsulation. The parallel co-flow stream contains the lysis comprising lysozyme introduced at the same flow rate. After passing through the device and being encapsulated in the droplets, unlysed *E. coli* appear as compact, bright puncta a few microns in diameter, while lysed cells appear as diffuse green fluorescence filling the encapsulating droplet. When no field is applied, 99% of cells remain unlysed, as shown in Figure 5.2A. By contrast, when we increase the electric field to 22.4×10^4 Vm^{-1} roughly half the cells lyse (Figure 5.2B) while at 23.5×10^4 Vm^{-1}, ~70% lyse (Figure 5.2C). These results can be rationalized based on the membrane structure of *E. coli*, which have an inner and outer membrane separated by a cell wall. Lysis occurs when the bacterial membrane is irreversibly permeabilized. While electroporation can create pores in the cell membrane, bacteria also possess a cell wall that protects their inner membrane. Lysozyme breaks down this cell wall to enhance lysis efficiency.(39, 40) Indeed, lysozyme lyses cells slowly over time, which is why it must be added immediately before encapsulation using co-flow droplet generation; if it was added to the cell suspension long before encapsulation, pre-lysis in the syringe would allow the lysates of different cells to mix, precluding the execution of pure single cell assays. Co-flow droplet generation enables this because cell and lysozyme solutions do not mix until they are encapsulated in the droplets, due to laminar flow conditions.(41)

The electric fields we apply are comparable to what's used in the food industry (20-40 kV/cm) to lyse microbes for food preservation. Multiple studies have investigated enzyme inactivation by exposure to such electric fields and have found, generally, that enzymes are more resistant to electric fields than microbes,(42, 43); above a threshold field, enzyme activity can be reduced, though the behavior depends on the enzyme under consideration.(44)

Achieving efficient cell lysis requires knowledge of the parameters that most greatly impact the electroporation process. To investigate this, we systematically vary parameters and observe the

impact on lysis efficiency, Figure 5.3. To measure the lytic effect for lysozyme, each series of experiments includes a control in which we do not apply an electric field; the lysis efficiencies of these experiments are consistently close to zero, which implies that on the timescale of our experiments, lysozyme alone is ineffective for efficient lysis. When we apply the electric field but do not include lysozyme, we obtain lysis efficiencies of <20%, shown by the red points in Figure 5.3A. Combining both lysozyme and electrical lysis improves the lysis efficiency significantly, resulting in lysis efficiencies up to 70% with these conditions.

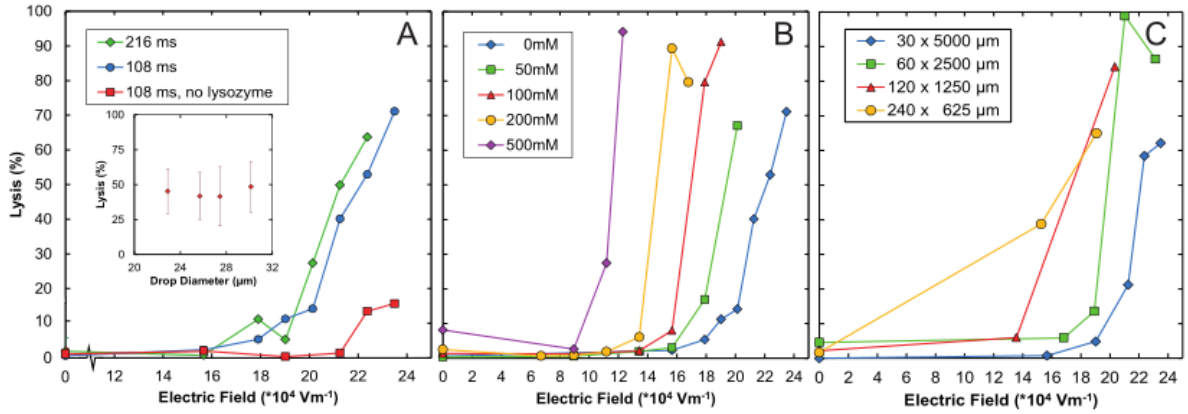

Figure 5.3 Dependence of lysis efficiency for different control parameters. A) Lysis efficiency as a function of voltage for different times of field exposure, with and without lysozyme. Inset) Lysis percentage versus drop diameter showing little dependence. Achieved by varying oil flow rate. B) Lysis efficiency as a function of voltage for different salt concentrations showing substantial dependence. Highest condition is equivalent to saltwater of the ocean. C) Lysis efficiency as a function of voltage for different channel dimensions, holding the time of field exposure for the cell constant.

An important parameter is the time the cell is exposed to the electric field, since this influences the duration that the pores are maintained through which lysozyme can enter. Millisecond pulses in the range of 1 KV/cm, comparable to what we apply, can yield pores with lifetimes of minutes, providing ample time for lysozyme to diffuse into the inter-membrane space,(28) where it can digest the cell wall. To vary this parameter, we adjust the flow rate of the cell solution using the 30 x 5000 μm device (Figure 3A). When lysozyme is present, the fraction of cells lysed strongly

increases with amplitude of the electric field, but does not depend strongly on the duration of field exposure for the range tested, as shown by the green and blue points in Figure 5.3a. This indicates that even the shortest pulse duration is able to generate pores sufficient for cell lysis. To confirm that these results do not depend on the size of the encapsulating droplets, which decreases as we reduce flow rate to increase field exposure time, we perform a second series of experiments holding exposure time and field strength constant, varying droplet size by adjusting carrier oil flow rate. However, again, there appears to be little dependence of lysis efficiency on this parameter, as shown in Figure 5.3A, inset.

Another parameter that impacts lysis efficiency is the conductivity of the buffer: Holding field amplitude constant, higher buffer conductivity increases electric current which can, in turn, impact lysis efficiency. To investigate this, we vary buffer conductivity by adjusting NaCl concentration while holding other parameters constant (Figure 5.3B). Similar to previous experiments, we find that, generally, the fraction of lysed cells increases strongly with electric field, with a range of low fields in which very little lysis is observed, followed by an abrupt increase in lysis above a threshold value. We also find that lysis efficiency depends on the conductivity of the buffer, with high conductivity buffers leading to cell lysis at lower fields than low conductivity buffers, as shown in Figure 5.3B. Hence, while salt concentration is an important parameter because it impacts the conductivity of the solution, high or low salt alone is not able to lyse the cells over the timescales we have tested, as shown by the low lysis efficiencies achieved for zero applied field.

The field in the electroporation channel depends on the applied voltage and resistivity of the path connecting the positive and ground electrodes which, in turn, depends on the length of the connecting channel. To investigate this, we vary the lengths and widths of these channels to maintain the time that the cells flow through the channel constant, Figure 5.3C. As expected, there

is only a weak dependence on the shape of the electroporation channel. Importantly, however, the device with wider, shorter channels achieves the needed electric fields to lyse cells at lower voltages; in addition, its hydrodynamic resistance is also lower, lowering the input pressure of the device. Hence, if low operating pressures and voltages are desired, a short, wide electroporation channel is preferable to a long, narrow one.

Our results indicate that there is a threshold field above which electrically-induced lysis becomes efficient and this field is lower when highly conductive buffers are used. Lysozyme, while ineffective on its own, greatly enhances lysis efficiency when used with electroporation. The time of electroporation, geometry of the channel, or size of the encapsulating droplets also affect lysis to varying degrees, as summarized in Figure 5.3

An important example of droplet-based microfluidic screening that relies on robust cell lysis is measuring enzyme catalysis at the single cell level, both for characterizing enzyme activity or enhancing it through droplet-based directed evolution.(17, 18) Chemical lysis is often undesirable because chemicals can interfere with the catalysis assay, whereas our electrical technique adds no interfering chemicals. To demonstrate this, we measure the activities of ß-glucosidase, an enzyme important in the conversion of biomass into biofuel, expressed in *E. coli* (Figure 5.4). We flow the cells through the 30 x 5000 µm electroporation channel at 100 µl/h, dispersing them in potassium phosphate buffer pH 7.2. When the cells are lysed, the enzyme expressed within them leaks into the encapsulating droplet where it catalyzes the breakdown of the substrate producing a fluorescent signal, as shown by the diffusely green-fluorescent droplets inset into Figure 5.4. In agreement with our previous studies utilizing GFP, we find that the percentage of lysed cells increases with electric field strength, with a threshold field of ~14×10^4 Vm^{-1}. To confirm that the observed catalysis results from cells, we stain the cells with DAPI prior to encapsulating them, so that they

appear as small red dots in the image, Figure 5.4. While there are indeed a small number (~20%) of encapsulated cells with no ß-glucosidase in the drops, the majority lyse releasing ß-glucosidase to catalyze the reaction. As a comparison, we repeat the experiment using a chemical lysing agent, BugBuster, to lyse the cells (blue point, 0 electric field Figure 5.4). While BugBuster outperforms electrical lysis for the conditions tested, it only does so by ~10%, and optimization of buffer conductivity and channel dimensions may enable comparable lysis efficiency. Moreover, BugBuster, which contains detergents, can interfere with sensitive catalysis assays.

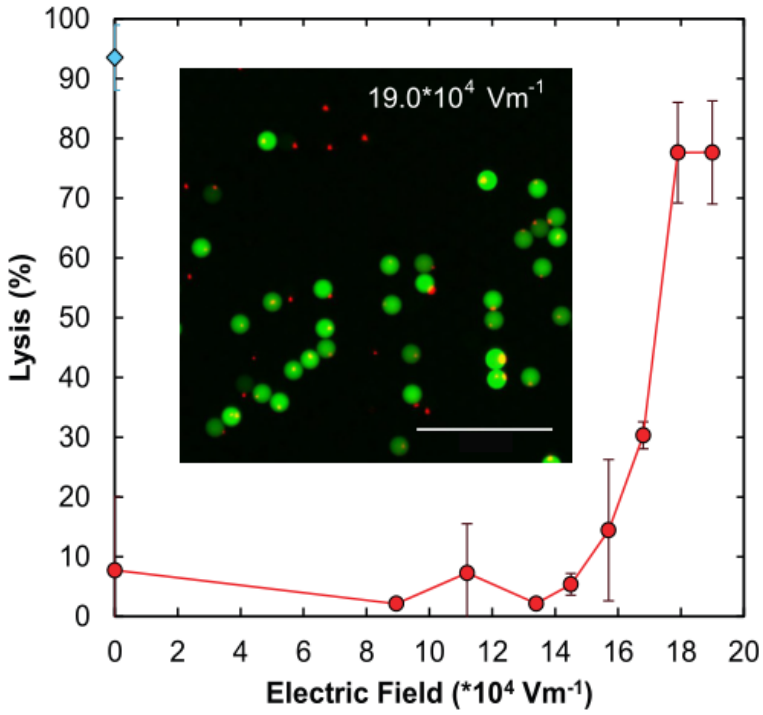

Figure 5.4 Application of electrical lysis for an enzymatic assay. Plot of efficiency of lysis as a function of electric field for E. coli cells expressing the enzyme ß-glucosidase (red curve). The substrate for the enzyme is included in the droplet by the second inlet of the coflow running parallel to the cells downstream of the electrical lysis region. A fluorescence image of the resulting droplets is shown in the inset where the small red dots correspond to the DAPI stained cells and the larger green circles correspond to the encapsulated droplets. The green fluorescence is the product of catalysis of the fluorogenic substrate of ß-glucosidase.

5.5 Conclusions

We have developed a robust method for lysing cells without the use of chemicals or detergents. Our approach is simple to integrate into microfluidic devices and compatible with high throughput single cell screening assays. While our method is limited in throughput by the upper rate at which monodisperse droplets can be generated and the Poisson loading that results in a majority of empty droplets, methods such as bubble-triggered droplet generation, geometrically mediated droplet breakup,(45, 46) and parallelization,(47, 48) can increase droplet generation rate markedly, while inertial ordering can massively reduce the number of empty droplets. (49) The use of high voltages and conductive buffers should be assessed when working with voltage sensitive or heat sensitive proteins. In addition, lysozyme may not be compatible with all assays, and thus may be left out when necessary, but will also reduce lysis efficiency. We anticipate our approach will provide an attractive alternative for applications that require cell lysis, but can be perturbed by the inclusion of common lysing agents, such as when characterizing binding or chemical activity of proteins, for screening and evolution applications. This method should also be valuable for lysing cells in droplets prior to mass-spectrometry analysis, which can be greatly hampered by the inclusion of common detergents. While we have demonstrated this approach with bacteria, we anticipate that it will prove equally effective for enhancing the lysis of other organisms, such as viruses, yeast, and mammalian cells.

References

1. S. Sakaguchi, D. A. Vignali, A. Y. Rudensky, R. E. Niec and H. Waldmann, Nature Reviews Immunology, 13, 461 (2013).
2. M. Hölzel, A. Bovier and T. Tüting, Nature Reviews Cancer, 13, 365 (2013).
3. A. Marusyk, V. Almendro and K. Polyak, Nature Reviews Cancer, 12, 323 (2012).
4. H. M. Davey and D. B. Kell, Microbiological reviews, 60, 641(1996).
5. M. T. Guo, A. Rotem, J. A. Heyman and D. A. Weitz, Lab on a Chip, 12, 2146 (2012).
6. A. J. Hughes, D. P. Spelke, Z. Xu, C.-C. Kang, D. V. Schaffer and A. E. Herr, Nature methods, 11, 749 (2014)
7. Huebner, M. Srisa-Art, D. Holt, C. Abell, F. Hollfelder and J. Edel, Chemical communications, 1218 (2007).
8. T. Konry, M. Dominguez-Villar, C. Baecher-Allan, D. A. Hafler and M. L. Yarmush, Biosensors and Bioelectronics, 26, 2707 (2011).
9. S. W. Lim, T. M. Tran and A. R. Abate, PloS one, 10 (2015).
10. D. J. Eastburn, A. Sciambi and A. R. Abate, Nucleic acids research, gku606 (2014).
11. S.-Y. Teh, R. Lin, L.-H. Hung and A. P. Lee, Lab on a Chip, 8, 198 (2008).
12. D. R. Link, E. Grasland-Mongrain, A. Duri, F. Sarrazin, Z. Cheng, G. Cristobal, M. Marquez and D. A. Weitz, Angewandte Chemie International Edition, 45, 2556 (2006).
13. A. R. Abate, T. Hung, P. Mary, J. J. Agresti and D. A. Weitz, Proceedings of the National Academy of Sciences, 107, 19163 (2010).
14. J.-C. Baret, O. J. Miller, V. Taly, M. Ryckelynck, A. El-Harrak, L. Frenz, C. Rick, M. L. Samuels, J. B. Hutchison and J. J. Agresti, Lab on a Chip, 9, 1850 (2009).

15. R. Novak, Y. Zeng, J. Shuga, G. Venugopalan, D. A. Fletcher, M. T. Smith and R. A. Mathies, Angewandte Chemie, 123, 410 (2011).
16. E. Shapiro, T. Biezuner and S. Linnarsson, Nature Reviews Genetics, 14, 618 (2013).
17. A. Fallah-Araghi, J.-C. Baret, M. Ryckelynck and A. D. Griffiths, Lab on a Chip, 12, 882 (2012).
18. J. J. Agresti, E. Antipov, A. R. Abate, K. Ahn, A. C. Rowat, J.-C. Baret, M. Marquez, A. M. Klibanov, A. D. Griffiths and D. A. Weitz, Proceedings of the National Academy of Sciences, 107, 4004 (2010).
19. G.-S. Du, J.-Z. Pan, S.-P. Zhao, Y. Zhu, J. M. den Toonder and Q. Fang, Analytical chemistry, 85, 6740 (2013).
20. J. Clausell-Tormos, D. Lieber, J.-C. Baret, A. El-Harrak, O. J. Miller, L. Frenz, J. Blouwolff, K. J. Humphry, S. Köster and H. Duan, Chemistry & biology, 15, 427 (2008).
21. X. Leng, W. Zhang, C. Wang, L. Cui and C. J. Yang, Lab on a Chip, 10, 2841 (2010).
22. D. J. Eastburn, A. Sciambi and A. R. Abate, Analytical chemistry, 85, 8016 (2013).
23. K. R. Rau, P. A Quinto-Su, A. N. Hellman and V. Venugopalan, Biophysical journal, 91, 317 (2006)
24. D. Di Carlo, L. Y. Wu and L. P. Lee, Lab on a Chip, 6, 1445 (2006)25H.
25. Zhang and W. Jin, Electrophoresis, 25, 1090 (2004)
26. P. Jen, T. G. Amstislavskaya, Y. H. Liu, J. H. Hsiao, and Y. H. Chen Sensors, 12, 6967 (2012)
27. M. D. Womack, D. A. Kendall and R. C. MacDonald, Biochimica et Biophysica Acta (BBA)-Biomembranes, 733, 210 (1983).
28. M.-P. Rols and J. Teissié, Biophysical journal, 75, 1415 (1998).

29. H.-Y. Wang, A. K. Bhunia and C. Lu, Biosensors and Bioelectronics, 22, 582 (2006).

30. H.-Y. Wang and C. Lu, Analytical chemistry, 78, 5158 (2006).

31. T. Geng, Y. Zhan, H.-Y. Wang, S. R. Witting, K. G. Cornetta and C. Lu, Journal of Controlled Release, 144, 91 (2010).

32. Y. Zhan, Z. Cao, N. Bao, J. Li, J. Wang, T. Geng, H. Lin and C. Lu, Journal of Controlled Release, 160, 570 (2012).

33. Luo, X. Yang, Q. Fu, M. Sun, Q. Ouyang, Y. Chen and H. Ji, Electrophoresis, 27, 1977 (2006).

34. Y. Zhan, J. Wang, N. Bao and C. Lu, Analytical chemistry, 81, 2027 (2009).

35. G. T. Roman, Y. Chen, P. Viberg, A. H. Culbertson and C. T. Culbertson, Analytical and bioanalytical chemistry, 387, 9 (2007)36

36. T. Geng and C. Lu, Lab on a Chip, 13, 3803 (2013)

37. S. Movahed, and D. Li, Microfluidics and Nanofluidics, 10, 703 (2011)

38. Y. Xia and G. M. Whitesides, Annual review of materials science, 28, 153 (1998).

39. de la Rosa and K. V. Kaler, 28th Annual International Conference of the IEEE, 4096 (2006).

40. M. Derde, V. r. Lechevalier, C. Guérin-Dubiard, M.-F. Cochet, S. Jan, F. Baron, M. Gautier, V. r. Vié and F. o. Nau, Journal of agricultural and food chemistry, 61, 9922 (2013).

41. T. M. Squires and S. R. Quake, Reviews of modern physics, 77, 977 (2005).

42. A. Van Loey, B. Verachtert and M. Hendrickx, Trends in Food Science & Technology, 12, 94 (2001).

43. S. Ho, G. Mittal and J. Cross, Journal of food engineering, 31, 69 (1997).

44. R. Yang, S. Li and Q. Zhang, Journal of Food Science, 69, 241 (2004).

45. R. Link, S. L. Anna, D. A. Weitz and H. Stone, Physical Review Letters, 92, 054503 (2004)

46. A. R. Abate and D. A. Weitz, Lab on a Chip, 11, 1911 (2011).

47. T. Nisisako, T. Torii, T. Takahashi and Y. Takizawa, Advanced Materials, 18, 1152 (2006).

48. M. B. Romanowsky, A. R. Abate, A. Rotem, C. Holtze and D. A. Weitz, Lab on a chip, 12, 802 (2012).

49. J. F. Edd, D. Di Carlo, K. J. Humphry, S. Köster, D. Irimia, D. A. Weitz and M. Toner, Lab on a Chip, 8, 1262 (2008).

Publishing Agreement

It is the policy of the University to encourage the distribution of all theses, dissertations, and manuscripts. Copies of all UCSF theses, dissertations, and manuscripts will be routed to the library via the Graduate Division. The library will make all theses, dissertations, and manuscripts accessible to the public and will preserve these to the best of their abilities, in perpetuity.

Please sign the following statement:

I hereby grant permission to the Graduate Division of the University of California, San Francisco to release copies of my thesis, dissertation, or manuscript to the Campus Library to provide access and preservation, in whole or in part, in perpetuity.

Author Signature

6-21-17

Date